

4.3.2 Dual ion ART-2a of Dynamometer Source Particles and Chemical Class Comparison to Los Angeles and Azusa Ambient Dataset

The mass spectra obtained for particles in Los Angeles and Azusa were matched to the source clusters generated from the El Monte dynamometer datasets for gas and diesel vehicles shown in Appendices L and M. The ambient data from SCOS97-NARSTO on August 21-22, 1997 were matched to the dynamometer dual ion ART-2a results (vigilance factor = 0.7). The Los Angeles site was expected to have more of a “fresh vehicle emission” signature. The Los Angeles dataset for these two days included 27,433 particles with mass spectral composition data (“hit” particles). The Azusa set included 19,177 “hit” particles.

The matching of particles to classes was done in a non-exclusive manner so that the number of particles classified in a given class was not affected by the presence of other similar classes. This means that a single particle can be in multiple classes, so long as it is within one vigilance factor of each class. This is different from the matching procedure presented previously in this report, which was done exclusively (each particle may only be matched to one class – the best match). The non-exclusive matching was feasible because we are using dual ion data. When positive ion only data are used, particles may be classified into many classes (particularly if the vigilance factor is 0.5). If matching is done non-exclusively with positive ion only data, it may be difficult to understand the meaning of the classification because there is no way to tell which particles matched well versus those that barely met the vigilance factor criteria. When dual ion data is matched to classes that were created with a higher vigilance factor, the classes are already more refined and the particles must match more closely to be classified in a given cluster. On average, a particle will only match 1 or 2 classes when a vigilance factor such as 0.7 has been employed with a dual ion dataset and the matching may be done in a non-exclusive manner. The non-exclusive matching has the advantage of allowing all the classes to be monitored for matches to all particles. Often a particle may be able to be classified into two somewhat similar classes and this information is maintained for non-exclusive matching. For example, the classes considering only the positive ion portion of a dataset may generate one sea salt cluster. The same classification with dual ion data may create two sea salt classes (i.e. one with more sulfate in the negative ion mass spectrum than the other class). Exclusive matching forces a particle with an border-line/intermediate amount of sulfate to be classified into only one of those classes, while the non-exclusive matching would properly identify both classes as a possible match.

Overall, the percentage of particles in Los Angeles that matched the car and diesel classes from the dynamometer was just slightly higher than for Azusa (Table 4.9, Figures 4.5 and 4.6, Appendix N). This is consistent with the hypothesis that Los Angeles particles are more similar to fresh emissions than Azusa particles. For example, 64 % of the ambient particles sampled in Los Angeles matched one or more car classes, while less than 60 % of the ambient particles sampled in Azusa matched one or more car classes sampled during the dynamometer study. The appearance of fresh emissions as well as transported emissions at the Azusa sampling site is consistent with its location, near the 210 freeway and impacted by diesel vehicle traffic. However, the whole story is not told by just the number of particles that match but by which classes they matched (or failed to match).

The distribution of the ambient particles matched to the dynamometer classes varied by site and time. The Azusa particles were more likely to match diesel class 1, in comparison to Los Angeles particles. Diesel class 1 has marker peaks for secondary species including m/z 58 and 86 (see Table 4.9). The particles at the more inland Azusa site were more likely to encounter

gas-phase pollutants and have undergone transformations. The Azusa particles were less likely to match the diesel classes 5 and 6, in comparison to Los Angeles particles. This favoring may be explained by instrumental factors. Clusters 5 and 6 lack negative ion mass spectra and as previously described, since it was the first dual ion experiment for this instrument, the Los Angeles instrument had some difficulty acquiring negative ion spectra (see previous chapter, section 3.3.5). Cluster 4 in Azusa is a surrogate for cluster 5 (nearly identical positive ion mass spectra). As the source test data are further examined and more data become available, we hope to be able to attribute to the factors which lead to the generation of certain particle types. The temporal profiles of the most common clusters are shown in Figures 4.7-4.9. Since particles can be matched to more than one class, similar classes are likely to have some particles in common and thus have similar temporal profiles. For example, car cluster 11 and diesel cluster 6 are similar and the Los Angeles temporal profiles are similar.

Table 4.9. Summary of similarity between particle classes identified by ART-2a for dual ion mass spectra from the vehicle dynamometer experiments and the ambient data (vigilance factor = 0.7).

Weight Matrix	Matched	Unmatched	Top Matching	Favored Clusters
Site	(%)	(%)	Clusters*	(for site)
To car clusters				
Los Angeles	64.0	36.0	7, 24, 2, 9, 22, 11	2, 7, 9, 11, 22, 24
Azusa	59.8	40.2	7, 24, 2, 9, 6, 22	1, 6, 8, 21
To diesel clusters				
Los Angeles	24.9	75.1	5, 6, 1	5, 6
Azusa	24.2	75.8	5, 6, 1, 4	1, 4

*non-exclusive

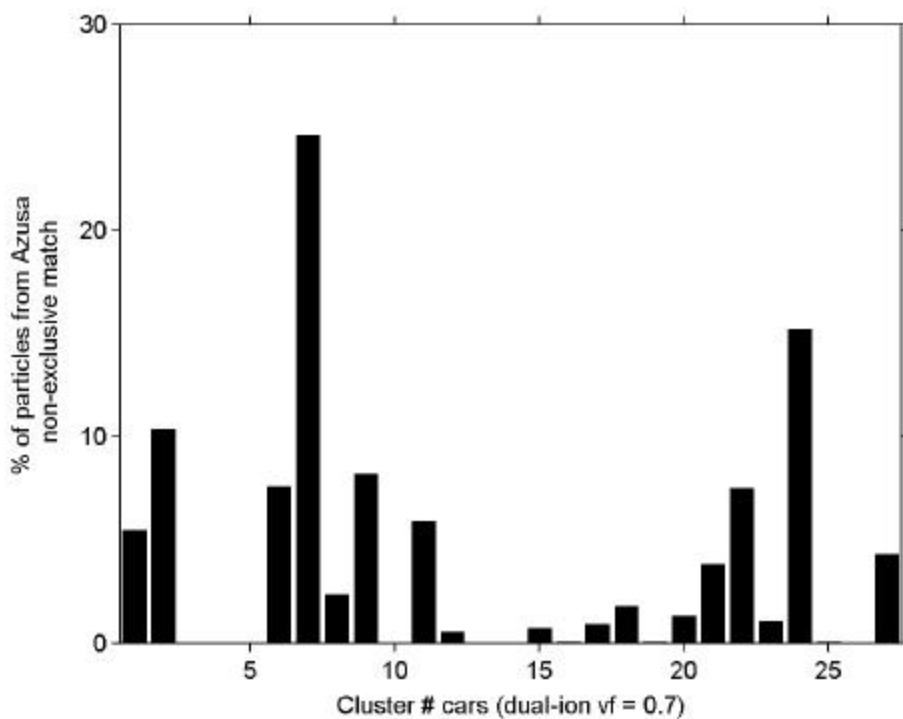
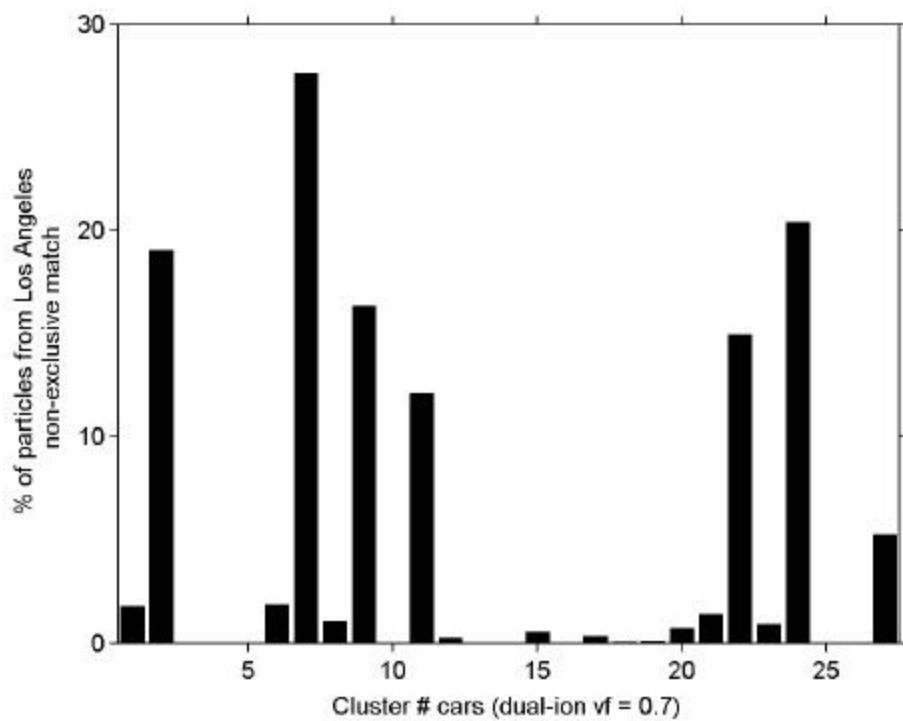


Figure 4.5: Number of particles per class, identified by ART-2a (vigilance, 0.7; classes generated from car dual ion data). Particles sampled by ATOFMS August 21-22, 1997 in Los Angeles (top) and Azusa (bottom), CA.

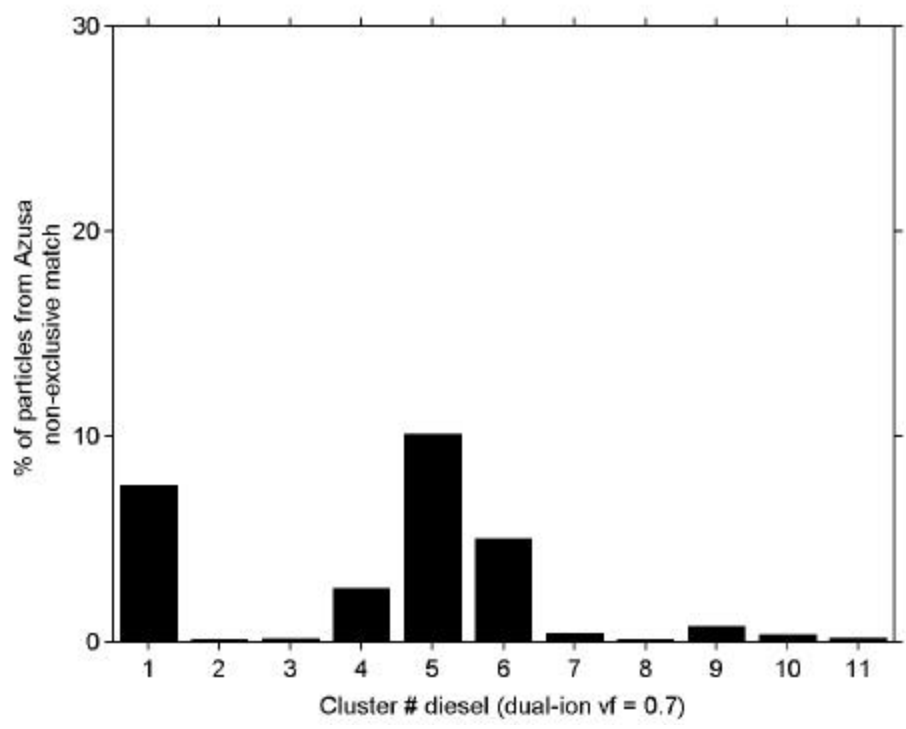
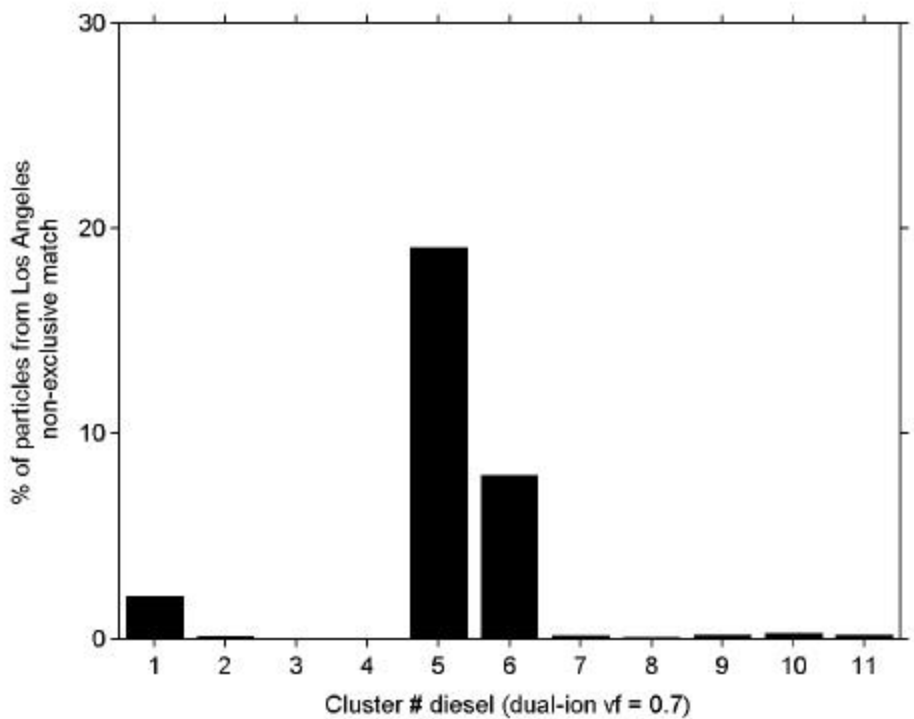


Figure 4.6: Number of particles per class, identified by ART-2a (vigilance, 0.7; classes generated from diesel dual ion data,). Particles sampled by ATOFMS August 21-22, 1997 in Los Angeles (top) and Azusa (bottom), CA.

On August 21-22, 1997, the number of particles in the diesel classes in Los Angeles drop when the afternoon winds bring in fresh marine air parcels (Figure 4.14 upper plot; for air mass trajectory information, see discussion of trajectory 1 in Chapter 3). A similar trend is noticeable in Azusa except for diesel cluster 5, which shows a major spike late in the afternoons (Figure 4.14 lower plot). This particle class appears to have marker peaks at m/z 58 and 86 that generally indicate secondary species. In addition, this particle type does not produce a detectable negative ion mass spectrum. The Los Angeles aerosol did not have any particles that matched the composition of diesel cluster 4 but Azusa had several percent of the particles with similar composition. Particle spectra in this class also have peaks that indicate secondary species (i.e. amine fragments at m/z 58 and 86); this was one of the unique diesel classes, showing little or no overlap with the car particle classes. Matching particles to the Los Angeles dataset was complicated by the fact that the dataset have very few negative ion spectra due to instrumental problems. The source sets and other ambient sets had both positive and negative ion spectra, therefore producing a higher amount of overall matches.

The results for matching to the car classes involved more clusters than the matching to diesel. Considering the most commonly matched car clusters, several have a temporal pattern similar to the particles matched to the diesel classes (Figure 4.15). The morning spike followed by an afternoon dip can be seen for car clusters 2, 9, 11, and 22 in Los Angeles. The particles matched to car cluster 7 spike when those clusters dip and cluster 7 matched particles spike on either side of the spike in those several classes on August 22. Clusters 7 and 24 have a fairly similar temporal pattern in Azusa. Again, the majority of classes build up and then decrease as cleaner air masses cross the region on August 21-22, 1997. Cluster 24 particles lack a negative ion mass spectrum and appear to be a metal-rich (i.e. $^{23}\text{Na}^+$, $^{27}\text{Al}^+$, $^{39}\text{K}^+$, $^{40}\text{Ca}^+$, $^{57}\text{Fe}^+$) organic carbon type. Car cluster 7 is a sea salt particle type with nitrate. This particle type was an ambient background particle type brought in by the dilution air and analyzed during the dynamometer experiment. Ultimately, particle types that are confirmed to represent only the background aerosol composition will be eliminated from the “source” database. In this case, a similar percentage of particles at Azusa and Los Angeles were matched to this class so there was no effect on the relative importance of the source classes (the absolute number of matched particles was inflated by about 25% if indeed this class is indeed a background particle type.)

Figure 4.16 shows the temporal profiles for three of the most abundant clusters in Azusa. Clusters 1 and 22 have markers for secondary organic species and cluster 8 is a sulfate-rich carbon type. The particles matched to these three clusters have a pattern that seems to follow the air mass exchange, as observed for many other classes.

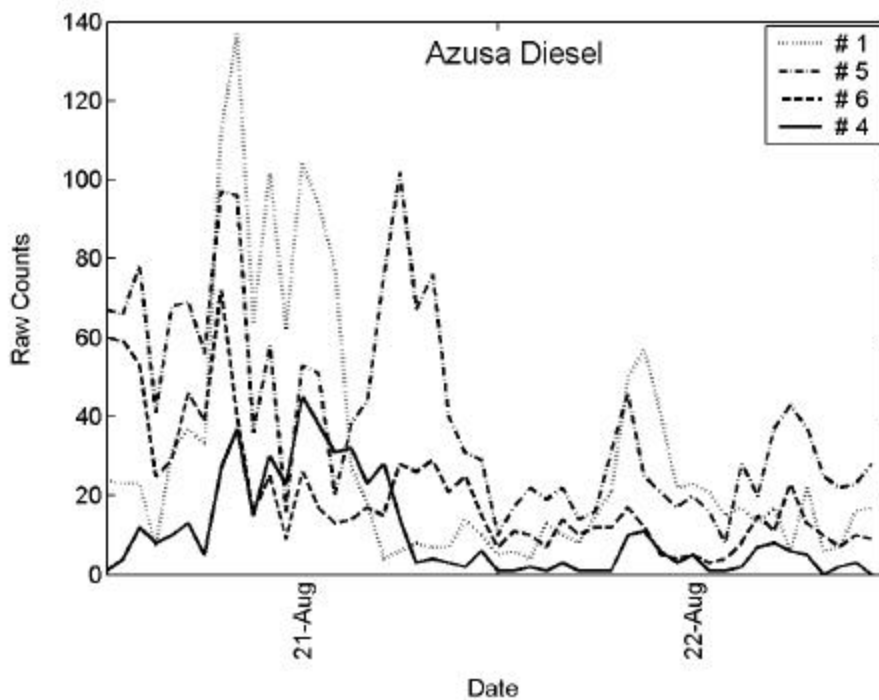
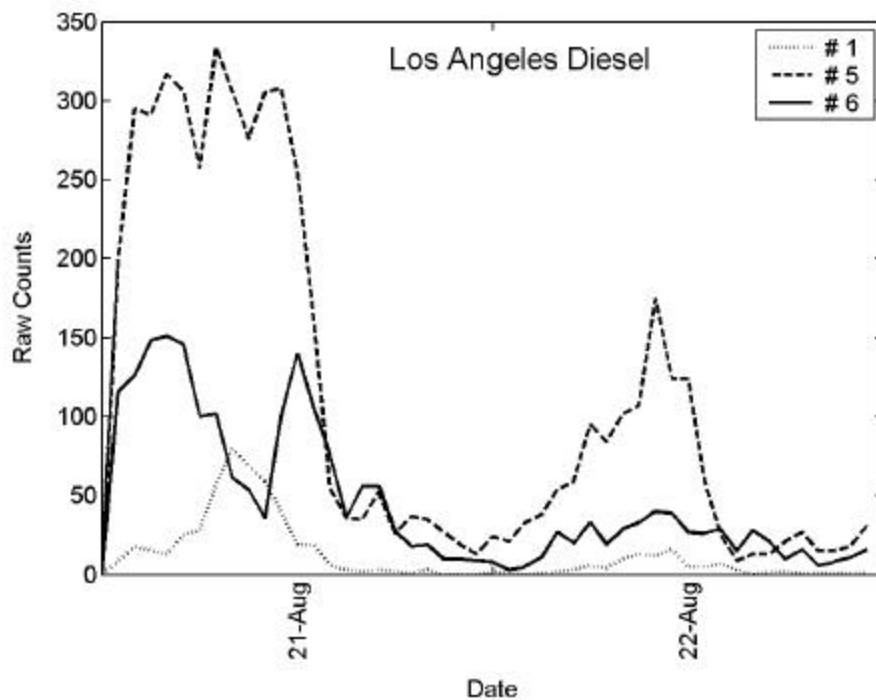


Figure 4.7: Time series plots for particles matched to classes generated from diesel dual ion data (vigilance, 0.7;). Particles sampled by ATOFMS August 21-22, 1997 in Los Angeles (top) and Azusa (bottom), CA. Temporal resolution is 1 hour.

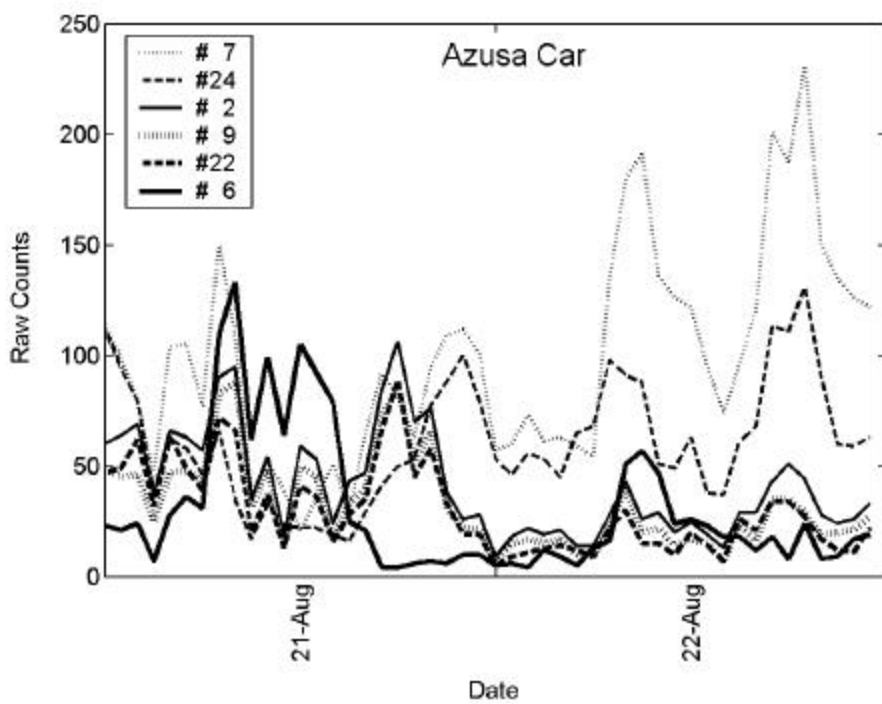
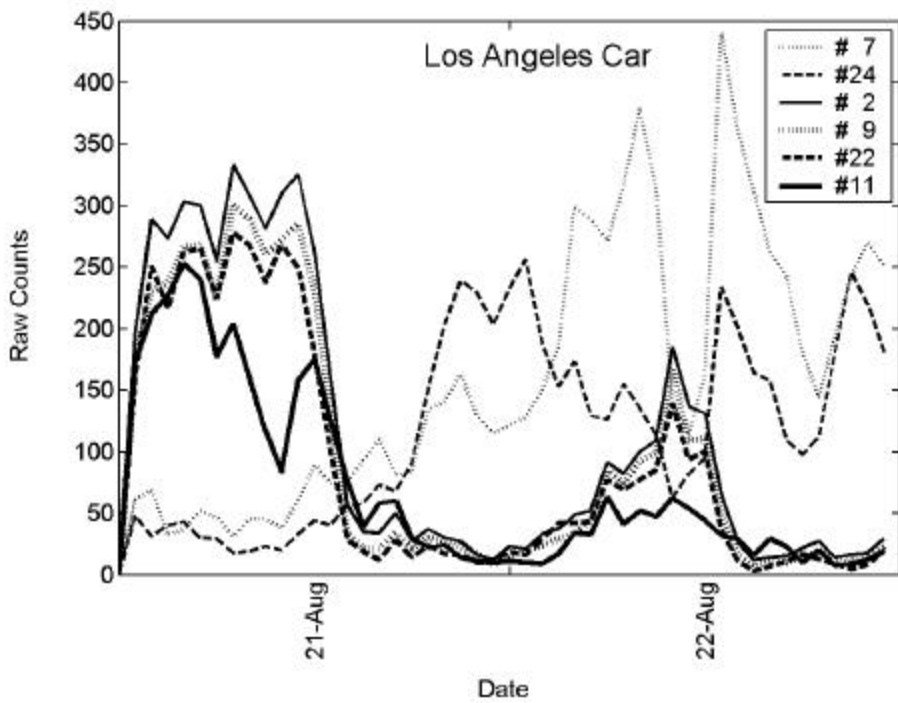


Figure 4.8: Time series plots for particles matched to classes generated from car dual ion data (vigilance, 0.7;). Particles sampled by ATOFMS August 21-22, 1997 in Los Angeles (top) and Azusa (bottom), CA. Temporal resolution is 1 hour.

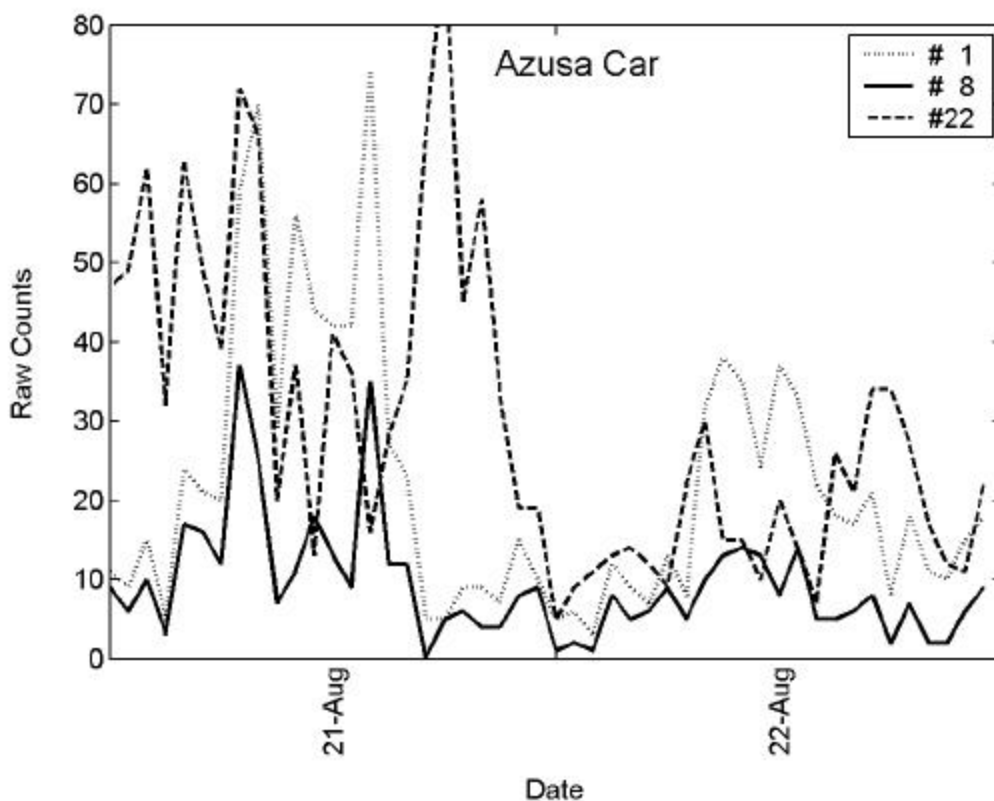


Figure 4.9: Time series plot for particles matched to classes generated from car dual ion data (vigilance, 0.7;). Particles sampled by ATOFMS August 21-22, 1997 in Azusa, CA. Temporal resolution is 1 hour.

In general, many of the major clusters generated from the dynamometer experiment are found in the ambient SCOS97-NARSTO data. The temporal profiles track the meteorology of the region. The classes that include fragments consistent with the presence of secondary species are more common at the inland site, Azusa. The Los Angeles particles were matched many of the dynamometer classes dominated by positive ions, indicating a close resemblance to fresh vehicle emissions. It should be noted that the Azusa site was near the 210 freeway and thus showed an influence from diesel vehicles as well as transported (transformed) emissions.

4.4 Conclusions

This chapter demonstrates the ability to create unique “fingerprints” from source characterization experiments. This is the first attempt to study and understand the overlap between ATOFMS source and ambient data using ART-2a. The degree of similarity between classes, including ambient classes of particles and classes of particles from a known source were calculated and plotted. Some clusters were found to be quite similar while others were unique. For source allocation, it is important to find potential unique “fingerprints” or types of particles for a source. This neural network method holds promise for determining source signatures. This demonstration lays the foundation for further investigation as part of another on-going CARB

project. As additional sources types are characterized (i.e. biomass, coal burning, meal cooking), they will be used to build a library of particle types that can be used as “seeds” for ambient source apportionment. In addition, additional diesel and gasoline characterization studies on much larger vehicle fleets have already been conducted for fine and ultrafine (<100 nm) particles to create significantly larger datasets under a variety of driving conditions. In the future, ambient particles will be compared to the source classes generated by experiments for multiple sources. The development of these source databases will also include the data from multiple dynamometer and tunnel studies currently under analysis.

The clusters generated from the dynamometer experiment are consistent with those observed during ambient sampling as part of SCOS97-NARSTO in Riverside, Azusa, and Los Angeles. The temporal profiles can be explained by the prevalent meteorology of the region. The classes that include fragments consistent with the presence of secondary species are more common in Azusa than Los Angeles and are even more abundant in Riverside, the most inland site. The Los Angeles particles match the dynamometer classes (both gas and diesel), indicating a closer resemblance to fresh vehicle emissions for many of the particles. However, as indicated, the matching was not quite as successful, given instrumental difficulties with the negative ion detection in the Los Angeles instrument.

Chapter 5

Mira Loma Aerosol and Nitrate-Oriented Trajectory

5.1 Introduction

This chapter focuses on the particle composition at a mid-region sampling site in Mira Loma during late September of 1997 (September 27-29, 1997) and the changes in the aerosol composition along the trajectory from Diamond Bar to Mira Loma to Riverside. These sites lie along typical late summer wind trajectory patterns that cross an agricultural area. These sites are (in order) upwind, adjacent to, and downwind of the ammonia emissions from livestock (dairy feedlots) and fertilizer use. For this study, the ATOFMS instrument from Azusa was moved to Mira Loma in late August and sampled in Mira Loma for the month of September. The Los Angeles ATOFMS was moved to Diamond Bar for particle sampling in September as well. The lab-based ATOFMS remained in Riverside. The Diamond Bar and Mira Loma sites were located approximately 1 mile south of the 60 freeway. The Mira Loma site was located in the back of a parking lot where new vehicles were offloaded from trains and loaded onto heavy duty diesel transport trucks. A primary goal of this study was to characterize the particles which contribute to the well documented high $PM_{2.5}$ mass concentrations observed in the Mira Loma and Riverside areas. Most of this has been attributed to accumulation of ammonium, nitrate, and secondary organic species (SOA) on particles under stagnant conditions encountered due to the mountainous geography. However, in this study it was determined the presence of diesel trucks in Mira Loma also appeared to have a significant effect on the particle population.

5.2 Experimental methods

As discussed in Section 2.3, ATOFMS was used to characterize individual ambient aerosol particles. The data are calibrated for size and the time axes are converted to m/z (see Section 2.2) and compiled in the YAADA database. As discussed in Chapter 2, neural network ART-2a analysis can be applied to ATOFMS data. In this chapter, the existing Riverside clusters are again incorporated into this analysis. The ambient particles sampled in Mira Loma are matched to existing classes from Riverside (see Section 3.2). In addition, digital mass spectra are used to display the trends in a set of several single particle mass spectra (see Section 3.2).

5.3 Results and Discussion

5.3.1 Mira Loma Single Particle Composition and Comparison to Riverside Ambient Positive ion ART-2a Classes

The particle size distribution of the single particle Mira Loma data exhibits a typical bimodal shape. There is a “notch” in the super- μm size mode, around 2.1-2.3 μm . The “notch” is a sampling artifact of the nozzle used in this instrument at this time. Based on other sizing measurements at the site, the actual size distribution falls off smoothly in this region.

The positive ion digital mass spectrum shows the particle composition above 1 μm includes a sea salt signature blended with elemental or organic carbon ion peaks (Figure 5.2). The sea salt markers highlighted include $^{23}\text{Na}^+$, $^{39/41}\text{K}^+$, $^{108}(\text{Na}_2\text{NO}_3)^+$ and $^{165}(\text{Na}_3\text{SO}_4)^+$. The marker peaks for the carbon ion clusters are highlighted: $^{12}\text{C}^+$, $^{24}\text{C}_2^+$, extending up to $^{144}\text{C}_{12}^+$. For the most part, the particle spectra dominated by a carbon-envelope (elemental carbon) and the sea salt particles are externally mixed. Particles with one percent of their relative area at m/z 60 or 72 do not have sea salt marker peaks. Only about five percent of the particles with at least one percent of their relative area at m/z 12 or 36 also show sea salt marker peaks (with at least one percent of their relative area at m/z 81 (Na_2Cl^+) or the nitrate-reacted sea salt marker m/z 108 (Na_2NO_3^+)). The most logical explanation for this blending of inorganic and organic peaks is that some of the sea salt particles possessed an organic coating. The negative ion digital mass spectrum for the super- μm particles shows large peaks for $^{46}\text{NO}_2^-$ and $^{62}\text{NO}_3^-$. Other peaks include $^{35}\text{Cl}^-$, $^{80}\text{SO}_3^-$, $^{97}\text{HSO}_3^-$, $^{147}\text{Na}(\text{NO}_3)_2^-$, and carbon cluster ion peaks including m/z -48, -60, and -72. Figure 5.3 shows the digital mass spectra for particles below 1 μm in aerodynamic diameter. Dominating the spectrum are peaks due to elemental carbon (carbon clusters) in both polarities (i.e. m/z 12, 24, 36, 48...144), showing the strong influence of diesel traffic in the area. Also, present are peaks due to organic carbon species at m/z 15, 27, 29, 39, 41, 43, 50, and 51.

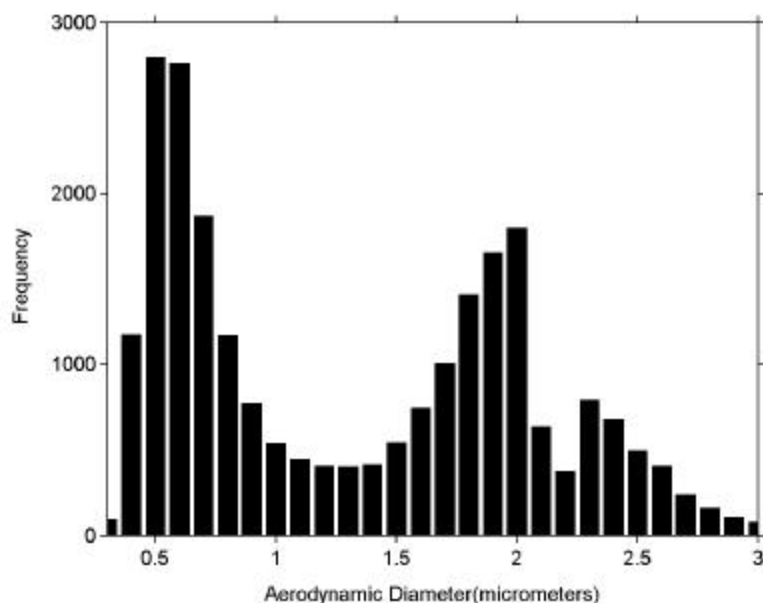


Figure 5.1: Size distribution plot for the particles sampled in Mira Loma, CA September 27-29, 1997.

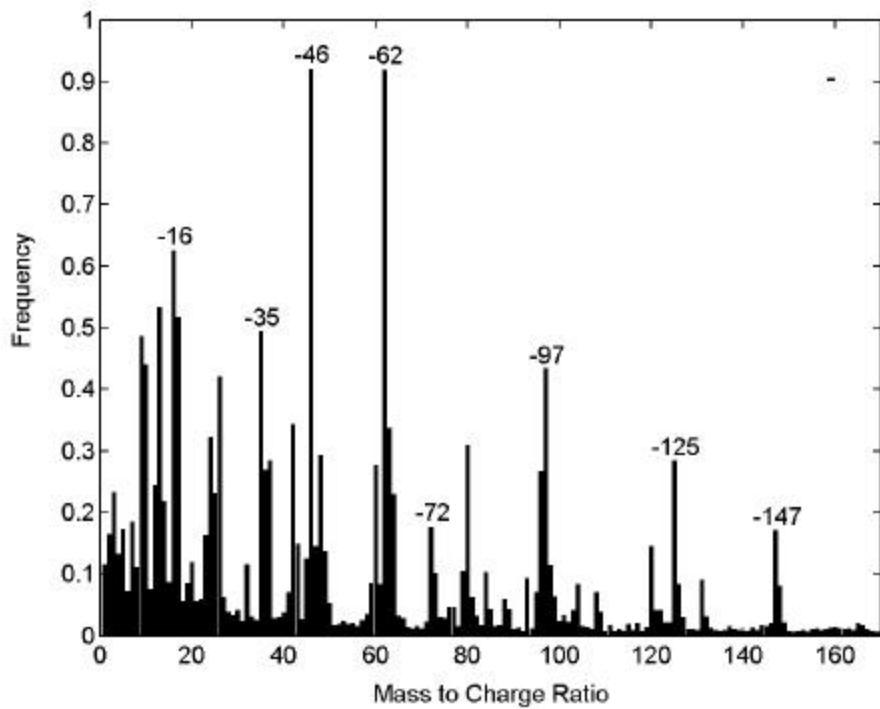
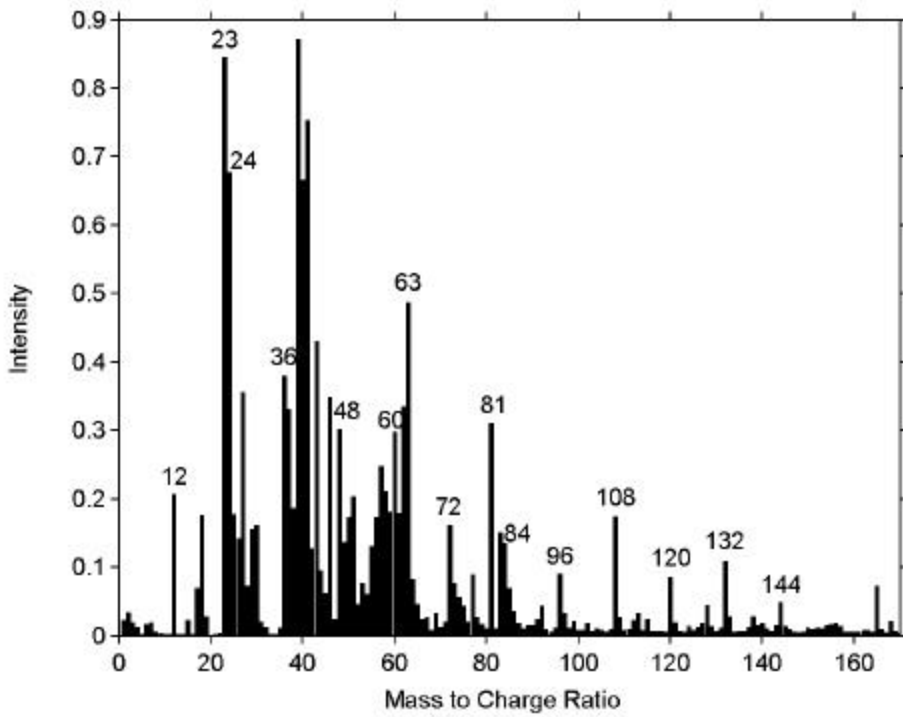


Figure 5.2: Positive- and negative ion digital mass spectra of super-mm particles sampled in Mira Loma, CA during September 27-29, 1997.

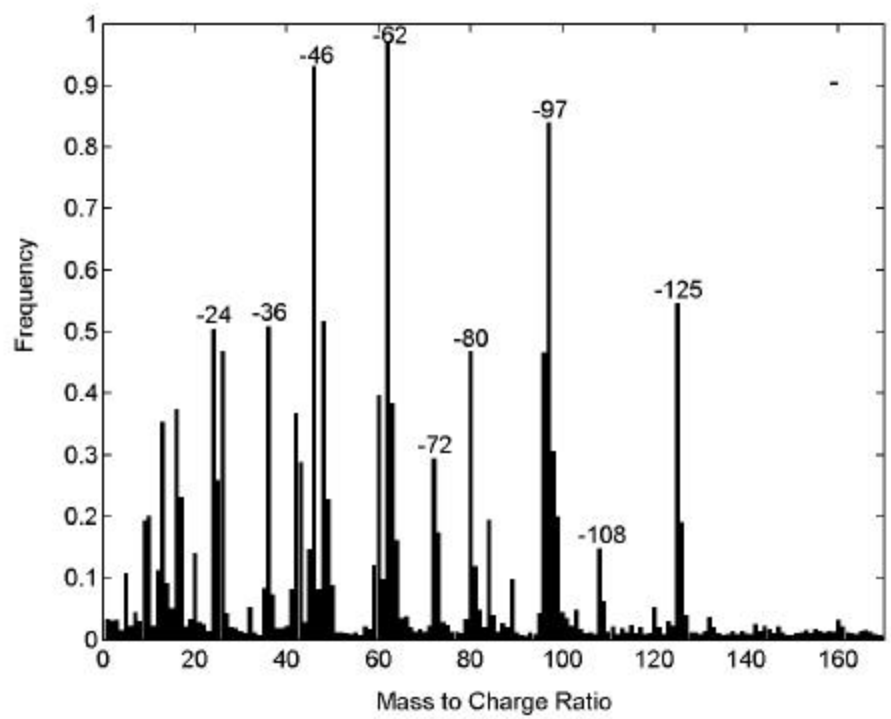
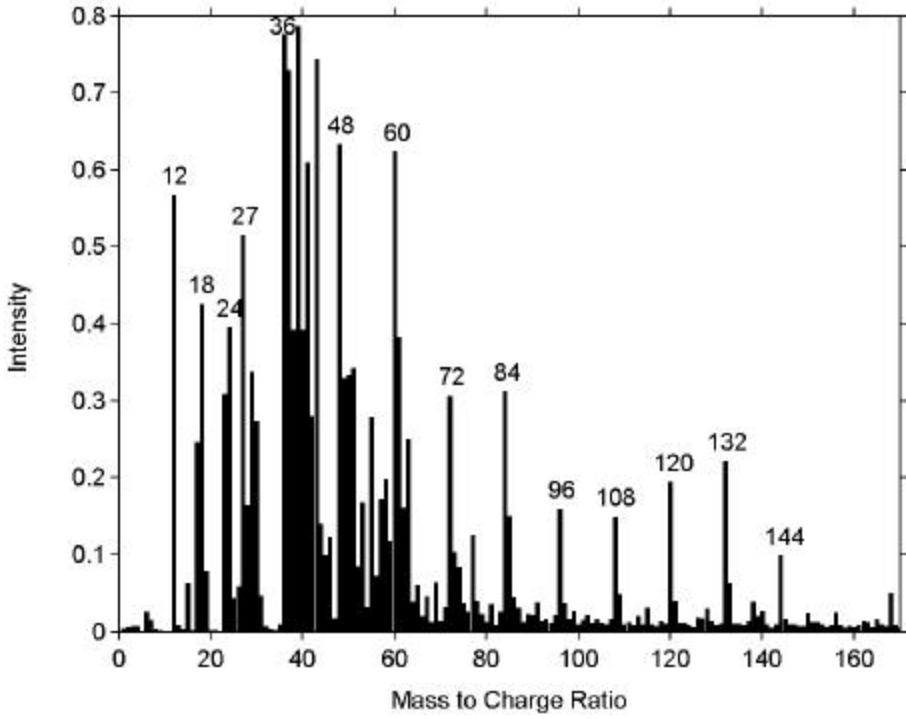


Figure 5.3: Positive- and negative ion digital mass spectra of sub-mm particles sampled in Mira Loma, CA during September 27-29, 1997.

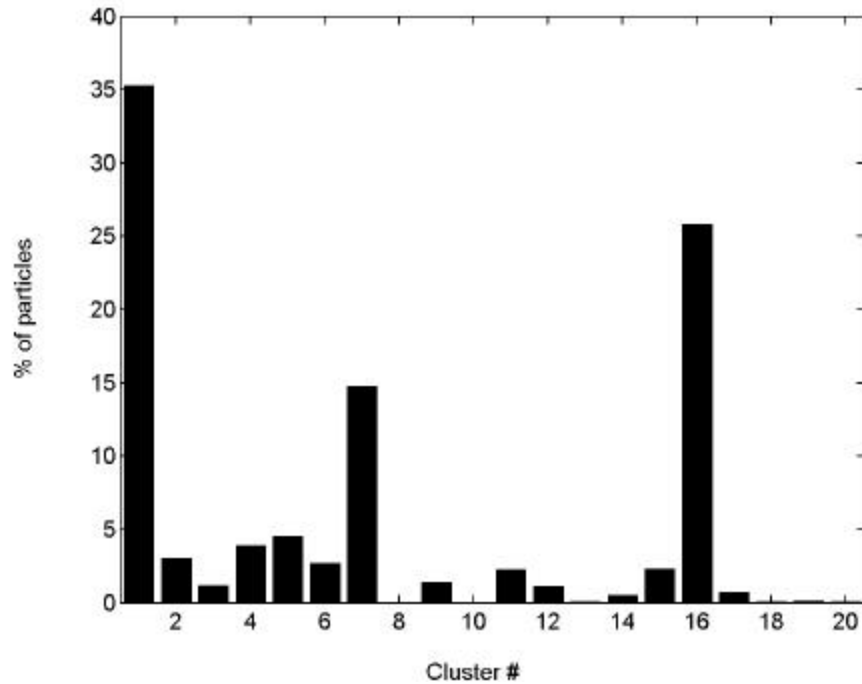


Figure 5.4: Number of particles matched to ART-2a classes (vigilance, 0.5; learning 0.05; 20 iterations, classes generated from Riverside data). Particles sampled by the ATOFMS in Mira Loma, CA during September 27-29, 1997.

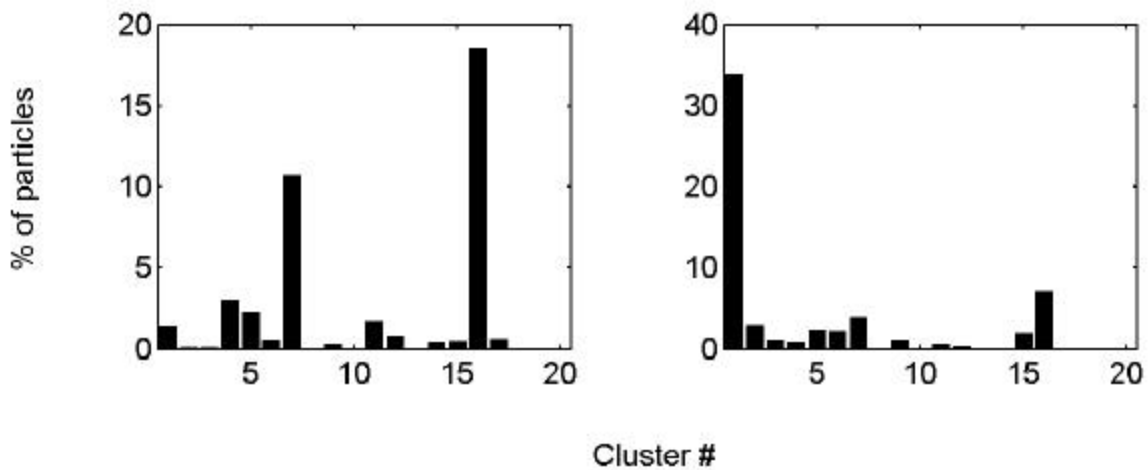


Figure 5.5: Number of sub- (left side) and super- mm (right side) particles matched to ART-2a classes, (vigilance, 0.5; learning 0.05; 20 iterations, classes generated from Riverside data). Particles sampled by the ATOFMS in Mira Loma, CA during September 27-29, 1997.

The positive ion mass spectra from the Mira Loma ambient particles were matched to the 20 most common classes from Riverside (described in Chapter 2). The process of using existing clusters to classify a new dataset, referred to as “matching” particles, is described in further detail in Chapter 3. The Mira Loma particles were matched to the existing ambient Riverside classes. Figures 5.4 and 5.5 show the number of particles matched to each ART-2a class (also see Appendix D for numerical results of matching). Using the matching routine, sea salt particles with nitrate (cluster 1) appear as the most commonly detected particles in Mira Loma of the original Riverside particle types. Note as described before, the relative fraction is determined by the fact that the ATOFMS detects larger particles more efficiently than smaller particles. Upon scaling, sub- μm particle types (i.e. cluster 16) will be the most abundant. Cluster 1 matched particles were mainly above 1 μm but a few fell just below 1 μm (notice the presence of some particles for cluster 1 in the plot on the left side of Figure 5.5). The temporal profile of the total, super- μm , and cluster 1 matched hits is provided in Figure 5.6. The second most commonly detected particle types were classified as elemental carbon particles, cluster 16, as described above. As discussed in Chapter 4, one of the top classes found in the diesel exhaust experiment resembled the elemental carbon cluster 16 (see Tables 4.2 and 4.3). The close proximity of the freeway, truck terminals, and warehouses, and the presence of many large diesel trucks in the lot where the sampling trailer was located may explain the strong elemental carbon signatures in this dataset. The temporal profiles of the total, sub- μm , and cluster 16 matched hits are provided in Figure 5.7. Figure 5.8 shows the strong anti-correlation observed between the temporal profiles for the elemental carbon (16) and sea salt (1) class particle types. These plots demonstrate how the arrival of particles in sea salt cluster 1 represented fresh air masses being transported in from the coast. The arrival of this air mass disrupted the stagnant conditions, reducing the overall contributions from local particle sources upon dilution. Finally, potassium-rich particles (cluster 7) were commonly observed in Mira Loma, particularly in the sub- μm fraction possibly indicating biomass or cooking emissions. Particles that were matched to cluster 7 in Riverside were super- μm as opposed to sub- μm , indicating a different source (most likely crustal in Riverside). The few super- μm cluster 7 particles observed in Mira Loma were more dust-like (i.e. possessed at least one percent relative area at m/z 23 and 56) and the sub- μm cluster 7 particles were more carbon-rich (i.e. possessed at least one percent relative area at m/z 12, 36, 48 and 60). The combination of size and composition of the K-rich particles in Mira Loma and Riverside cluster 7 particles suggests a different source. Further source tests are necessary to allow apportionment of these particle types.

There is a noticeable absence of organic carbon with high amounts of ammonium and nitrate (clusters 8 and 13) in Mira Loma. One possible explanation for this observation is that the ammonium sources were too close to the site to allow the necessary time for significant ammonium nitrate to form on the surface of existing particles. Another possibility, as shown in Figure 5.3, is the ammonia partitioned preferentially to elemental carbon particles given their much higher abundance and surface area. The downwind Riverside site is episodically impacted by the particle enriched in ammonium nitrate. However, after sea salt and elemental carbon particles, the next most detected particle types in Mira Loma (which would be ranked much higher upon scaling) were clusters 4 and 11. These are organic carbon particle types with ammonium and nitrate, and represent the most common sub- μm particles detected in Riverside. Their relatively lower ranking in Mira Loma is due mostly to the higher relative abundance of elemental carbon particles in the area relative to Riverside. In the next section, the chemical

composition of the three trajectory sites will be analyzed more closely and detailed observations regarding changes in the ammonium and nitrate content of particles will be discussed.

The size-segregation of the matched results shows the consistent associations between particle size and composition. The sub- μm particles match the elemental carbon, potassium-rich, and organic carbon clusters, while the super- μm particles mainly match clusters of sea salt particles with nitrate and elemental carbon (cluster1 and 16).

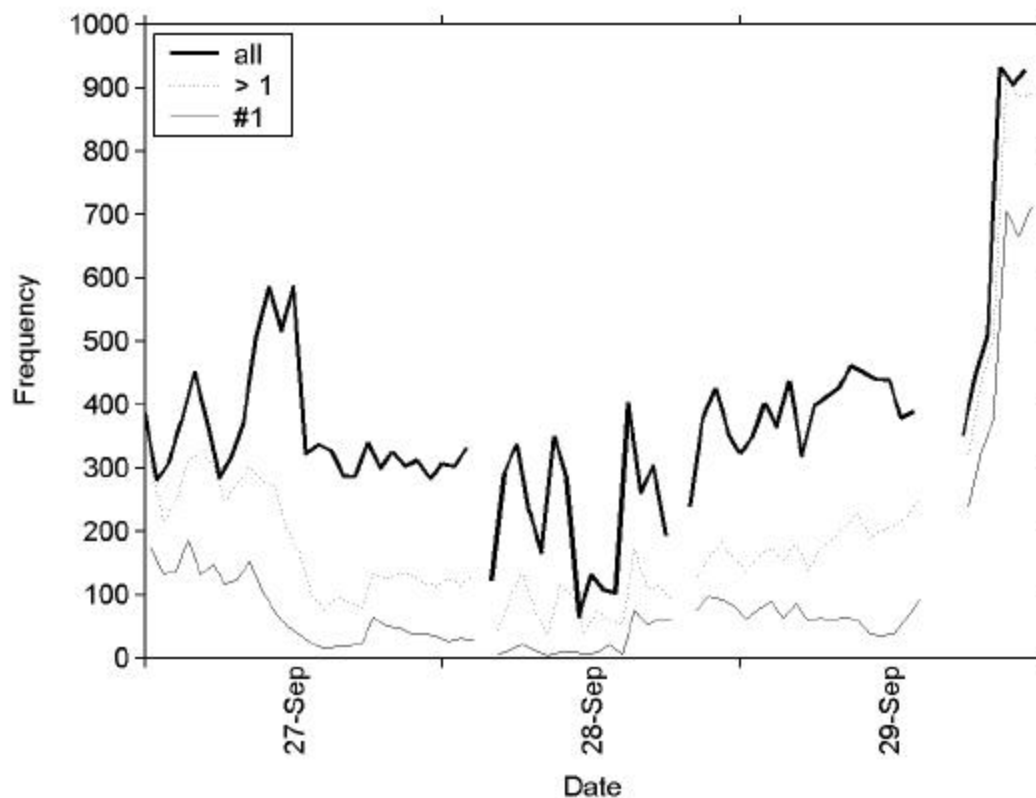


Figure 5.6: Times series plots of ATOFMS data from Mira Loma, CA. Total, super- μm , and particles matched to ART-2a sea salt class 1 (vigilance, 0.5; learning 0.05; 20 iterations, classes generated from Riverside data). ATOFMS data displayed with 1-hour resolution.

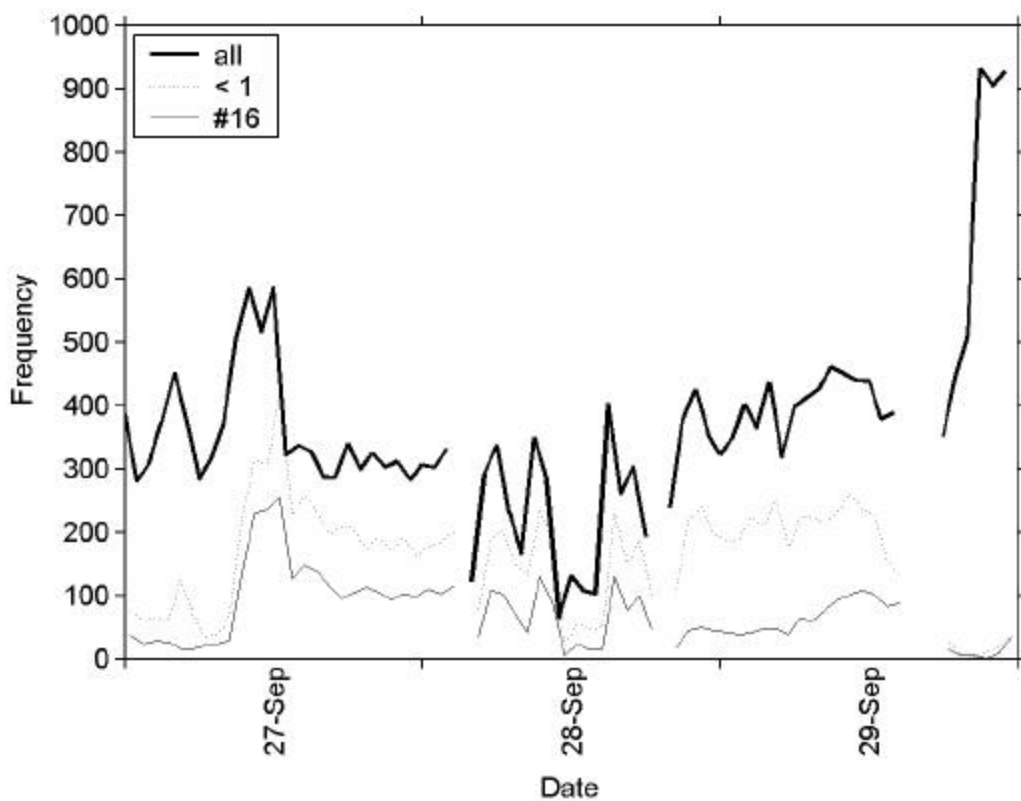


Figure 5.7: Times series plots of ATOFMS data from Mira Loma, CA. Total, sub- mm, and particles matched to ART-2a elemental-carbon class 16 (vigilance, 0.5; learning 0.05; 20 iterations, classes generated from Riverside data). ATOFMS data displayed with 1-hour resolution.

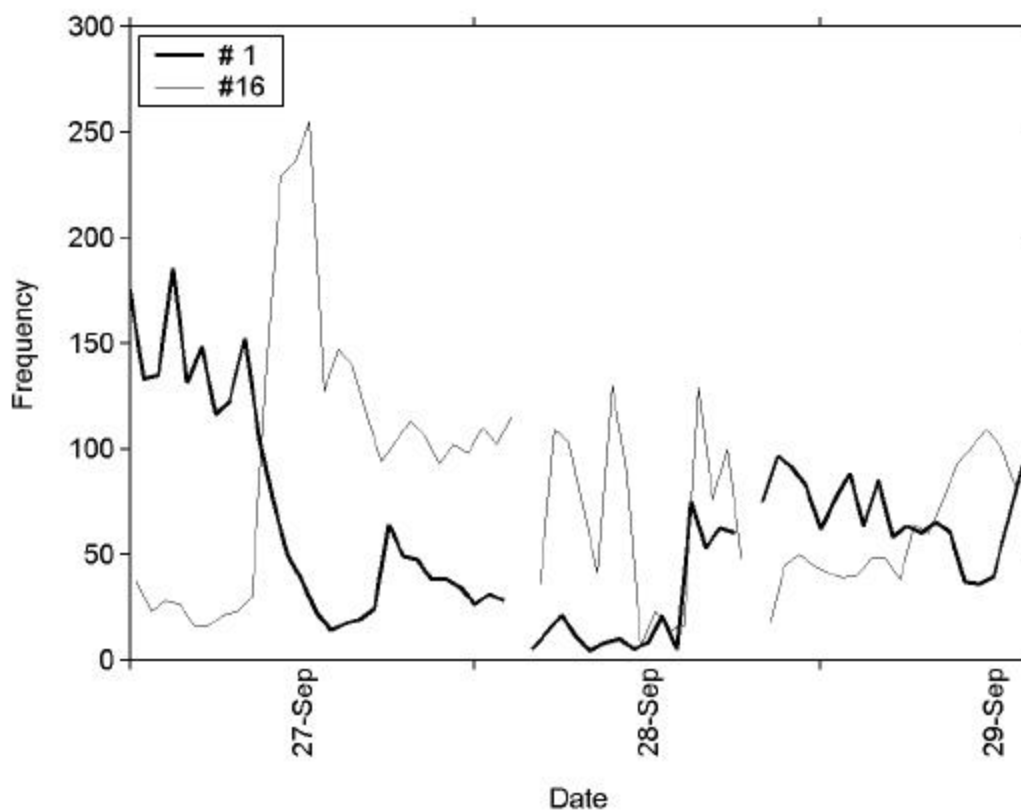


Figure 5.8: Times series plots of ATOFMS data from Mira Loma, CA. Particles matched to ART-2a sea salt class 1 and elemental-carbon class 16 (vigilance, 0.5; learning 0.05; 20 iterations, classes generated from Riverside data). ATOFMS data displayed with 1-hour resolution.

5.3.2 Particle Composition along the Diamond Bar-Mira Loma-Riverside Trajectory

To observe the changes in particle composition across the Diamond Bar-Mira Loma-Riverside trajectory path, a series of ART-2a classification and matching steps include:

1. Create ART-2a classes for the upwind site (Diamond Bar):
 - 1.1. Create classes for Diamond Bar particles by ART-2a
 - 1.2. Sort the classes according to the number of particles per class
 - 1.3. Truncate the classes with less than the arbitrary threshold number/percent of particles (consider only clusters containing a statistically significant number of particles)
2. Determine “new” classes for the mid-region site (Mira Loma):
 - 2.1. Match Mira Loma particles to the set of classes from Diamond Bar (i.e. the upwind site)
 - 2.2. Find the Mira Loma particles that were not matched to the set of classes from Diamond Bar
 - 2.3. Create “new” classes for “unmatched” Mira Loma particles by ART-2a
 - 2.4. Sort the classes according to the number of particles per class
 - 2.5. Truncate the classes with less than the arbitrary threshold number/percent of particles
 - 2.6. Combine the set of classes from Diamond Bar with the set of “new” classes from Mira Loma
3. Determine “new” classes for the downwind site (Riverside):
 - 3.1. Match Riverside particles to the combined set of classes from Diamond Bar/Mira Loma
 - 3.2. Find the Riverside particles that were not matched to the set of classes from Diamond Bar/Mira Loma
 - 3.3. Create “new” classes for “unmatched” Riverside particles by ART-2a
 - 3.4. Sort the classes according to the number of particles per class
 - 3.5. Truncate the classes with less than the arbitrary threshold number/percent of particles
 - 3.6. Combine the set of classes from Diamond Bar/Mira Loma with the set of “new” classes from Riverside
4. Match the particles from each site to the combined Diamond Bar/Mira Loma/Riverside classes

By following these steps, we began the ART-2a analysis at the cleanest site (Diamond Bar), created clusters, matched sequentially to the next most inland site (Mira Loma), and finally matched these clusters to particles sampled at the most inland site (Riverside). We expected to see more particles and new particle types as the air masses move inland and the air pollution levels increased. The parameters for the ART-2 analysis (for all three sites) included: a vigilance factor of 0.7, a learning rate of 0.05, a maximum of 40 iterations, and a range of the first 350 m/z (m/z) units of the positive ion mass spectra for creating the vectors. The times selected for each site were determined by the back-wind air-parcel-trajectory calculations. Based on the calculations for Riverside for September 28-29, 1997, the times for when these air masses had passed over Diamond Bar and Mira Loma were determined.

Table 5.1: List of ATOFMS selected sampling times for each site.

Start Date/Time	End Date/Time	Sampling Location	ATOFMS instrument
September 28, 1997 0:00	September 29, 1997 24:00	Riverside	lab-based (BST)
September 27, 1997 15:00	September 29, 1997 19:00	Mira Loma	transportable (ELD)
September 27, 1997 11:00	September 29, 1997 14:00	Diamond Bar	transportable (JKE)

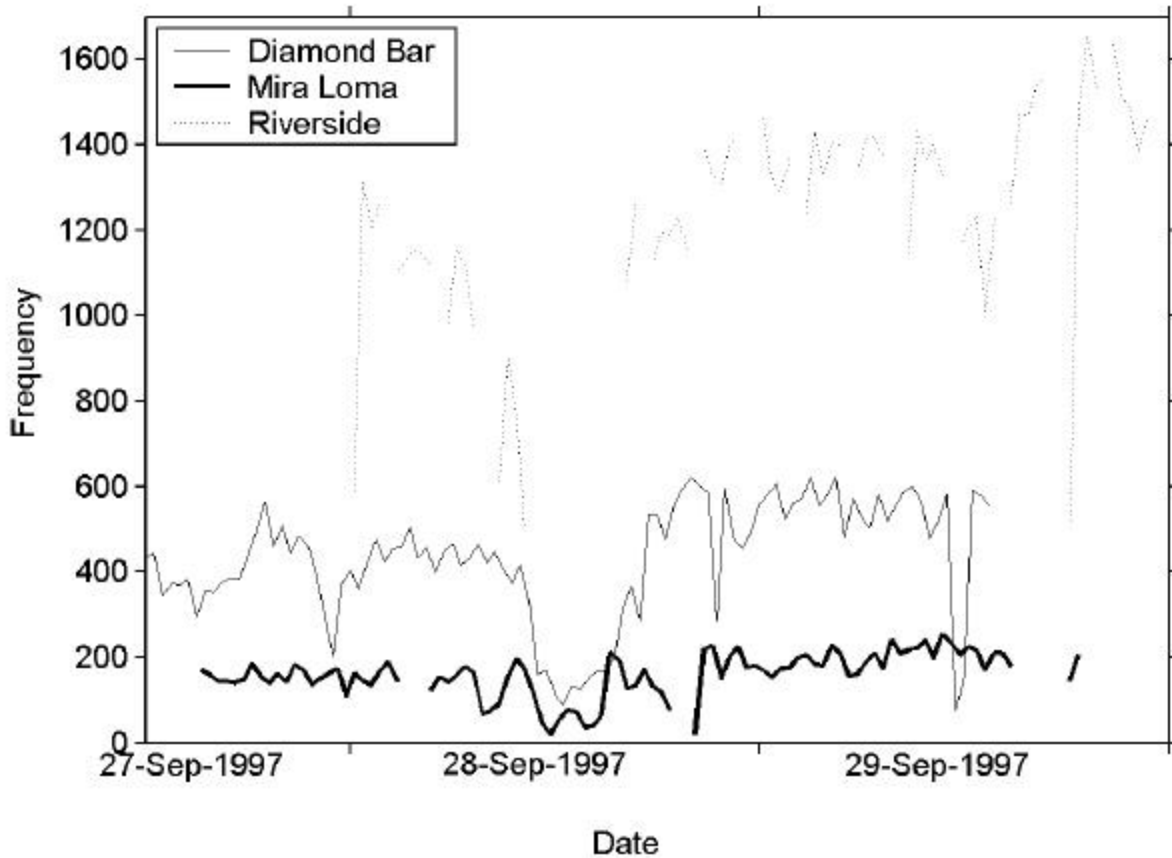


Figure 5.9: Times series plots of ATOFMS data from Diamond Bar, Mira Loma, and Riverside, CA. Particles selected for trajectory matched times. ATOFMS data displayed with 30 min resolution on x-axis (time period 9/27/97 12:00 – 9/29/97 24:00).

As discussed in Chapter 2, the plotted temporal profile of positive ion mass spectral data for the Riverside ATOFMS are not continuous because the mass spectrometer was switched to negative ion mode periodically. The times listed for each site in Table 5.1 will ultimately be matched to the combined set of classes created by the ART-2a neural network analysis from Diamond Bar, Mira Loma and Azusa. In order to carry out the classifications, the initial datasets

from each site were selected (10,000 – 20,000 particles per dataset). The ART-2a inputs were truncated where necessary while still capturing a representative sample by selecting times throughout the trajectory period. More particles were selected the further inland the site was located to insure that there would be a reasonable number of “unmatched” particles to screen with ART-2a for “new” classes. For Diamond Bar data, all the positive ion mass spectra for September 28, 1997 during odd-numbered hours were considered, totaling 8,913 positive ion mass spectra from 9,136 particles. For Mira Loma, all the positive ion mass spectra for the time range indicated in Table 5.1 were considered, totaling 11,774 positive ion mass spectra (from 14,766 particles - the remaining particles had only a negative ion mass spectra). For Riverside, the 1-hour time periods starting 0:30, 5:30, 10:00, 16:00, 20:30 on September 28 and 3:00, 6:30, 13:00, 18:00 on September 29, 1997 were considered, totaling 21,421 particles (all had positive ion only mass spectra).

For the Diamond Bar initial set, ART-2a analysis yielded 30 major particle composition classes (each contained at least 0.67 % of the number of input spectra or at least 60 particles). An additional 12 classes were added from the Mira Loma dataset (classes 31-42, each contained at least 1.6 % of the number of input spectra or at least 19 particles). Finally, the Riverside dataset contributed 15 additional classes (classes 43-57, each class contained at least 1.4 % of the number of input spectra or at least 35 particles). Table 5.2 lists the top ion peaks from each of the clusters. Appendix O shows the weight matrices of each of the 57 clusters.

Table 5.2. Summary of particle classes identified by ART-2a of positive ion mass spectra from Diamond Bar-Mira-Riverside (vigilance factor = 0.7).

Class	Diamond Bar	Mira Loma	Riverside	Top 12 Peaks (m/z) Please see the Appendix for a list of m/z values with possible mass spectral peak assignments.											
	No. in Class			Major classes created by the initial set of positive ion Diamond Bar mass spectra											
1	10,175	437	4320	23	39	24	63	41	40	62	108	46	81	59	30
2	3825	71	62	23	63	39	24	41	62	40	81	46	108	92	83
3	5779	910	37,075	23	24	39	41	40	63	36	62	46	26	30	68
4	2946	172	836	23	39	41	40	24	30	18	108	36	63	43	58
5	2222	253	14,181	23	24	39	63	40	81	41	62	46	108	25	26
6	2102	218	454	23	36	39	12	41	24	37	40	48	60	30	18
7	895	154	88	23	39	43	27	37	36	41	38	18	30	40	24
8	1033	202	238	36	23	37	12	48	43	60	39	24	27	30	38
9	718	312	256	36	37	43	12	27	39	38	48	24	29	50	60
10	529	141	428	36	37	12	43	27	39	38	24	30	29	18	50
11	728	442	836	36	12	37	24	43	48	27	39	38	17	50	29
12	540	331	759	36	12	37	24	43	27	30	48	18	39	17	38
13	638	72	66	23	36	37	27	43	39	12	38	30	18	50	24
14	745	1584	2169	39	41	40	23	57	56	43	36	27	37	140	18
15	428	198	272	36	37	43	27	39	12	38	50	18	29	30	51
16	686	102	922	40	57	56	23	41	96	113	39	24	44	86	58
17	713	64	2756	40	23	57	39	24	41	56	63	96	113	108	58
18	591	893	267	36	48	37	60	23	12	43	39	24	61	27	49
19	614	277	520	39	23	41	40	56	36	24	43	57	48	27	60
20	492	1065	80	36	60	48	37	72	43	84	23	12	61	39	132
21	502	479	1255	39	40	41	23	56	57	140	43	42	27	18	213
22	391	238	1521	40	23	57	56	41	39	24	1	27	42	44	2
23	565	229	40	23	36	60	48	37	43	84	61	72	39	132	41
24	310	147	1006	36	37	18	12	30	43	39	27	24	17	38	50
25	384	445	423	39	36	37	12	60	48	41	43	24	18	27	30
26	211	174	301	43	27	37	39	36	38	29	50	51	41	30	18
27	374	178	594	39	56	41	40	23	57	27	73	30	43	18	64
28	317	316	560	37	27	39	18	43	36	38	50	29	51	30	41
29	365	219	597	56	39	23	57	54	27	73	24	40	55	72	41
30	259	153	149	36	39	12	37	24	43	27	30	18	48	41	38

(Table 5.2 is continued on the following page)

Table 5.2. (CONTINUED)

Class	Diamond Bar	Mira Loma	Riverside	Top 12 Peaks (m/z)											
		No. in Class		New classes created by positive ion Mira Loma mass spectra											
31	264	90	157	41	24	23	2	27	57	28	58	42	59	1	25
32	72	249	10	60	132	84	120	36	72	48	108	96	61	43	144
33	24	67	1	132	120	60	84	180	144	168	36	61	72	96	108
34	209	204	167	39	43	18	55	41	27	51	63	69	57	58	77
35	49	78	10	132	61	43	18	60	84	85	37	36	120	48	109
36	227	45	108	55	27	39	2	40	24	23	137	154	57	1	26
37	57	35	0	43	39	55	69	41	18	58	57	95	163	81	152
38	134	39	431	27	23	28	39	70	64	44	30	29	56	43	155
39	30	56	9	64	23	43	39	27	58	32	63	37	51	66	40
40	50	24	70	64	48	27	39	65	23	56	62	46	63	81	66
41	171	22	16	42	23	39	24	56	141	57	27	2	40	48	30
42	39	50	179	51	67	43	58	27	68	52	39	56	23	18	41
				New classes created by initial set of Riverside mass spectra											
43	1	0	967	30	18	46	19	35	17	31	1	39	36	37	27
44	0	4	894	30	18	35	17	36	31	46	19	86	39	27	43
45	6	9	1444	30	18	12	19	43	36	37	27	24	39	17	35
46	3	0	753	1	23	12	16	14	24	39	2	17	40	30	25
47	1	0	289	1	16	30	14	12	17	18	32	39	15	19	2
48	3	0	357	22	23	39	2	35	40	38	29	34	82	111	1
49	0	2	434	2	24	17	28	27	29	26	41	40	25	39	30
50	0	0	752	30	12	18	24	36	19	27	17	43	37	35	29
51	3	12	528	2	40	24	28	27	17	25	29	26	42	23	30
52	24	19	509	18	30	37	36	19	27	43	12	17	39	58	29
53	3	0	384	30	39	18	12	24	43	27	19	23	36	37	17
54	1	2	358	2	23	17	27	25	28	26	40	29	24	39	41
55	44	17	216	38	35	40	22	39	23	17	36	137	86	50	85
56	9	0	346	86	30	18	58	37	27	12	102	39	87	118	43
57	2	6	257	37	36	43	19	39	15	35	18	61	84	29	12

Of the first 30 clusters detected (initially by analyzing the Diamond Bar dataset), among the most common marker peaks are $^{23}\text{Na}^+$, $^{39,41}\text{K}^+$, $^{54,56,57}\text{Fe}^+$, $^{81,83}\text{Na}_2\text{Cl}^+$, $^{108}\text{Na}_2\text{NO}_3^+$, $^{12}\text{C}^+$, $^{36}\text{C}_3^+$, $^{48}\text{C}_4^+$, and $^{60}\text{C}_5^+$. The first seven classes are various sea salt types, indicative of the bias of the instrument to larger particles. It should be pointed out that the presence of m/z 24 in these mass spectra most likely results from a large sodium peak at m/z 23 (rather than a carbon or magnesium peak). The presence of m/z 40 in these mass spectra may be the result of a large potassium peak at m/z 39 or a calcium peak. Care must be taken when assigning a peak such as m/z 40, if the neighboring peak is very intense. Some of the clusters are characterized by nitrate marker peaks at m/z 30 and 108. Clusters 8-12 are carbon-rich, 14 is potassium-rich, 15 contains organic carbon, 16-17 are calcium-rich, 18 is carbon-rich, 20 has even more intense signal from larger carbon envelopes, 25 is potassium-rich with carbon envelopes, ammonium and nitrate, and 29 is iron-rich.

An additional 27 classes complete the set. The classes 31-42, added upon analysis of the Mira Loma dataset, are dominated by elemental carbon particle spectra. These spectra (many of

which contain a peak at m/z 132) are consistent with elemental carbon signatures based on laboratory studies, showing m/z 132 is a very stable carbon cluster ion. Clusters 31 and 36 appear to be soil dust with peaks for aluminum, iron, and 1. Cluster 42 is vanadium-rich, indicative of vehicle traffic. Added by the Riverside analysis, clusters 43-47 and 52-53 are ammonium-rich and nitrate-rich, indicating accumulation occurred on the particles before reaching the Riverside site. Almost all of the Riverside types showed markers due to ammonium and nitrate, sometimes so strong the core organic carbon signature was masked. New dust clusters types unique to Riverside include 46-49, 49, 51 and 54. These soil dust types most likely originated from a local source near Riverside and downwind of Mira Loma.

The appearance of new particle types indicates the evolution of the particles and/or the appearance of new particle types from local sources. The Mira Loma site showed particle spectra with elemental carbon peaks, indicating local diesel traffic in the area was a significant PM source. The contribution from soil dust increased as the air mass moved inland. The Riverside particles are richer in ammonium and nitrate than any of the other sites. The percent of particles that fall into each cluster at each site can be assigned. Overall, about 97 % of the particles from each site were matched to the combined set of 57 clusters created from Diamond bar, Mira Loma, and Riverside data (listed in Table 5.2). The result of matching particles at each site to the combined set is shown in Figures 5.10, 5.11, and 5.12. The top clusters in Diamond Bar include clusters 1-6. For Mira Loma, clusters 1, 3, 11, 14, 18, 20, and 25 were the most common. Based on unscaled numbers of particles (which favors the super- μm size mode), over 40% of the detected particles in Riverside were classified into sea salt cluster 3, followed by 5 and 1 (other sea salt variations). Also popular were clusters 14, 17, 21-22, and 43-46. Cluster 14 is potassium-rich and clusters 43-45 are ammonium nitrate-rich (see Table 5.2 for details on classes).

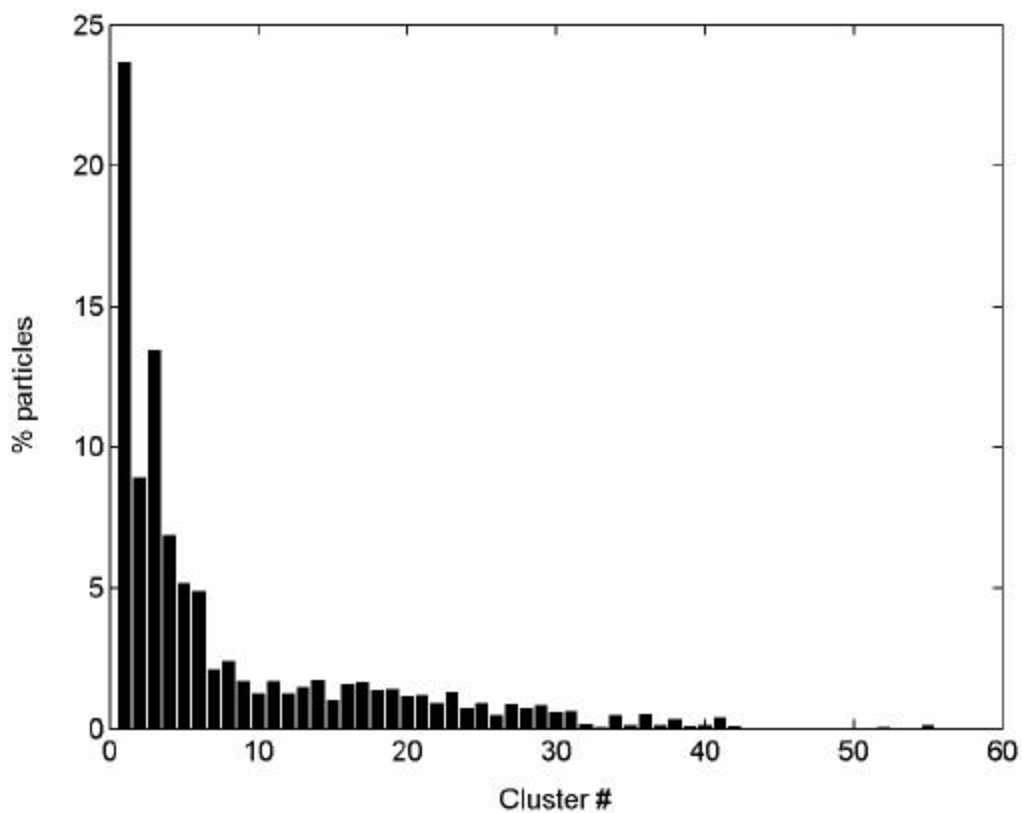


Figure 5.10: Percent of particles per class, identified by ART-2a (positive ion, vigilance 0.7, from ATOFMS data sampled in Diamond Bar, Mira Loma, and Riverside, CA for trajectory-matched times). Particles sampled in Diamond Bar, CA September 27, 1997 11:00 – September 29, 1997 14:00.

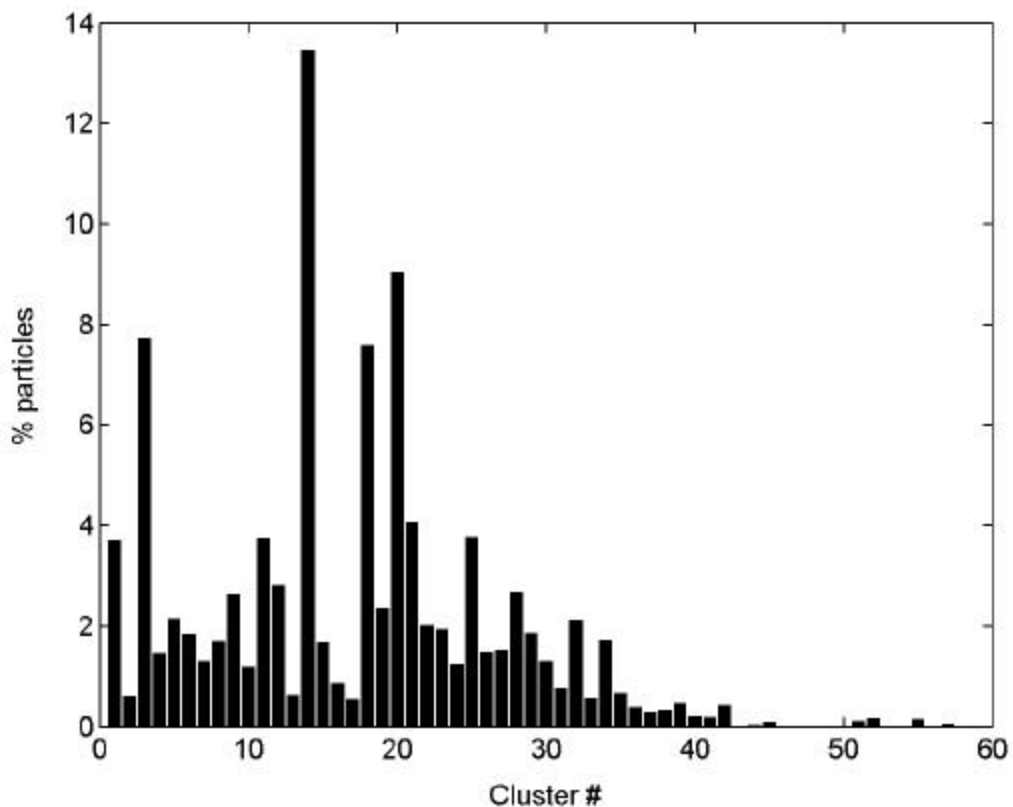


Figure 5.11: Percent of particles per class, identified by ART-2a (positive ion, vigilance 0.7, from ATOFMS data sampled in Diamond Bar, Mira Loma, and Riverside, CA for trajectory-matched times). Particles sampled in Mira Loma, CA September 27, 1997 15:00 – September 29, 1997 19:00.

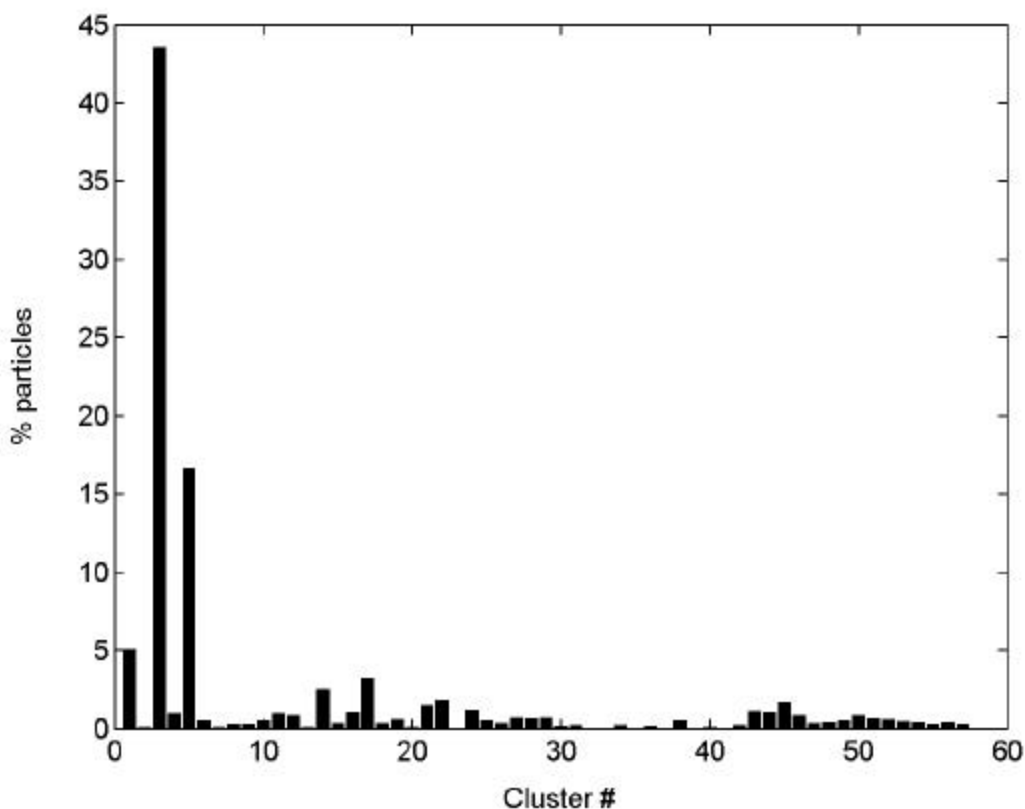


Figure 5.12: Percent of particles per class, identified by ART-2a (positive ion, vigilance 0.7, from ATOFMS data sampled in Diamond Bar, Mira Loma, and Riverside, CA for trajectory-matched times). Particles sampled in Riverside, CA September 28, 1997 00:00 – September 28, 1997 24:00.

As discussed in Chapter 3, the matched results can be considered with a size break at 1 μm . To visualize the changes in the percent of particles that match each class as the air mass moves inland, Figures 5.13-5.16 compare the matching results between two sites. The y-axis is the difference in percent of particles per class. The classes with positive-going bars are more prevalent at the site listed in the upper portion of the plot compared to the site listed in the lower portion. The distinguishing characteristics of the sub- μm particles show a general trend from Diamond Bar to Mira Loma to Riverside of organic carbon- to elemental carbon- to ammonium nitrate-rich organic carbon, respectively. The distinguishing characteristics of the super- μm particles show a general trend from Diamond Bar to Mira Loma to Riverside of sea salt types (classes 1 and 2) to potassium-rich and elemental carbon particle types to reacted sea salt (classes 3 and 5).

It is interesting to see how the particle types vary over time. The temporal profiles of clusters 1 and 10 in Diamond Bar are shown in Figure 5.17. Cluster 1 is a sea salt particle type with nitrate, 10 is an organic carbon type. Consistent with other figures in this report, the number of detected organic-carbon type particles builds when the air stagnates as indicated by the lower sea salt contributions.

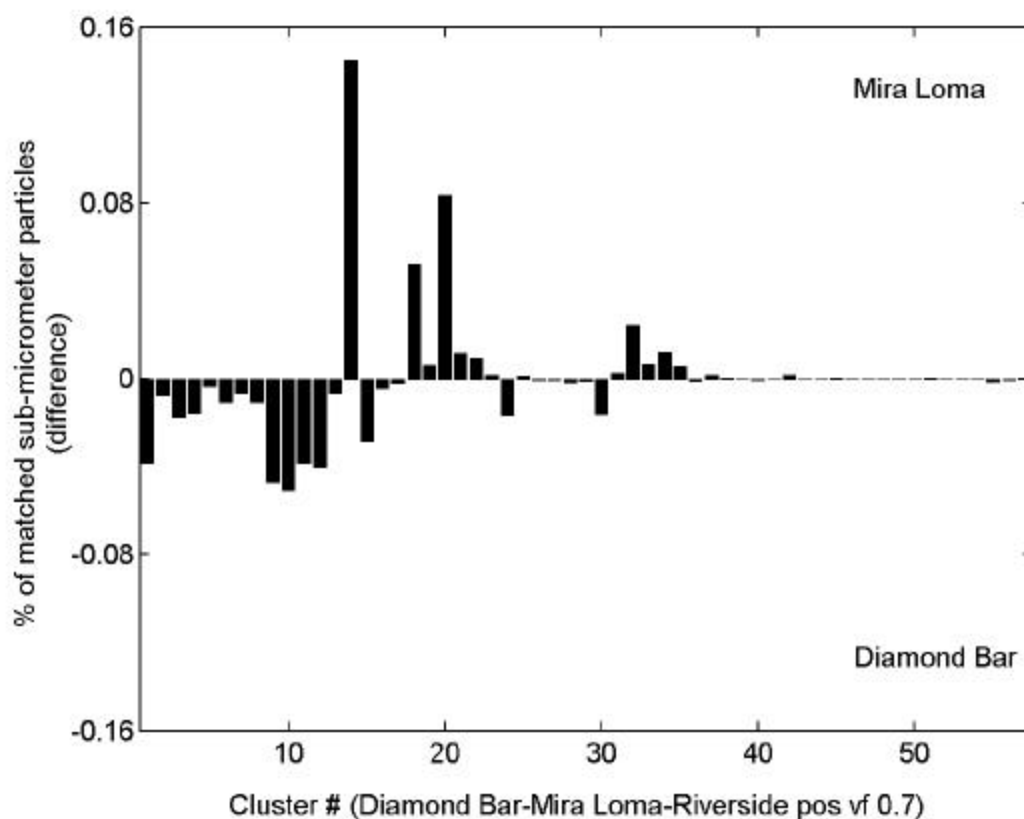


Figure 5.13: Difference in the fraction of sub- mm particles matched per class, identified by ART-2a (y-axis is Mira Loma minus Diamond Bar; classes generated from Diamond Bar, Mira Loma, and Riverside, CA for trajectory-matched times, positive ion, vigilance 0.7). Particles sampled by the ATOFMS in Mira Loma and Diamond Bar, CA on August 27-29, 1997 (see Table 5.1 for time ranges at each site).

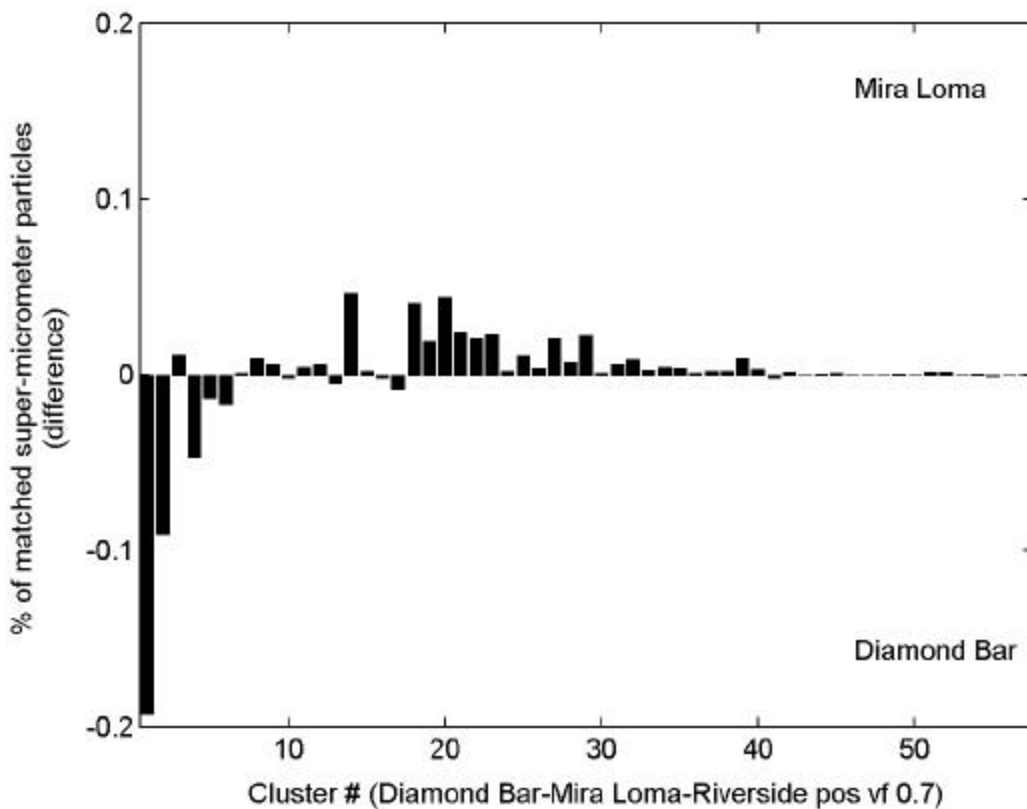


Figure 5.14: Difference in the fraction of super- mm particles matched per class, identified by ART-2a (y-axis is Mira Loma minus Diamond Bar; classes generated from Diamond Bar, Mira Loma, and Riverside, CA for trajectory-matched times, positive ion, vigilance 0.7). Particles sampled by the ATOFMS in Mira Loma and Diamond Bar, CA on August 27-29, 1997 (see Table 5.1 for time ranges at each site).

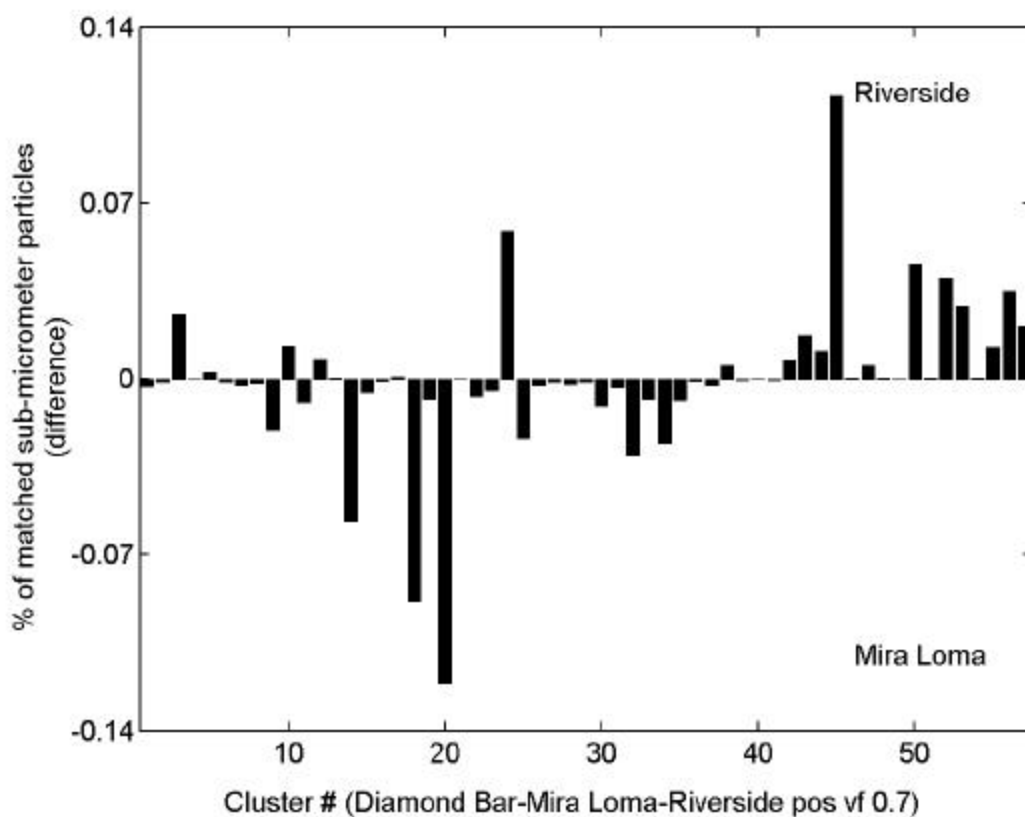


Figure 5.15: Difference in the fraction of sub- mm particles matched per class, identified by ART-2a (y-axis is Riverside minus Mira Loma; classes generated from Diamond Bar, Mira Loma, and Riverside, CA for trajectory-matched times, positive ion, vigilance 0.7). Particles sampled by the ATOFMS in Riverside and Mira Loma, CA on August 27-29, 1997 (see Table 5.1 for time ranges at each site).

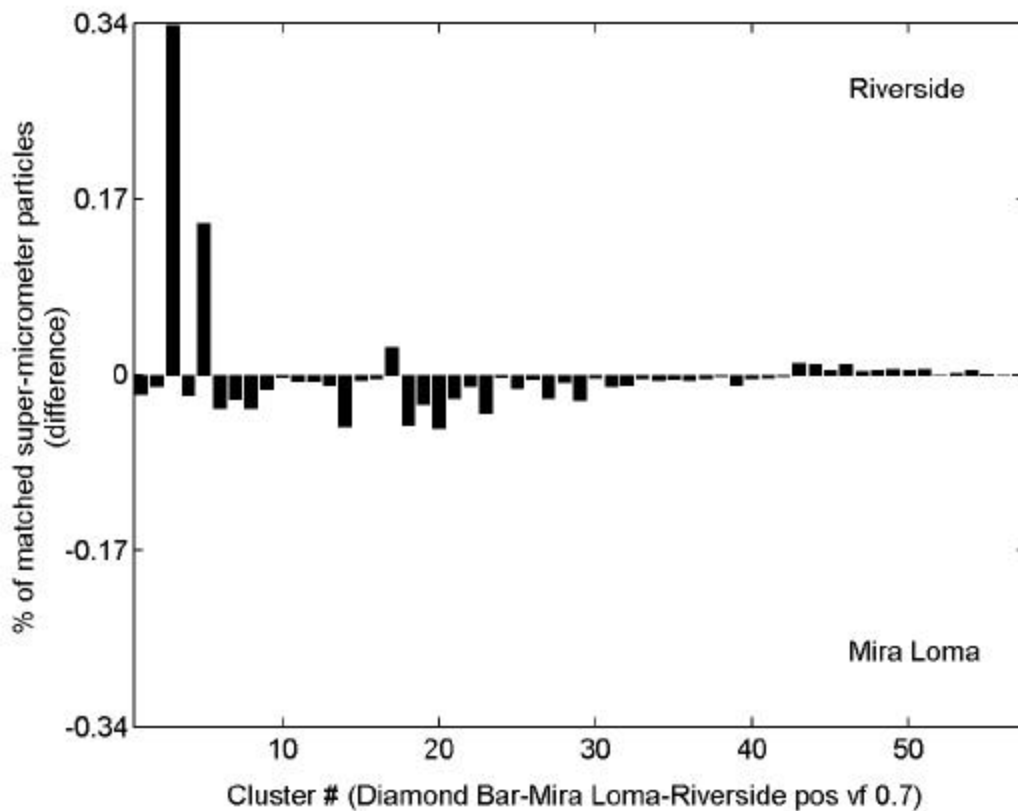


Figure 5.16: Difference in the fraction of super- mm particles matched per class, identified by ART-2a (y-axis is Riverside minus Mira Loma; classes generated from Diamond Bar, Mira Loma, and Riverside, CA for trajectory-matched times, positive ion, vigilance 0.7). Particles sampled by the ATOFMS in Riverside and Mira Loma, CA on August 27-29, 1997 (see Table 5.1 for time ranges at each site).

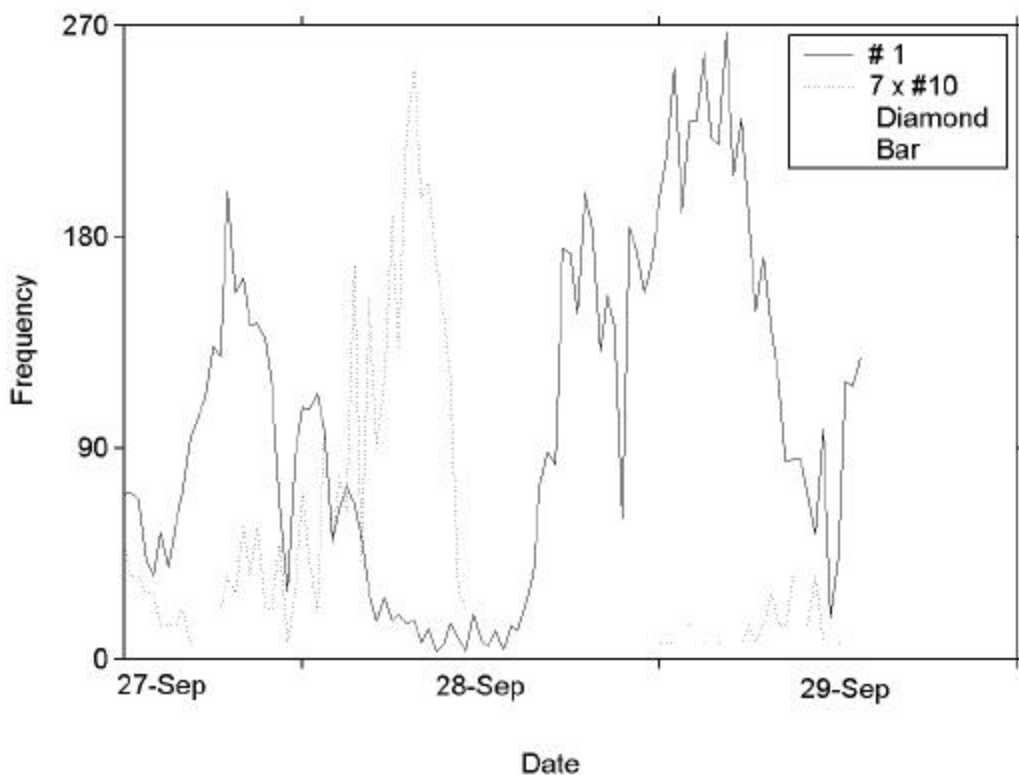


Figure 5.17: Times series plots of ATOFMS data from Diamond Bar, CA. Particles matched to ART-2a sea salt cluster 1 and elemental-carbon class 10 (vigilance, 0.7; learning 0.05; 40 iterations, classes generated from Diamond Bar, Mira Loma, and Riverside data). ATOFMS data displayed with 30-min resolution.

5.3.3 Particle Transformations in Diamond Bar, Mira Loma, and Riverside during Trajectory 3

To examine the changes in the particle composition within an air mass, the back-wind trajectory data were used to determine the path of the air masses of interest. One air mass that crossed reasonably close to the sites of interest arrived in Riverside during September 29, 1997 13:00-15:00. The air mass had passed near Mira Loma during September 28 17:20-21:50 and Diamond Bar during September 28 13:00-16:00. The trajectory (trajectory 3) begins with a relatively clean air mass in Diamond Bar. The time of origin in Diamond Bar is between the morning spike of cluster 10 and the afternoon spike of cluster 1 (see Figure 5.17). It passed quickly to Mira Loma and stagnated before reaching Riverside. The air mass should have already been enriched with the ammonia from the agricultural Mira Loma area before stagnation because it already passed through the Mira Loma site before it stagnated.

The particles from each site during trajectory 3 times were matched to the combined set of classes generated (listed in Table 5.2). Figure 5.18 summarizes the fraction of particles matched

per class at each of the three sites. Figure 5.19 shows the difference in the fraction of particles matched per class between pairs of sites.

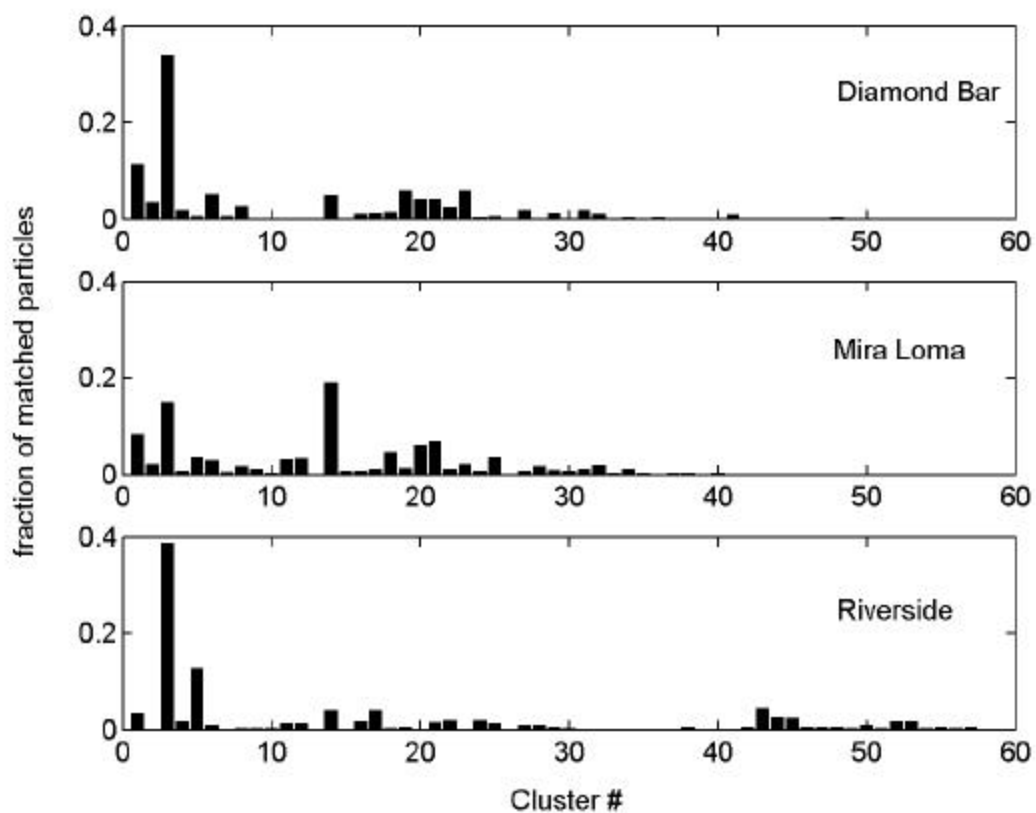


Figure 5.18: Fraction of particles matched per class, identified by ART-2a (classes generated from Diamond Bar, Mira Loma, and Riverside, CA for trajectory-matched times, positive ion, vigilance 0.7). Particles sampled by the ATOFMS in Mira Loma and Diamond Bar, CA on August 28-29, 1997 (trajectory 3 times).

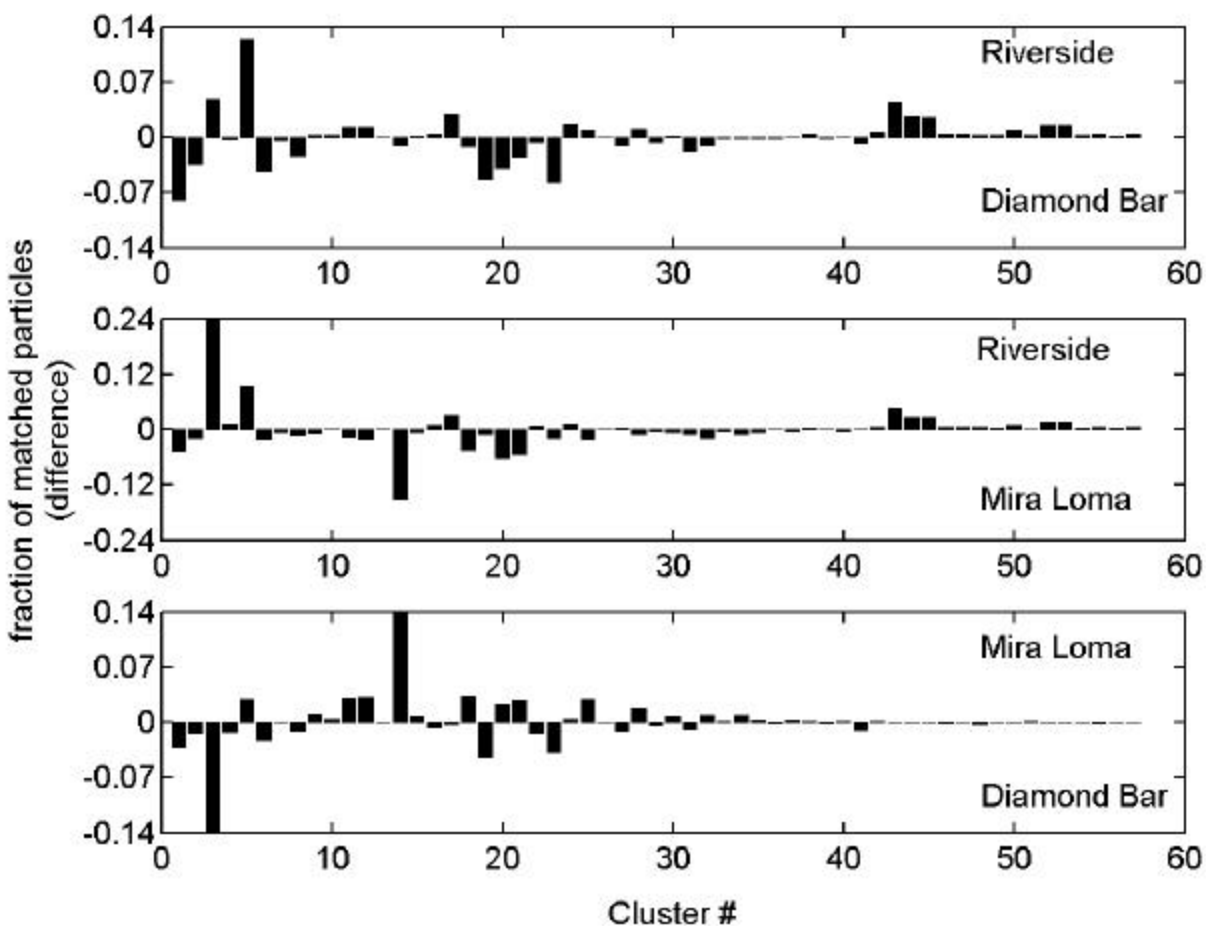


Figure 5.19: Difference in the fraction of particles matched per class, identified by ART-2a (classes generated from Diamond Bar, Mira Loma, and Riverside, CA for trajectory-matched times, positive ion, vigilance 0.7). Particles sampled by the ATOFMS in Mira Loma and Diamond Bar, CA on August 28-29, 1997 (trajectory 3 times).

These plots demonstrate that as the trajectory 3 air mass traveled across the region, the particle composition changed. Table 5.3 lists the favored classes at each site, based on Figure 5.19. The weight vector (class composition) data in Table 5.2 provides an indication of important peaks. The weight vectors for the favored classes at each site are provided in Figures 5.20-5.22. Overall, the Diamond Bar mass spectra show sodium- and potassium-rich particles, Mira Loma mass spectra show more elemental carbon envelopes in the particle mass spectra, and Riverside mass spectra show more ammonium and nitrate coated on organic carbon particles. The individual weight vectors show a representation of the favored classes at each site (use Table 5.2 as a guide to identify the m/z of each peak).

Table 5.3: List of the characteristic particle classes from trajectory 3 sampling times for each site.

Favored Classes (top 8)	Sampling Location	ATOFMS instrument
3, 5, 17, 43, 44, 45, 52, 53	Riverside	lab-based (BST)
6, 14, 18, 20, 21, 25, 28, 32	Mira Loma	transportable (ELD)
1, 2, 6, 8, 19, 22, 23, 41	Diamond Bar	transportable (JKE)

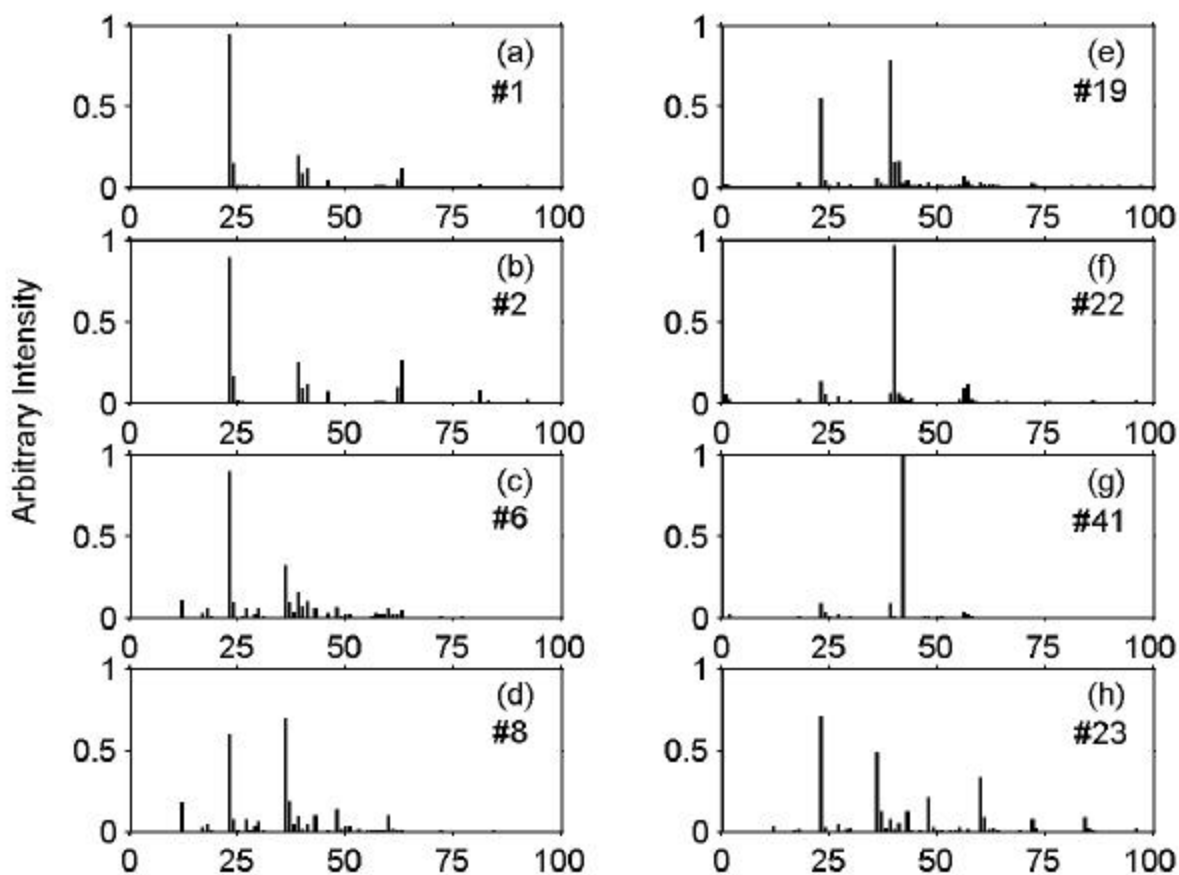


Figure 5.20: Normalized weight vectors for favored particle classes detected in Diamond Bar trajectory 3. Classes were identified by ART-2a, generated from Diamond Bar, Mira Loma, and Riverside, CA for trajectory-matched times, positive ion, vigilance 0.7.

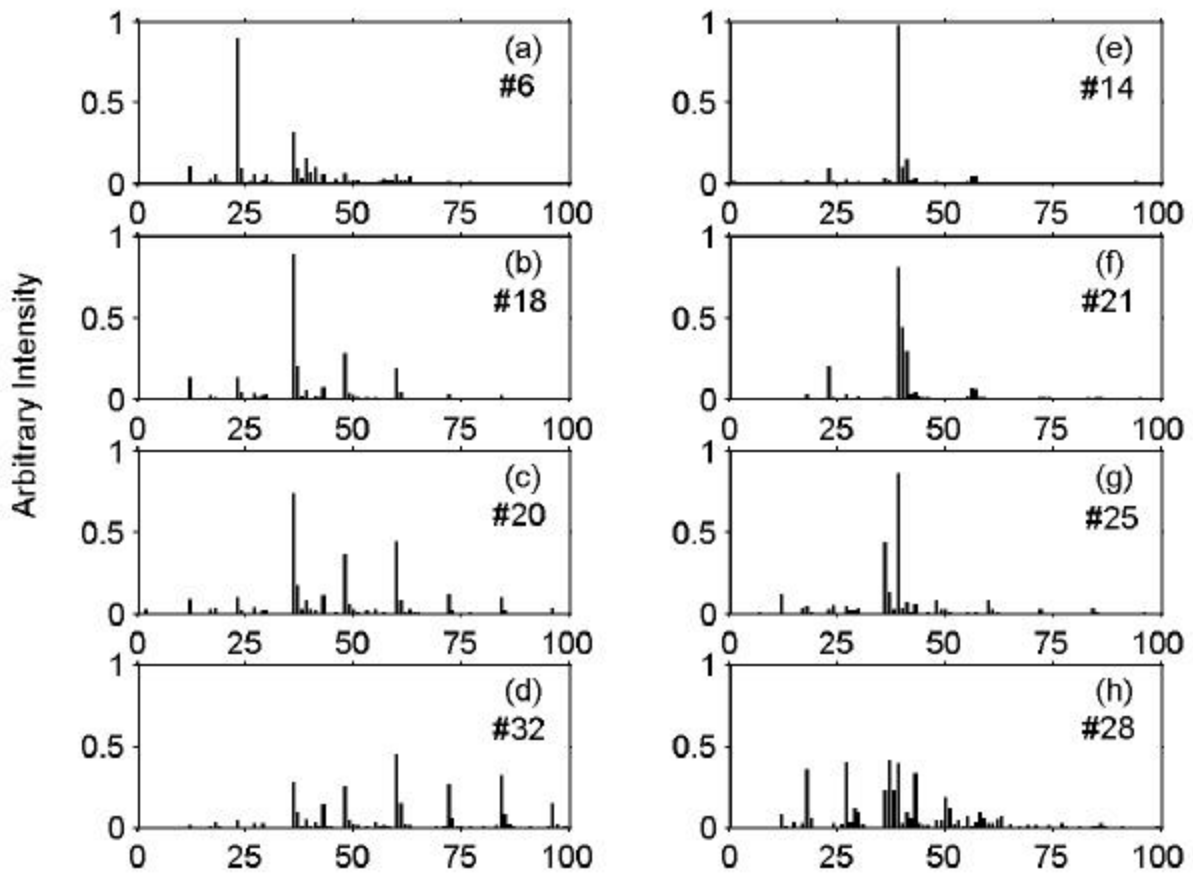


Figure 5.21: Normalized weight vectors for favored particle classes detected in Mira Loma trajectory 3. Classes were identified by ART-2a, generated from Diamond Bar, Mira Loma, and Riverside, CA for trajectory-matched times, positive ion, vigilance 0.7.

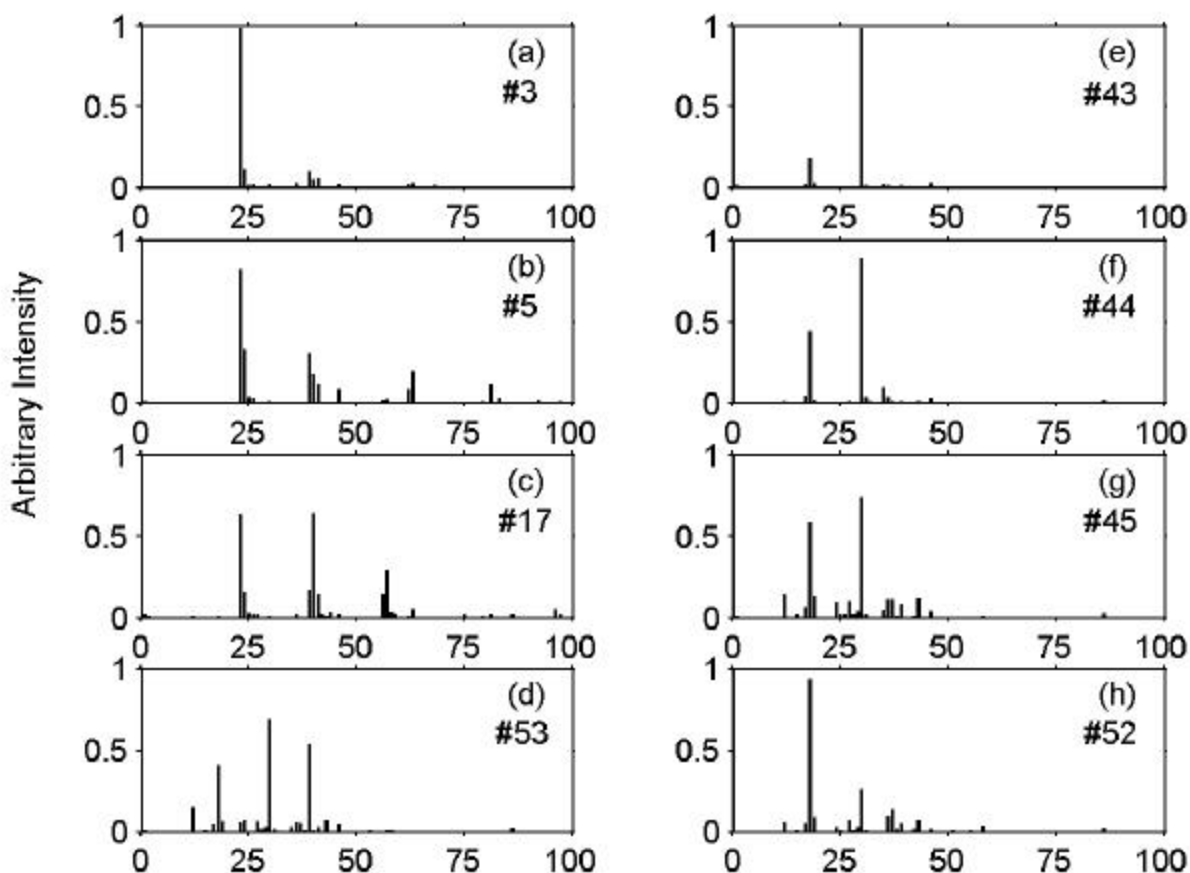


Figure 5.22: Normalized weight vectors for favored particle classes detected in Riverside trajectory 3. Classes were identified by ART-2a, generated from Diamond Bar, Mira Loma, and Riverside, CA for trajectory-matched times, positive ion, vigilance 0.7.

5.4 Conclusions

This chapter began by examining the size and composition of particles in Mira Loma, CA during September 27-29, 1997, using the size distribution and digital mass spectra of sub- and super- μm particles. The particles were matched to the classes generated in Chapter 2 and the temporal trends of contrasting classes were examined. The temporal trends of the super- μm sea salt particles and sub- μm particles were anti-correlated for the period September 27-29, 1997 in Mira Loma.

The Diamond Bar-Mira Loma-Riverside trajectory was considered. The air masses arriving in Riverside during September 28-29, 1997 were traced back to determine the times when they had been present at the sampling sites in Diamond Bar and Mira Loma. These trajectory-matched times for all three sites were used to create classes using a neural network. The resulting 57 classes (Appendix O) were used to classify the particles at each site. The temporal trends of clusters 1 and 10 in Diamond Bar were presented. The temporal profile of

these chemically/source contrasted particle types shows how the air mass movement patterns strongly affects the particle population in a given location. Stagnation leads to the accumulation of certain organic carbon particle types (cluster 10), and the movement of the fresh air masses brings sea salt particles inland (cluster 1), leading to an immediate reduction of the carbon particle types. The particle types in one air parcel trajectory that passed through the three sampling sites were examined (trajectory 3). The fraction of particles in each class at each site was presented along with the chemical differences between sites. The composition (weight vector) of the favored classes for each site clearly shows the particles at each site were quite distinct. The single particle mass spectra sampled from the trajectory 3 air mass show substantial contributions from ammonium and nitrate when the particles arrive in Riverside. The spectra dominated by ammonium and nitrate detected in Riverside were not observed in Mira Loma. This suggests a number of possible explanations: 1) a certain period of time is required between the time of enrichment of the air mass with gas-phase ammonia and the observation of particle-phase ammonium by ATOFMS, 2) the site could have been nitric acid limited and thus unable to form ammonium nitrate in the particles, 3) meteorology must change such as higher relative humidity and/or lower temperatures through day/night cycling to promote partitioning of ammonia and nitric acid from the gas to particle phase. The observed enrichment of the ambient air in Mira Loma with elemental carbon particles shows a major influence of diesel truck activity in this area.

A great deal of insight was provided into possible particle sources and chemistry in three spatially distinct regions by comparison of the particle types observed at these 3 sites. However, the comparison is limited by the fact that only single polarity spectra were compared since the Riverside instrument could only detect one polarity of ions. It is quite possible, more particle types would be present (as demonstrated in the ART-2a analysis of vehicles in Chapter x) and different sources and chemistry would be more obvious with the addition of negative ion spectra. This study suggests a follow-up trajectory study using three dual polarity instruments along a common trajectory would provide even further information on sources and chemistry in the region.

Chapter 6

Trends in Riverside Aerosol

6.1 Introduction

The previous chapters focus on ATOFMS data taken during short time periods at various sites during the SCOS97-NARSTO study. In general, this report captures highlights from an enormous amount of data collected by the ATOFMS instruments during this study. This chapter illustrates trends within a nearly continuous dataset acquired in Riverside between August 19, 1997 and September 27, 1997, containing over one million mass spectra. The particle composition is compared to the classes generated in Chapter 2 for ambient Riverside data (vigilance 0.5). In addition, the particle composition will be compared to the classes generated by car and diesel vehicle exhaust studies (vigilance 0.5). Size and composition trends will be presented and summarized.

6.2 Experimental methods

As discussed in Section 2.3, ATOFMS was used to characterize individual ambient aerosol particles. The data are calibrated for size and the time axes are converted to m/z (see Section 2.2) and compiled in the YAADA database. In this chapter, the existing Riverside clusters detailed in Chapter 2 have been incorporated in this analysis. Matching ambient particles from this longer dataset from Riverside will indicate which ambient particles have compositions similar to the particles from Riverside during the time discussed in Chapter 2.

6.3 Results and Discussion

6.3.1 Composition and Size Characteristics of Ambient Riverside Particles

Upon matching the ambient Riverside particles from this large dataset to the clusters previously created in Chapter 2, a total of 1,112,927 of the 1,141,941 particles were classified (over 97%). This indicates that the composition over the 40-days was similar to the smaller subset of data used to create the classes, August 21-23 time in Riverside (see Chapter 2). The most common particle type remained the sea salt class due to the fact this analysis was performed on unscaled ATOFMS data which shows a size bias towards larger particle sizes. Figure 6.1 shows the results of the matching process.

The relatively high sea salt particle number counts make it difficult to judge the frequency of the other classes, so the information for clusters 4-20 is displayed with a zoomed-in x- and y-axes in Figure 6.2. The more populated clusters include potassium-rich dust clusters 5, 7, and 9, soil dust cluster 10, and calcium-rich cluster 6. Vanadium-rich cluster 14 is the least popular cluster and shows a major diurnal trend, appearing each day in relatively short time bursts around noon. The trends for this particle type track the ammonium nitrate particle types, suggesting this particle type may be power plant related.

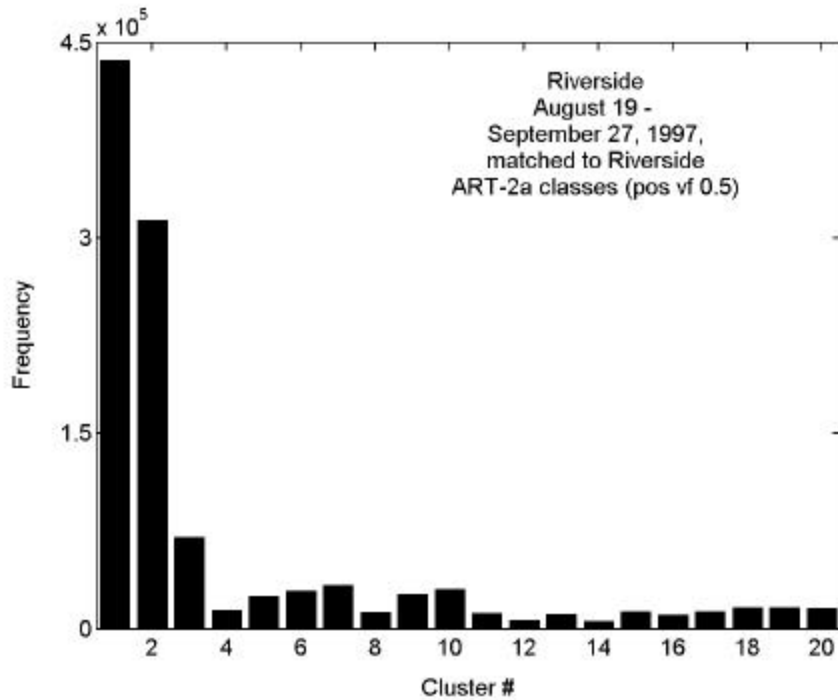


Figure 6.1: Number of particles per class, identified by ART-2a generated from August 21-23 in Riverside. Particles sampled in Riverside, CA August 19 - September 27, 1997.

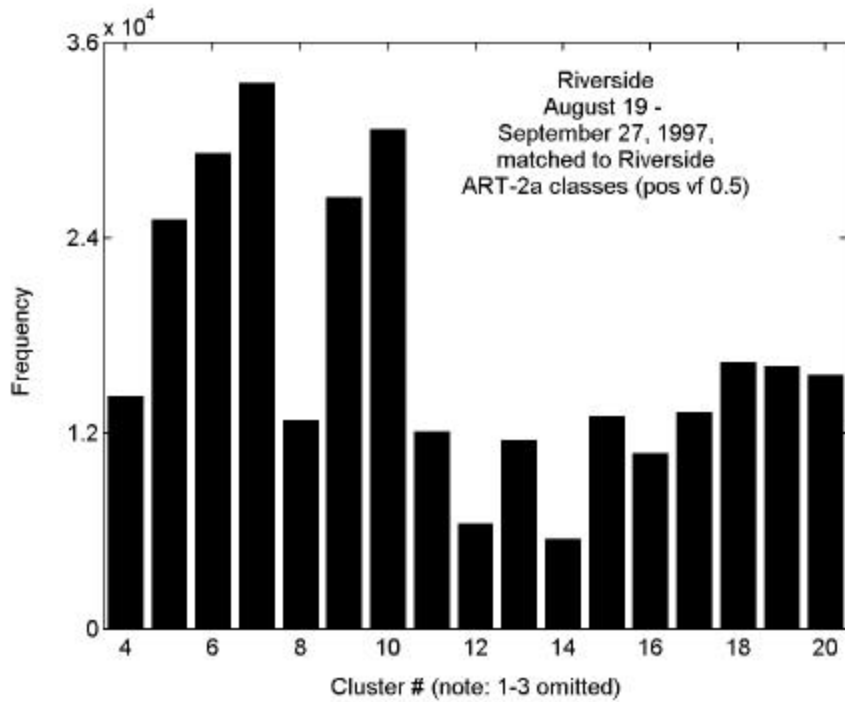


Figure 6.2: Number of particles per class, identified by ART-2a generated from August 21-23 in Riverside. Particles sampled in Riverside, CA August 19 - September 27, 1997.

The particle size distributions for the period between August 19-September 27, 1997 in Riverside displayed a bimodal shape with a break around 1 μm . Figure 6.3 shows the size distributions for all days (August 19-September 27) with 12-hour resolution (the data are plotted for midnight to noon, and noon to the following midnight each day). During the average 12-hour period, 13,824 particles were analyzed. The distribution obtained from noon to midnight on August 24, 1997 was omitted because the instrument was offline most of the time. It is not important to note which 12-hour period corresponds to each distribution but rather to observe, as a whole, the particle size trends. The average size distribution is included in Figure 6.3. For comparison, the same information for the period discussed in Chapter 2, August 21-23, 1997, is plotted in Figure 6.4.

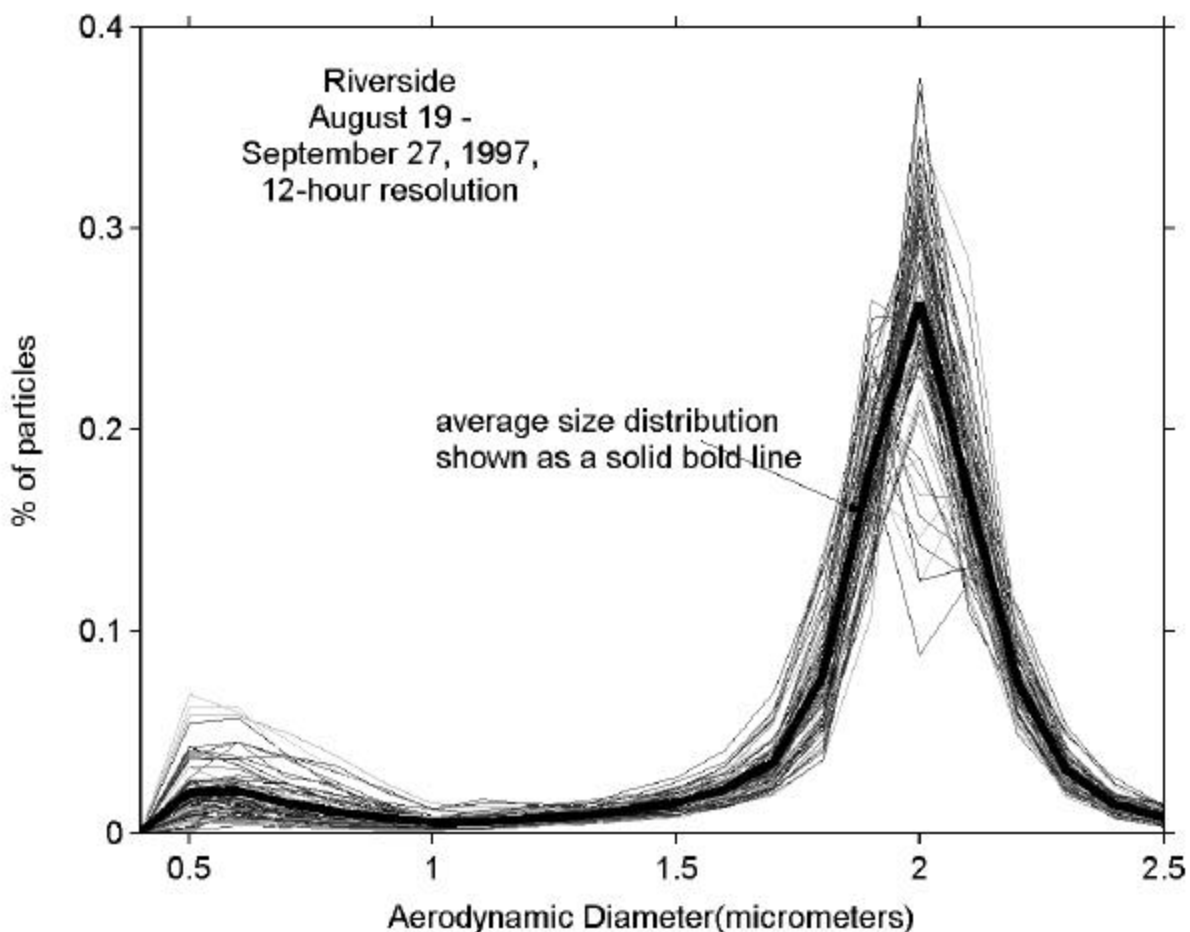


Figure 6.3: Size distribution plots for particles sampled in Riverside, CA August 19 - September 27, 1997. Size resolution is 0.1 mm; each line represents data from a 12-hour period.

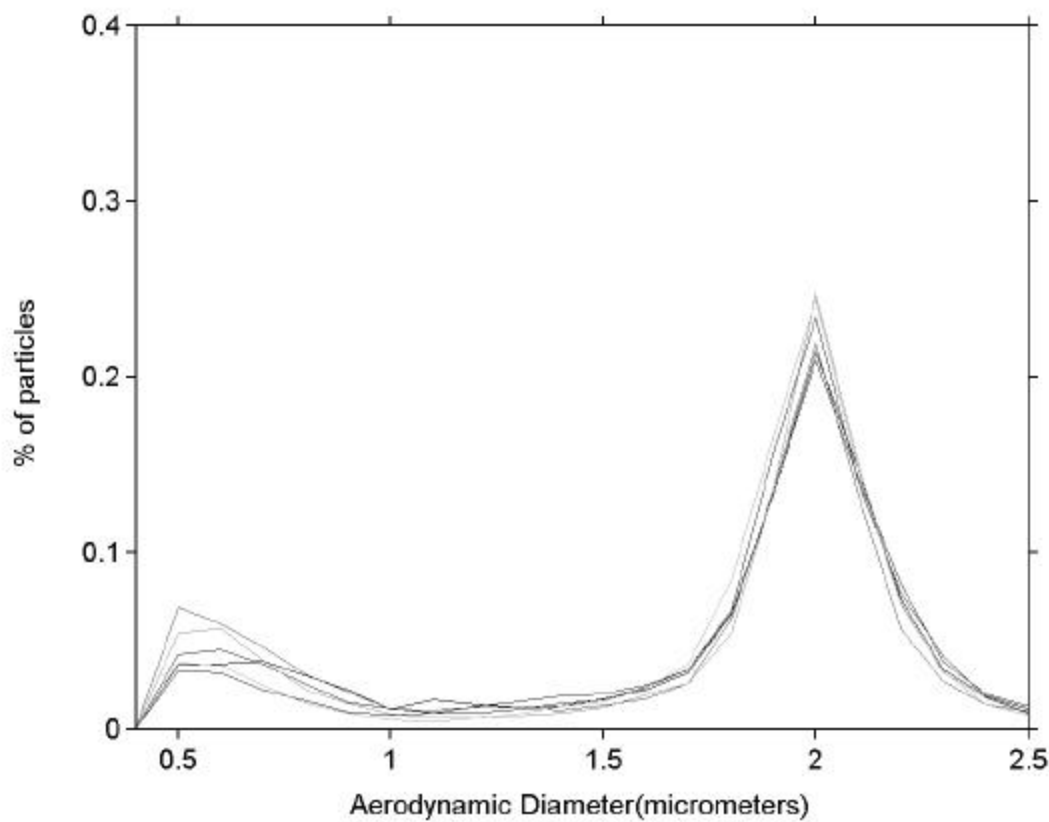


Figure 6.4: Size distribution plots for particles sampled in Riverside, CA August 21-23, 1997. Size resolution is 0.1 mm; each line represents data from a 12-hour period. No corrections have been made for offline time (shapes may be compared but intensity should not).

6.3.2 Temporal Trends of Riverside Particle Classes

Appendix Q shows the temporal profiles for the top 20 classes. The long-term temporal trends of major particle types detected during this study were determined. For example, the ammonium-nitrate-organic-carbon cluster 8 particles showed interesting temporal trends for August 21-23 (see Chapter 2 for details) and now with the larger dataset may be examined over a time period of more than 5 weeks. Trends in particle composition over extended periods of time (on relatively short time scales) will add a great deal of information to our existing knowledge of particle chemistry in the atmosphere.

The particles in this dataset that were matched to cluster 8, ammonium nitrate organic carbon particles, account for 1.2 % of the total number of matched particles in the period August 19 - September 27, 1997. Almost twenty percent (19.6 %) of the cluster 8 matched particles appear during August 21-23 (discussed in Chapter 2). As mentioned in Chapter 2, the afternoon episodes of August 21-23 were characterized by the increased presence of sub- μm , carbon-rich particles, especially ammonium-nitrate-organic carbon particles that correlated with increased ozone levels. Other days exhibit spikes indicating the appearance of ammonium nitrate organic carbon particles. From viewing these long term temporal figures, the relative significance of

these particle types over time can be determined. Figure 6.5 shows the temporal trend for cluster 8 with 3-hour resolution. The greatest number of cluster 8 particles in a single 3-hour period occurred on September 17, 1997 (17.0 % of total particles matched to cluster 8). The maximum ozone level for that September 17 was about 70 ppb and the maximum PM_{10} was about $50 \mu g m^{-3}$.

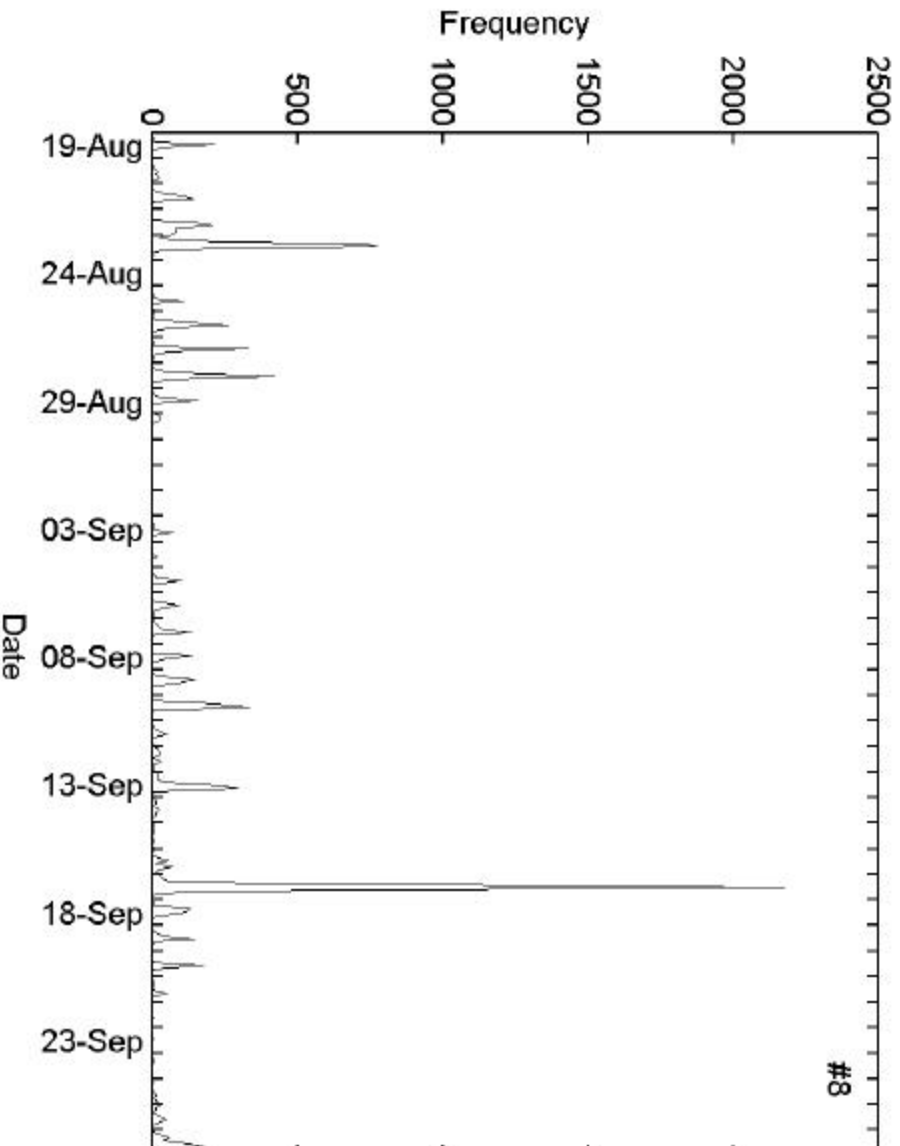


Figure 6.5: Time series plot for particles matched to cluster 8 – organic carbon with ammonium nitrate I. Temporal resolution is 3 hours for the single particle data.

The particles on September 17, 1997 showed a typical bimodal size distribution commonly detected by the ATOFMS during these studies, although the large mode dominates the overall size distribution (Figure 6.6). When the particles are matched to the existing Riverside clusters, clusters 8 and 13 become apparent (Figure 6.7).

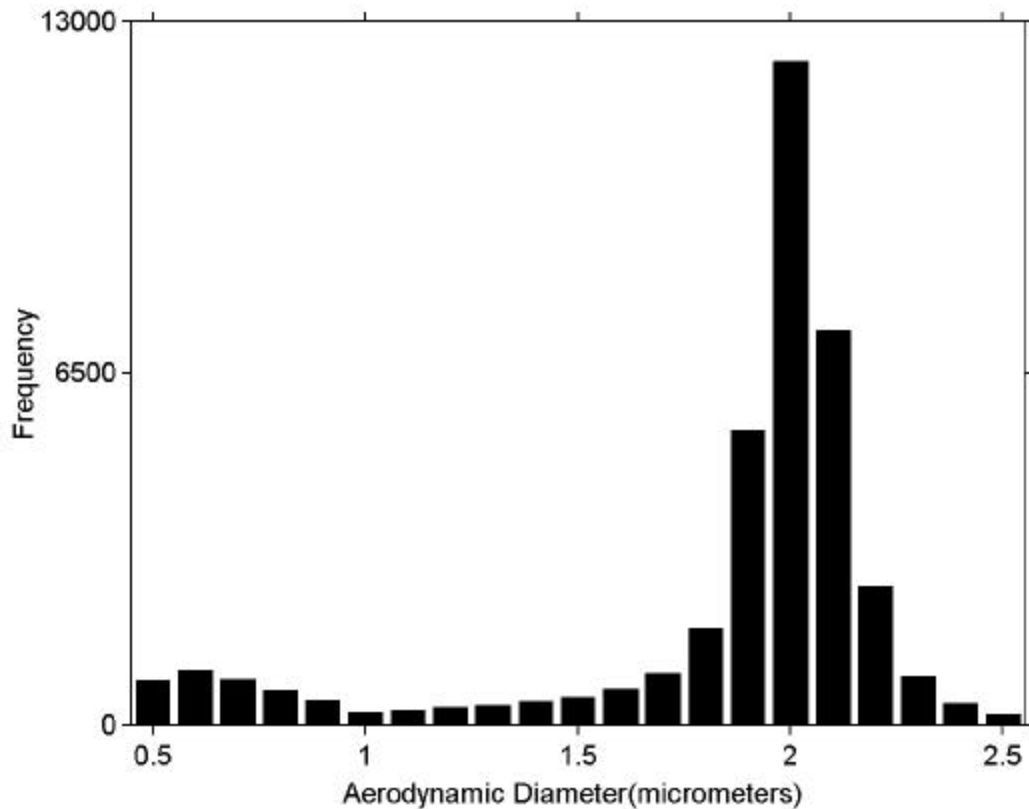


Figure 6.6: Size distribution plot for the particles sampled in Riverside, CA September 17, 1997

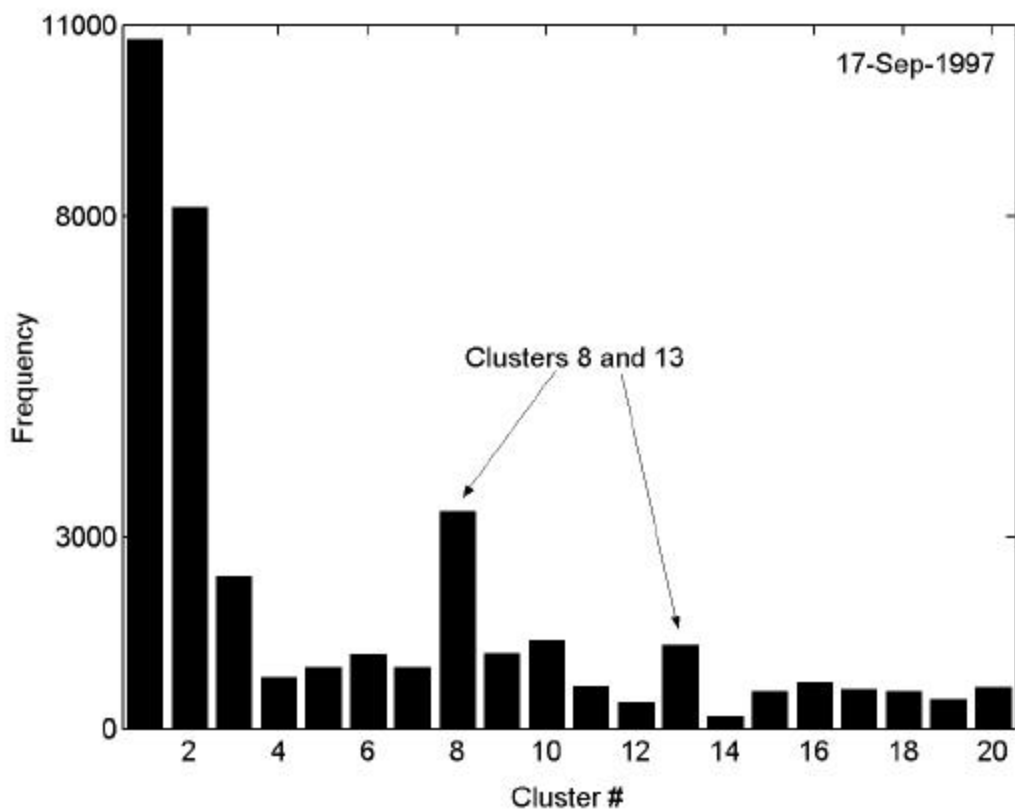


Figure 6.7: Number of particles matched to ART-2a classes (vigilance, 0.5; learning 0.05; 20 iterations, classes generated from Riverside data). Particles sampled by the ATOFMS in Riverside, CA on September 17, 1997.

Cluster 13 is another ammonium nitrate carbon particle type. The particles in this dataset that were matched to 13 account for 1.0 % of the total matched particles. During the period August 21-23, 14.3 % of the particles matched cluster 13. The two ammonium nitrate organic carbon classes (8 and 13) can be compared to determine whether they follow a similar temporal pattern, which would be expected based on the August 21-23 data (see Section 2.3.4). The temporal profile for particles matching cluster 13 is plotted in Figure 6.8 (3-hour resolution). A trend similar to that observed for particles in cluster 8 is observed for particles matching cluster 13. An episode of these particles also occurs on September 17, 1997, although not as pronounced as the peak in cluster 8.

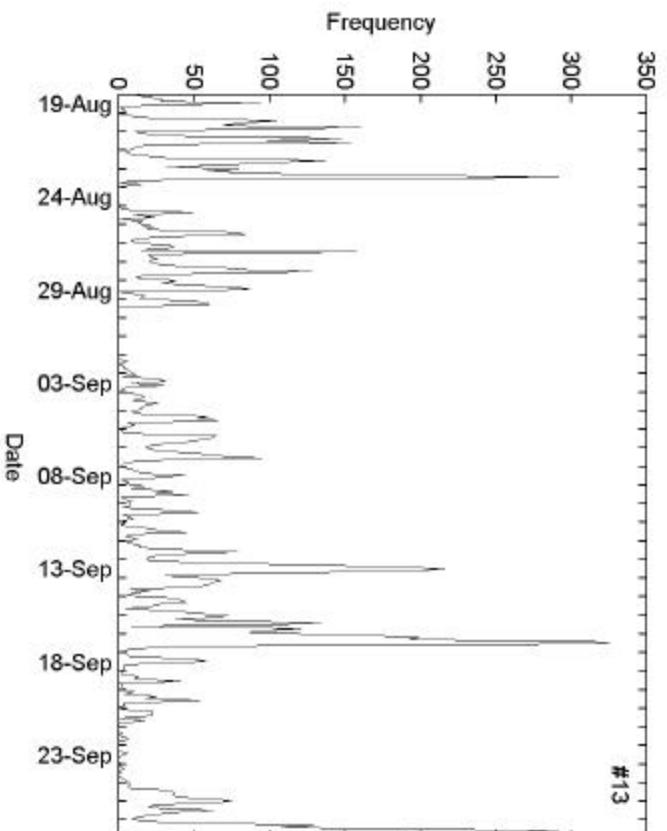


Figure 6.8: Time series plot for particles matched to cluster 13 – organic carbon with ammonium nitrate II. Temporal resolution is 3 hours for the single particle data.

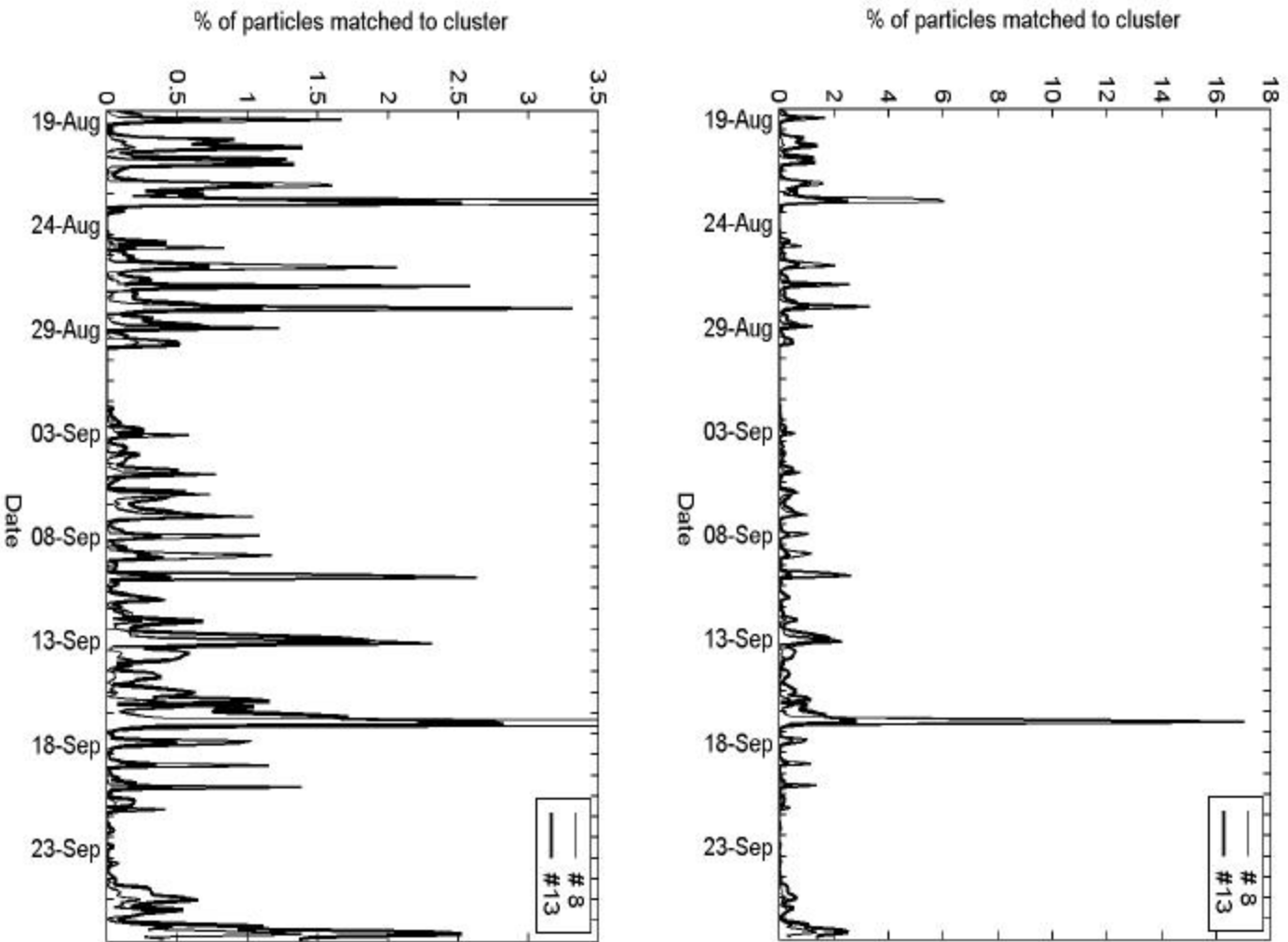


Figure 6.9: Time series plots for particles matched to organic carbon with ammonium nitrate clusters 8 and 13. Temporal resolution is 3 hours for the single particle data. The lower plot has a “zoomed-in” y-axis.

The temporal profiles of particles matching clusters 8 and 13 are plotted together in Figure 6.9. The y-axis has been changed from “frequency” to “% of matched particle to cluster” so both temporal trends more evident. The timing of the peaks is very similar. To investigate the apparent diurnal temporal pattern with clusters 8 and 13. The data from the same time bins on each of the 40 days were averaged. The particles in clusters 8 and 13 displayed a distinct diurnal pattern with a maximum between 12:00-15:00.

To increase the temporal resolution, the particles were divided in 30-min time bins. The percent of particles matched to each cluster per time bin per day was calculated. The average over the 40 days was calculated. The total percent for all 48 time-bins is 100% and the percent per bin would be 2.08 % if the particles were randomly distributed throughout the different time bins of each day. Instead the bins had a range of values with the highest percent for clusters 8 and 13 in the 13:30-14:00 time bin (Figures 6.10 and 6.11). The average percent of particles matched to cluster 8 for the 13:30-14:00 time bin per day was 10.74 %, and for cluster 13, 6.19 %. The time bins on either side of the maximum are appropriately increasing and then decreasing. The peaks in clusters 8 and 13 are observed in the early afternoon. The peak for cluster 8 particles is somewhat more narrow and intense. The peaks at m/z 18 and 30 have a greater relative intensity for cluster 8 than 13 (see Table 2.1 and Figure 2.2e-f). It appears that cluster 8 particles are only present at the peak of an ammonium nitrate episode. Cluster 13 particles appear to be a more general indicator of an ammonium nitrate episode, appearing slightly before and after cluster 8 particles. Coupling the real-time ATOFMS data acquisition to a real-time particle classification tool would provide a means for recognizing certain episodes immediately in the field. This type of “trigger” could be used, for example, to alert others to sample and capture specific events of interest with filter-based techniques. In the case of ammonium and nitrate, cluster 13 would predict the coming episode and cluster 8 would signify the center of the episode.

This 40-day-long single particle dataset from Riverside allows one to observed trends in particle composition, the regularity of the diurnal patterns, and the variability of magnitude. A better perspective is gained by examining this 40-day long period, in contrast to a few isolated IOP data points. Cluster 8 particles on September 13 and 17 appear as isolated spikes in the temporal profile while peaks on August 21-23, 25-28, and September 5-8 appear as sets of days with increasing peak frequency values (Figure 6.5). Having this wider perspective on the air quality with high resolution, these data can yield a broader understanding of the atmosphere and create regulations to control/minimize air pollution.

As mentioned in Chapter 2, the lab-based instrument was periodically switched to negative ion mode (these data were not considered for this investigation because the spectra are not directly comparable). The normal schedule of negative ion data acquisition can be seen in these plots. The times for negative ion mode will not have matches and generally include the time bins: 2:00-2:30, 5:00-5:30, 8:00-8:30, 11:00-11:30, 14:00-14:30, 17:00-17:30, and 20:00-20:30.

In general, ammonium nitrate organic carbon clusters (8 and 13) disappeared as sea salt clusters (1 and 2) appeared during August 21-23 (see Chapter 2). The peak and fall-off of the ammonium nitrate organic carbon cluster 8 (bars) are followed by the rise and peak (solid line) for the sea salt with nitrate cluster 2 (Figure 6.12). Similar temporal trends are consistently observed throughout the study. Some of the easiest times to pick out such trends include August 25-28.

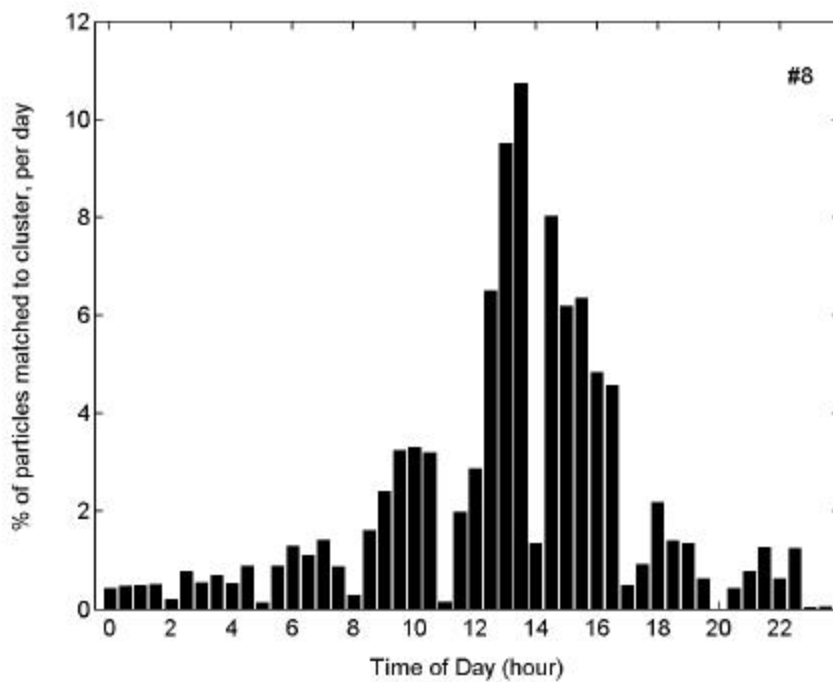


Figure 6.10: Time of day correlation plot for particles matched to organic carbon with ammonium nitrate cluster 8. Temporal resolution is 30 min for the single particle data.

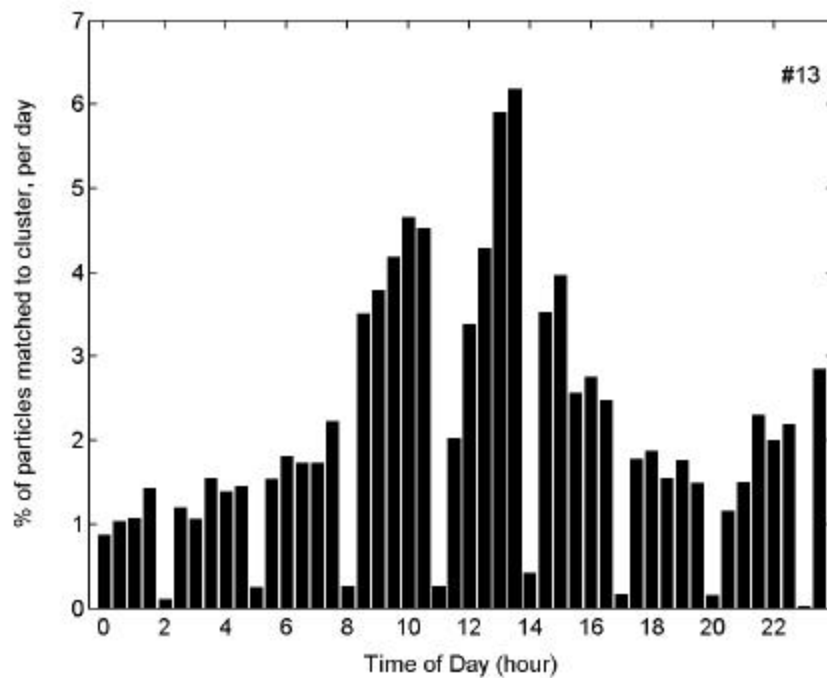


Figure 6.11: Time of day correlation plot for particles matched to organic carbon with ammonium nitrate cluster 13. Temporal resolution is 30 min for the single particle data.

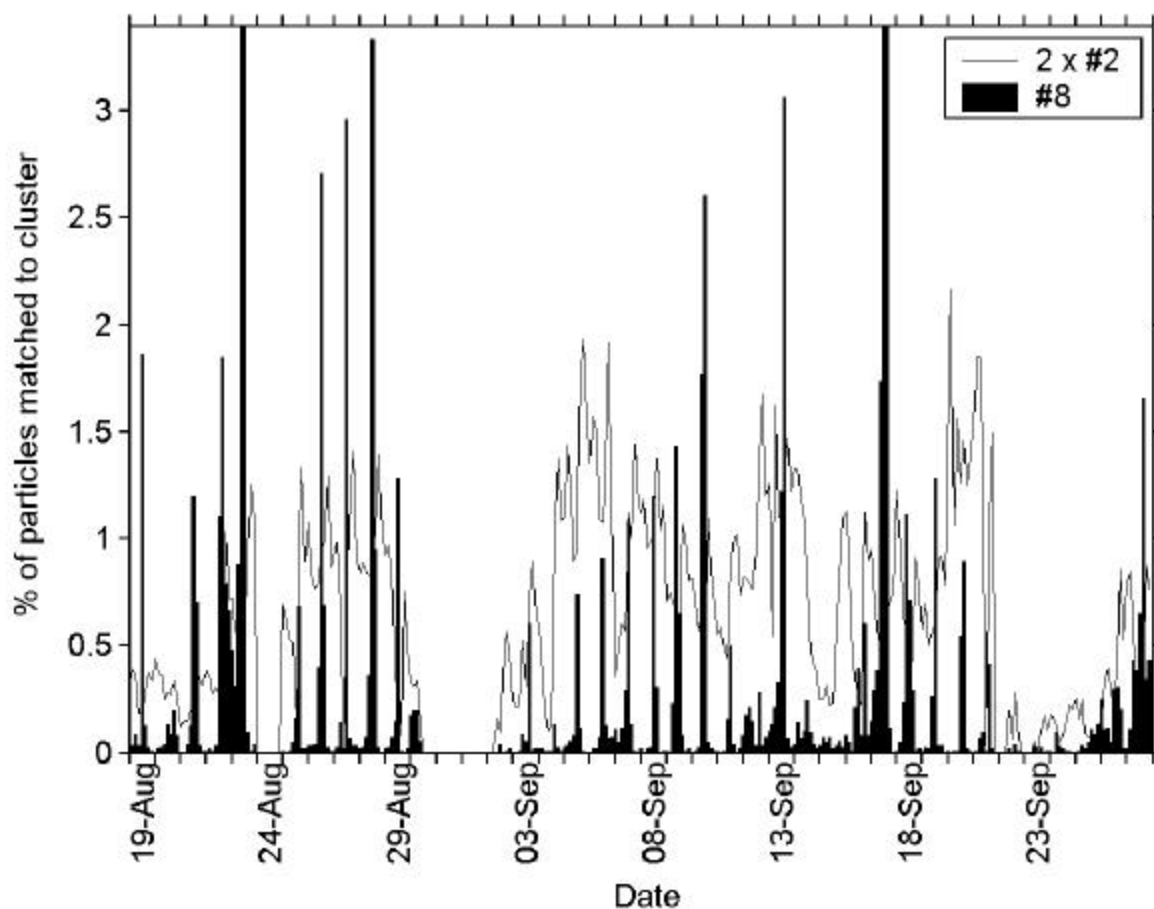


Figure 6.12: Time series plot for particles matched to sea salt with nitrate cluster 2 and ammonium nitrate organic carbon 8. Temporal resolution is 3 hours for the single particle data. Because the values for cluster 2 were multiplied by a factor of 2, the full height of the peaks for August 23 and September 17, 1997 extends beyond the y-axis limit of 3.4 %.

The particles in cluster 2, sea salt, were not randomly distributed throughout the day but instead displayed a diurnal peak with a maximum in the 18:00-21:00 time bin. These sea salt particles are transformed by NO_x reactions and represent a reacted form of sea salt. Ironically though, for the average day in Riverside during this period, the arrival of the air masses enriched with these particles mark the arrival of air masses with the shortest time over land. While the particles in this air mass are reacted, the air mass overall is among the cleanest to arrive in the inland site of Riverside. With the temporal resolution increased to thirty minutes per time bins, the time of day correlation for cluster 2 particles is shown in Figure 6.13. The highest value for clusters 2 was in the 18:30-19:00 time bin. The average percent of particles matched to cluster 2 in the 18:30-19:00 time bin is 3.81 %, almost twice the amount expected if the particles were distributed evenly over all 48 bins. One would expect 2.08 % ($100/48$) of the particles matched to the cluster to appear in each bin of the 48 30-minute time bins (or perhaps to be more generous, 2.44 % if you assume only 41 bins per day because approximately 7 bins per day do

not have positive ion data). Figure 6.13 is an inverse plot of time over land because the particles in cluster 2 are associated with short time over land.

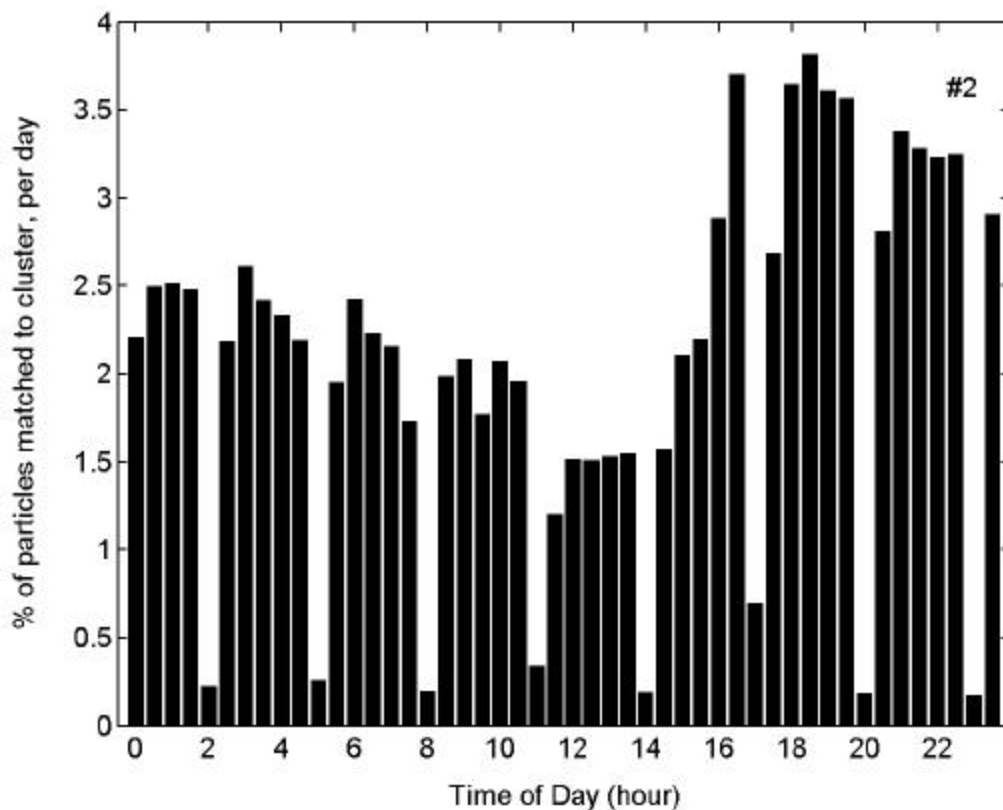


Figure 6.13: Time of day correlation plot for particles matched to sea salt with nitrate cluster 2. Temporal resolution is 30 min for the single particle data.

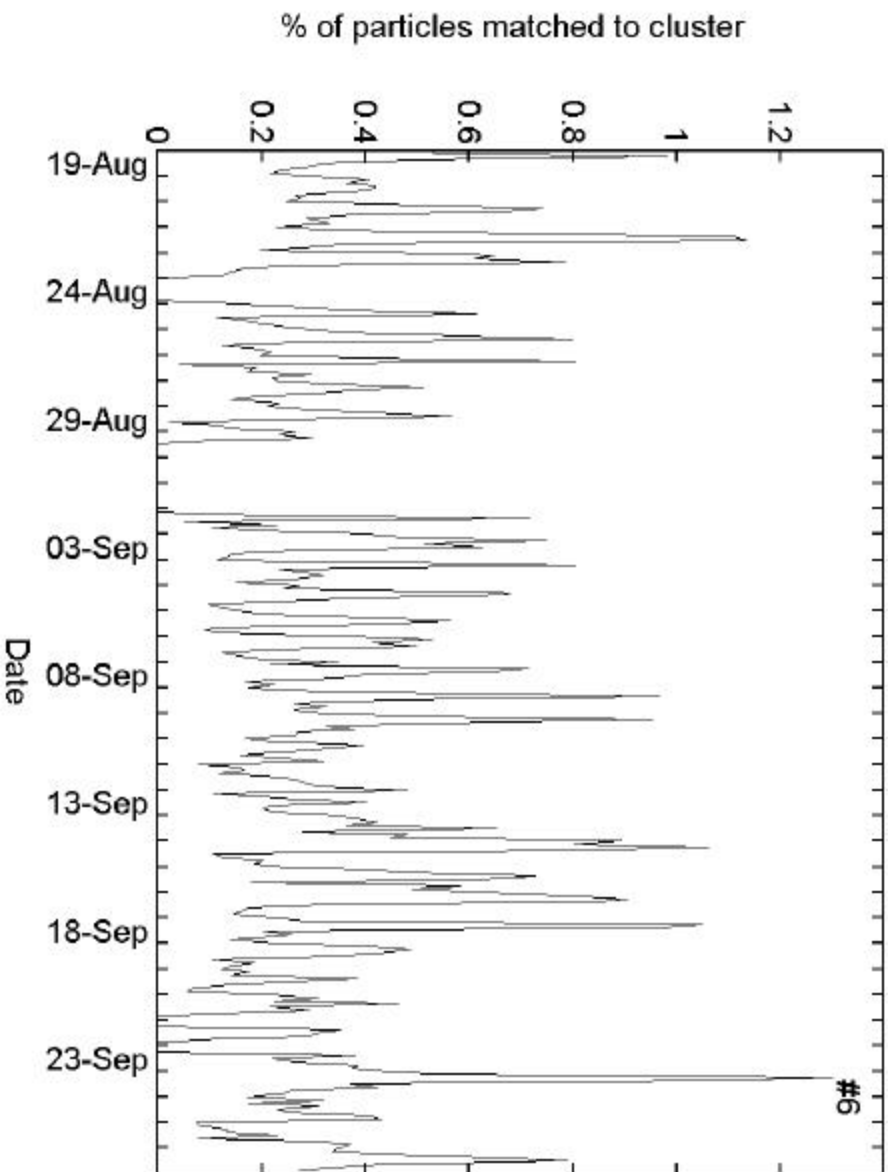


Figure 6.14: Time series plot for particles matched to calcium-rich dust cluster 6. Temporal resolution is 3 hours for the single particle data.

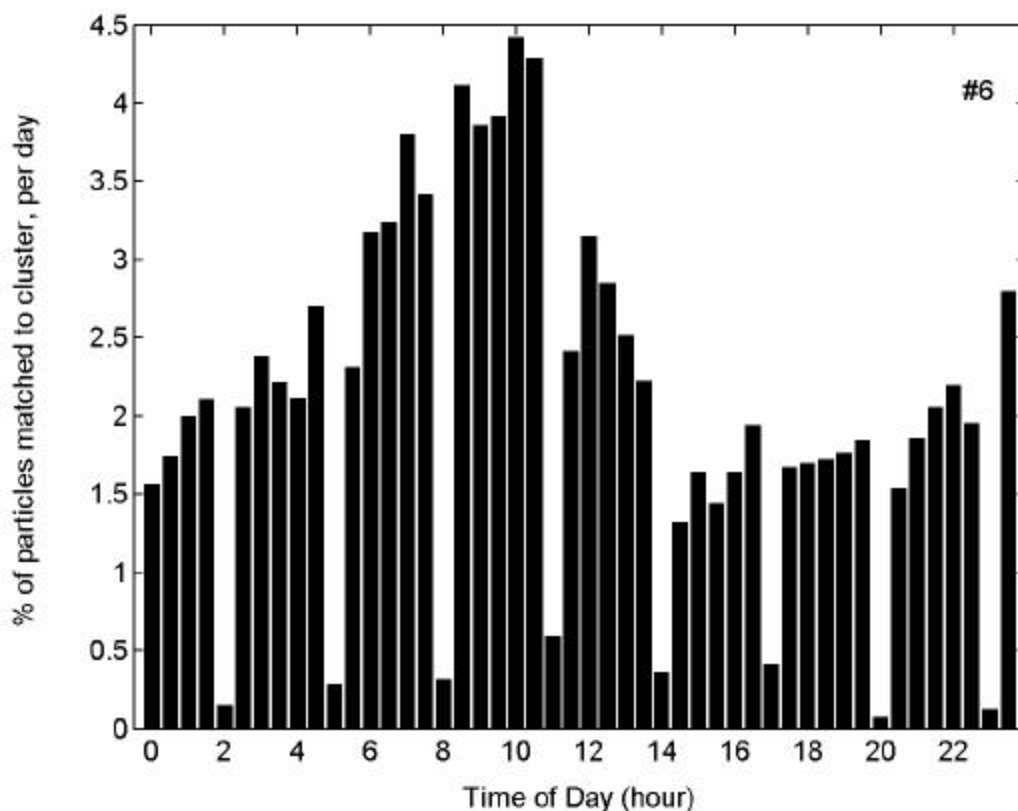


Figure 6.15: Time of day correlation plot for particles matched to calcium-rich dust cluster 6. Temporal resolution is 30 min for the single particle data.

Finally, Figure 6.14 shows the time series plots for cluster 6, a super- μm , calcium-rich dust type. The temporal profile of cluster 6 particles shows a regular pattern of peaks with similar intensity each day. The daily wind patterns in Riverside are a likely explanation for the temporal trend of the soil/crustal origin class. The time-of-day correlation plot in Figure 6.15 shows a morning peak. The maximum value is 4.43 % in the 10:00-10:30 time bin. Further correlation of with wind speed should shed light on the origin of this particle type.

Each of the different classes shown in this section has a unique diurnal pattern. A morning peak was observed for calcium-rich dust cluster 6, an early afternoon peak for the ammonium nitrate organic carbon cluster 8, and an evening peak for the sea salt with nitrate cluster 2 particles. The single particle nature of the ATOFMS data allows for a unique analysis of temporal trends in particle composition. At the time of SCOS97-NARSTO sampling, the current Matlab database and application of the ART-2a neural network for analysis were not even available yet. However, the single particle nature of the data has allowed it to be stored, combined, and reanalyzed in many ways. The species of interest need not be defined before the analysis and in fact may be discovered as a close look is taken at the mass spectra during more detailed analysis. The high temporal resolution of the ATOFMS instruments allows for flexible selection of time bins (and similarly for size). These advantages were demonstrated in this section. The data were displayed with 3-hour resolution to observe the trends over the course of many weeks and then with 30-minute resolution to examine the daily trends.

6.3.3 Composition of Ambient Riverside Particles - Matching to Car and Diesel

Forty days of ambient Riverside particle spectra were classified into diesel and car types (positive ion only vigilance 0.5) observed during the dynamometer test (see Chapter 4 for details). Diesel classes 2 and 3 do not resemble any of the car particles, providing unique signatures for diesel vehicles. As an example of the temporal trends for source-matched particles, the temporal profiles of diesel classes 2 and 3 appear in Figures 6.16 and 6.17, respectively. The composition of diesel cluster 2 is characterized by a large peak at m/z 40 and smaller peaks including 12, 24, and 36, thus representing an elemental carbon calcium-rich type. For cluster 3 particles, there is a less intense peak for calcium and the carbon peaks are more intense. The peaks in the temporal profile of cluster 3 have more magnitude and variability. The diesel cluster 2 particles peak at 4:30-5:00 and 22:30-23:00 (Figure 6.18) and display a minimum at 14:00. In contrast, cluster 3 has a peak at 10:00 (Figure 6.19). This appears to be related to the morning rush hour traffic.

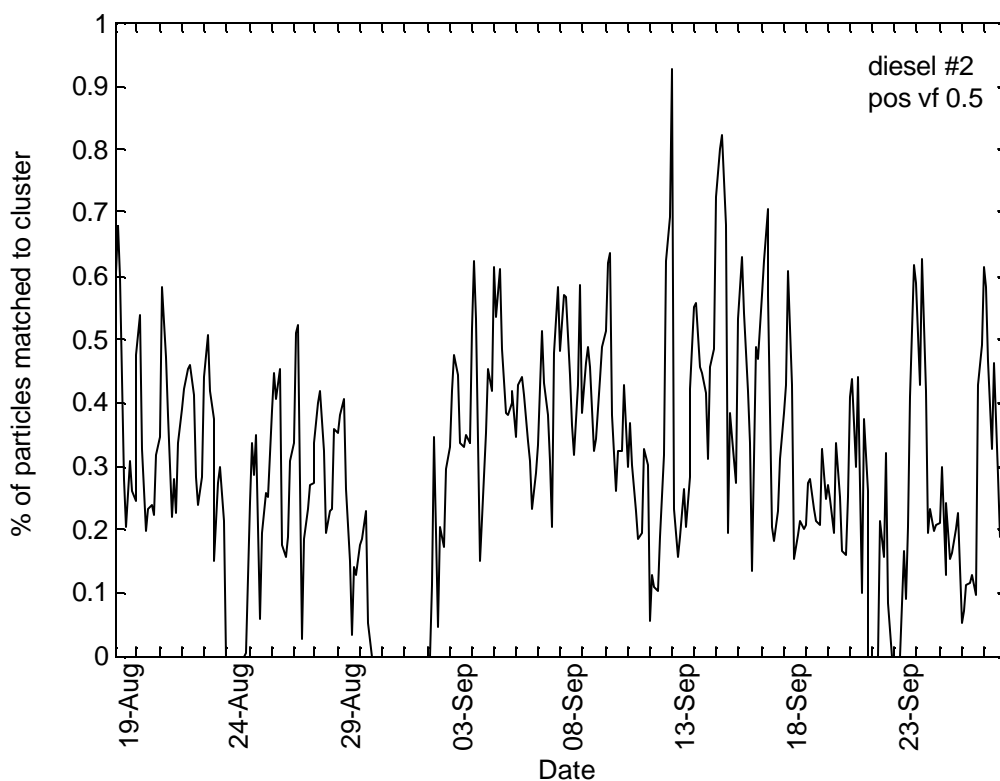


Figure 6.16: Time series plot for particles matched to calcium-rich diesel exhaust cluster 2. Temporal resolution is 3 hours for the single particle data.

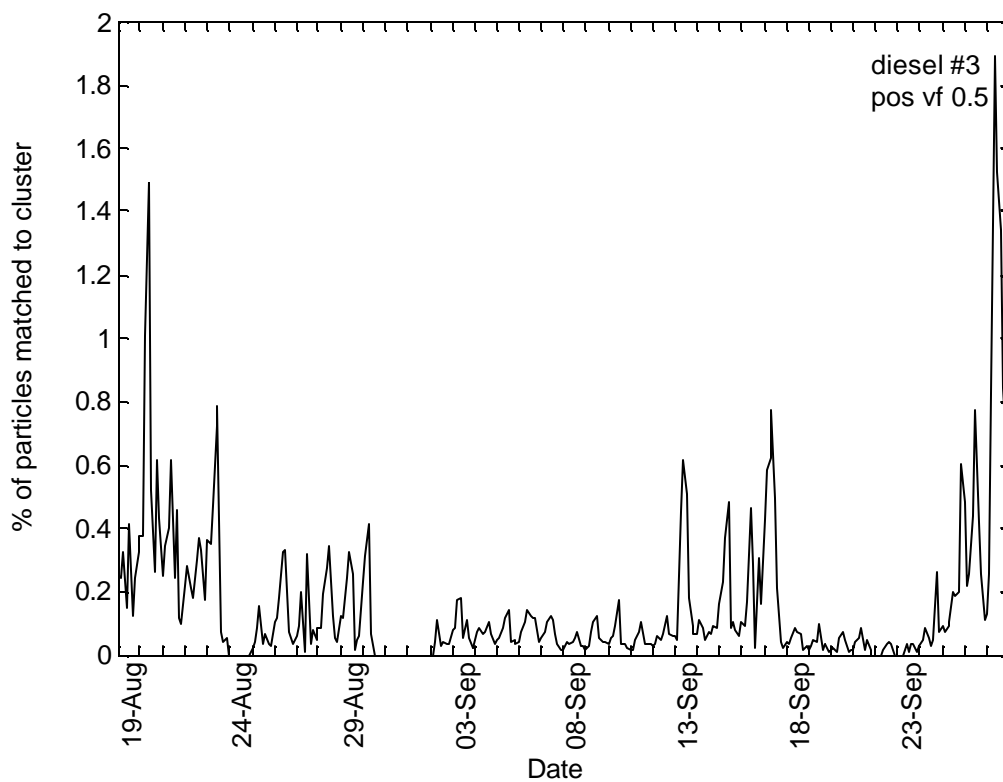


Figure 6.17: Time series plot for particles matched to elemental carbon with calcium diesel exhaust cluster 3. Temporal resolution is 3 hours for the single particle data.

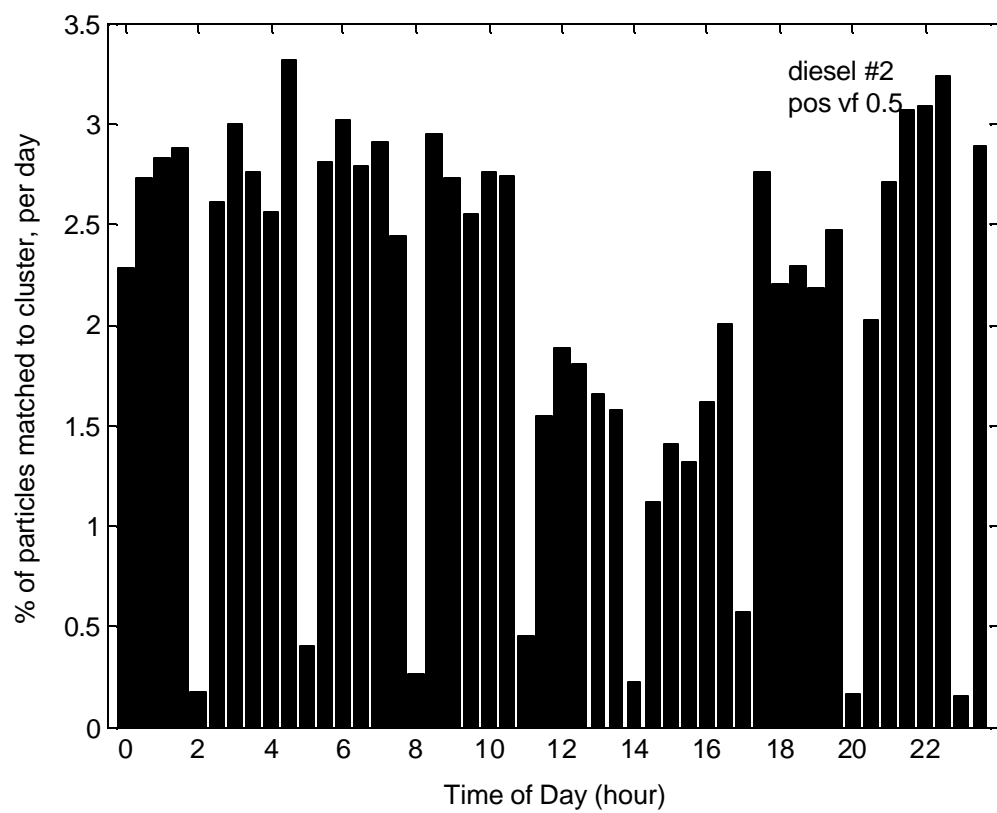


Figure 6.18: Time of day correlation plot for particles matched to diesel cluster 2. Temporal resolution is 30 min for the single particle data.

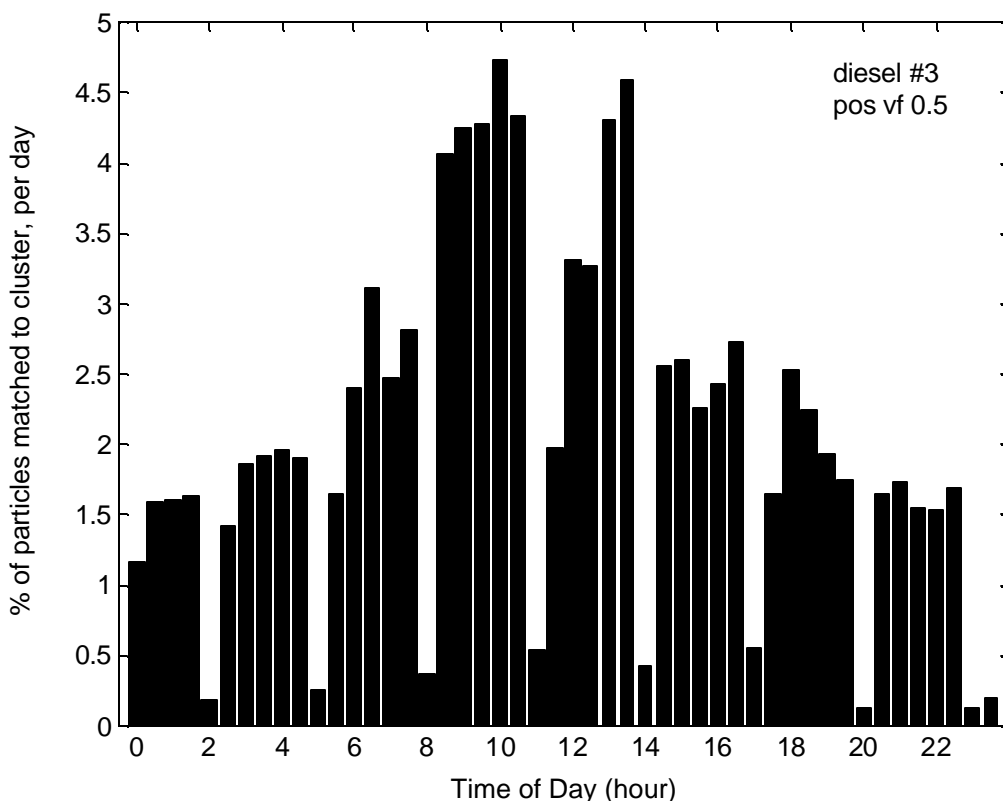


Figure 6.19: Time of day correlation plot for particles matched to diesel cluster 3. Temporal resolution is 30 min for the single particle data.

As an example of the matching to car exhaust data, the temporal profile of particles matched to car cluster 2 is shown in Figure 6.20 (positive ion only, vigilance factor 0.5). There is a peak each day at 13:00 in the time of day correlation plot for car cluster 2, which contrasts the temporal profiles of the diesel vehicle particles types (Figure 6.21). The fact this type grows in a mid-day suggests these are transformed vehicle particles produced in the morning. A higher (tighter) vigilance factor would allow for separation of fresh gasoline emissions from aged particles. This type of long term analysis may be used for each cluster in ambient or source data. Further analysis of the source-matched particles with more comprehensive source datasets is underway.

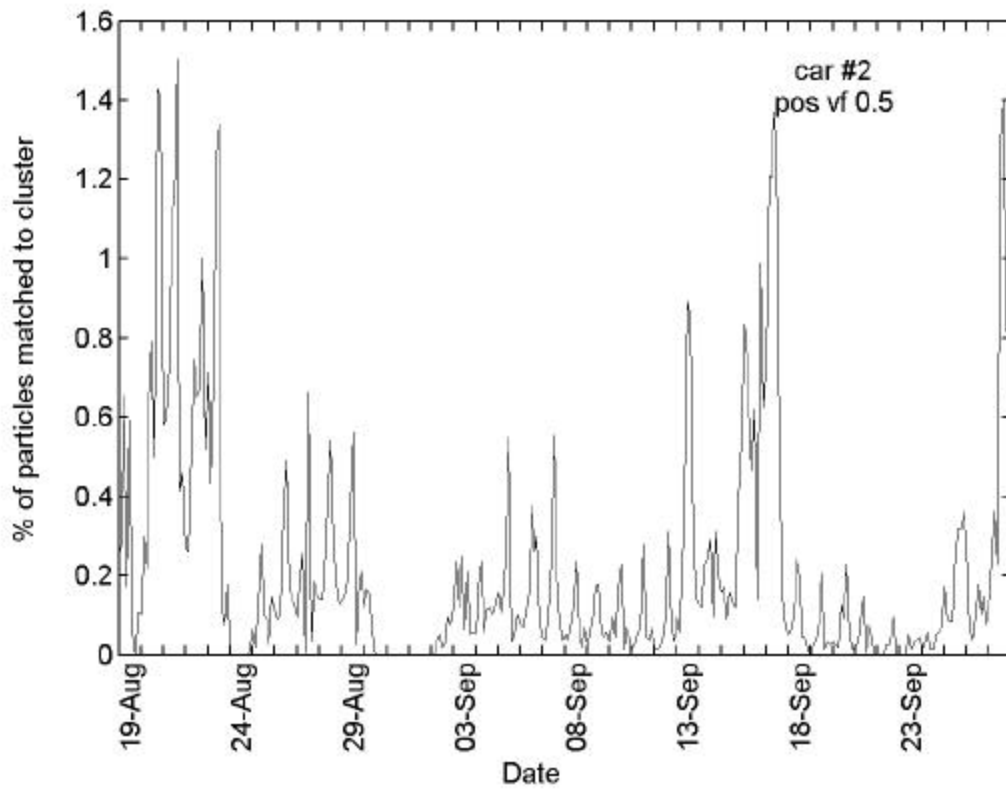


Figure 6.20: Time series plot for particles matched to car cluster 2. Temporal resolution is 3 hours for the single particle data.

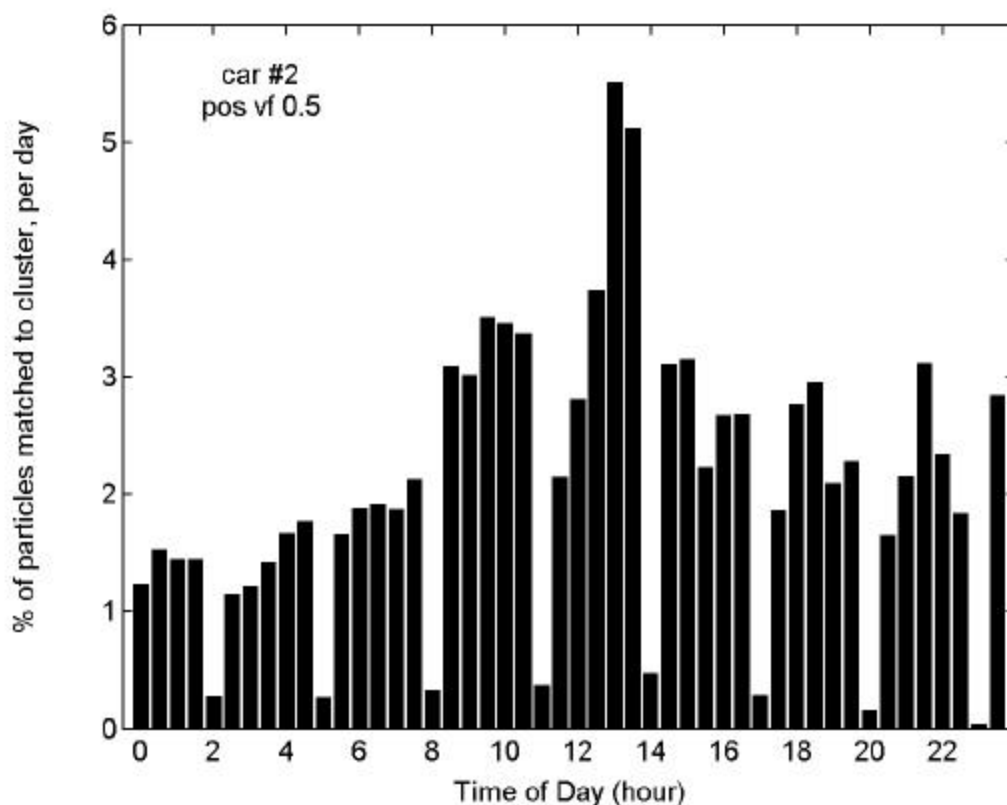


Figure 6.21: Time of day correlation plot for particles matched to car cluster 2. Temporal resolution is 30 min for the single particle data.

6.4 Conclusions

In this chapter, patterns of particle size and composition as determined by the ATOFMS over a several week period were examined. The chemical composition of over one million positive ion single particle mass spectra were classified into clusters created using a neural network (details of classes in Chapter 2). The size distributions were plotted. The temporal trends of several clusters were detailed.

The temporal profiles of many particle types showed repetitive diurnal patterns. The ammonium nitrate organic carbon cluster 8 showed a significant peak on September 17, 1997. The size profile and number of particles matched per class for September 17, 1997 were shown. The temporal profile of another ammonium nitrate organic carbon cluster, cluster 13, was presented and compared to cluster 8. A time-of-day correlation plot was produced to determine if the peaks for a given cluster occurred at a consistent time of day. Clusters 8 and 13 were found to peak at the same time of day but the peak for cluster 8 was a bit narrower in time, on average. The temporal trends and time-of-day plots for sea salt cluster 2 and calcium-rich dust cluster 6 each showed unique temporal behaviors. The three types of particles each showed characteristic diurnal patterns.

Based on the Chapter 4 (specifically, Figure 4.5), the diesel clusters 2 and 3 were selected as example source particle types. The temporal profiles were plotted, and the time-of-day plots

indicated peak times for these clusters in Riverside occur at 10:00 for cluster 3 and show a minimum at 14:00 for cluster 2. These temporal trends contrast the temporal profiles for the unique car particle types (most likely aged + fresh emissions), thus indicating they can serve as unique markers to discriminate between the emissions sources in ambient studies.

Chapter 7

Establishing ATOFMS quantitation procedures

7.1 Introduction

ATOFMS instruments collect continuous, single particle data. To generate accurate number and mass concentrations of particles, the ATOFMS measurements must be scaled to account for the sampling and detection biases of the instrument. Recent steps have been taken to scale number concentrations of the ATOFMS using scanning mobility particle sizing (SMPS) instruments and aerodynamic particles sizers (APS). These sizing instruments cover two size ranges between 50 nm to 500 nm (for the UF-ATOFMS) and 200 nm to 2.5 μm for the standard ATOFMS. It is important to scale the ATOFMS data to account for size biases in particle detection and derive atmospherically relevant particle concentrations for size-resolved ATOFMS data. Furthermore, scaling is a necessary step for the data before chemical composition data can be quantified. Allen et al. determined that ATOFMS instruments undercount particles by a factor, ϕ , that follows a power law dependence on aerodynamic particle diameter, D_a (Allen 2000).

During discrete times of SCOS97-NARSTO, cascade impactors were used to determine distributions of particles mass and composition side-by-side with the ATOFMS instruments. The impactors are considered the standard for quantitative chemical analysis, and ATOFMS scaling factors (to account for the ATOFMS particle detection efficiencies) are generated to reconstruct the aerosol mass loadings and species concentrations measured by the impactors. These calibration methods for the ATOFMS instruments allow for conversion between ATOFMS number counts for particles sampled and MOUDI mass concentrations. In addition, the ion signals from ammonium and nitrate may be used to quantify the concentrations of these species (Bhave 2002). In future studies, similar procedures will be applied for quantifying sulfate, chloride, OC, EC, and various metals in the particles. The driving force for such calibrations is the ATOFMS, once calibrated, can provide continuous information on the concentration of chemical species with higher temporal resolution (30-60 minutes) than most off-line sampling techniques while providing information on the chemical associations between the key species of interest. This will represent a much more cost effective way to obtain size-resolved particle composition data. Unprecedented data with high size, temporal, and spatial resolution will be available on atmospheric aerosols.

7.2 Experimental methods

Sampling periods where the MOUDI was operating side-by-side with the ATOFMS which yielded calibration points included August 21-23 (V1) and 27-29 (V2), September 27-30 (N1), and October 31-November 1, 1997 (N3). Data from each of these periods generate 20 potential data points for the three instruments. Seven of these data points are for Riverside sampling during V1, V2, and N3. This contrasts our first calibration study in 1996 where we only had 4 calibration points and thus this will provide a more accurate calibration.

The techniques developed and applied for the 1996 field study as part of our previous CARB contract are being used as a model (Allen 2000). ATOFMS counts are converted to apparent mass for comparison with mass concentration data collected with micro-orifice uniform deposition impactors (MOUDI). The impactor stages that overlap with the size range of particle detection by ATOFMS include 0.32-0.56, 0.56-1.0, and 1.0-1.8 μm . For the 1996 trajectory study (T96), a power law dependence on aerodynamic particle diameter was used to model the ATOFMS undercounting particles and create a scaling factor, Φ :

$$\Phi = \alpha D_a^\beta$$

To apply this model, the aerosol mass concentration measured for a sample collected on stage i of a cascade impactor is designated m_i . The impactors are considered the standard and this m_i is the reference measurement of the aerosol mass concentration between the cut-off diameters of the stage. The ATOFMS data are divided into size bins selected so that 10 sub-bins (j) fit within each impactor bin i . Then the counts per bin, sum of the number of hit (mass spectrum acquired) ATOFMS particles per bin (j), are divided by the volume of air sampled. The apparent mass concentration (m_j) in a narrow ATOFMS size bin is calculated where the particles are assumed to be spherical and of uniform density ($\rho_p = 1.3 \text{ g cm}^{-3}$),

$$m_j^* = n_j^* (\Pi/6) \rho_p \overline{D_{p,j}}^3 \quad (\text{Equation A})$$

and $\overline{D_{p,j}}$ is the logarithmic mean particle diameter in size bin j . The ratio of aerosol mass as measured by an impactor to that estimated from ATOFMS data, is a measure of the particle detection efficiency. This ratio, Φ , is the inverse of the mass detection efficiency.

The model operates under the hypothesis that the ATOFMS particle counts can be reliably scaled by the inverse mass detection efficiency to yield atmospheric aerosol concentrations and that the scaling functions are dependent only on particle aerodynamic diameter, D_a . This model is then expressed as:

$$m_i = \sum \Phi(\overline{D_{a,j}}) m_j^* + \epsilon_i \quad (\text{Equation B})$$

where $\Phi(\overline{D_{a,j}})$ is the scaling function and ϵ_i is the residual aerosol mass concentration. Plots of Φ versus D_a suggest that Φ follows a power law relationship in D_a .

$$\Phi = \alpha D_a^\beta \quad (\text{Equation C})$$

Parameters α and β were determined by non-linear regression of impactor mass concentration data on ATOFMS particle data with the ATOFMS data in narrow size bins.

For SCOS97-NARSTO, one subtle but noteworthy change to the scaling procedure has been made (does not appear in the T96 publication). In T96, ATOFMS data were aggregated into 10 sub-bins (j) of equal logarithmic width, corresponding to each impactor particle size bin (i). The mass concentration of particles in each sub-bin (m_j^*) was then estimated by multiplying

the apparent number concentration of particles in this sub-bin (n_j^*) by the mass of a single particle which has a physical diameter equal to the logarithmic *mean* particle diameter. The n_j^* 's within each impactor bin are then summed and regressed against the corresponding impactor measurement, based upon their logarithmic *mean* aerodynamic diameter. Combining equations A, B, and C would yield:

$$m_i = \sum_{j < i} \left(a \overline{D_{a,j}}^b n_j^* \frac{\rho}{6} r_p \overline{D_{p,j}}^3 \right) + e_i \quad (\text{Equation D})$$

In the revised methodology, the ATOFMS data are *not* aggregated into MOI sub-bins before scaling. Each particle (k) is scaled based upon its individual diameter ($D_{a,k}$). Equation D would be rewritten as follows:

$$m_i = \sum_{k < i} \left(a D_{a,k}^b n_k^* \frac{\rho}{6} r_p D_{p,k}^3 \right) + e_i \quad (\text{Equation E})$$

This method is more accurate because there is no averaging of particle size, mass, etc. Moreover, it simplifies the procedure of scaling up data, because any group of particles can be multiplied by αD_a^β to get the number concentration of particles of that type. In the previous methodology, the procedure used to calculate α and β was slightly different than the procedure followed to scale up the data.

For species quantitation, the data are first scaled for detection efficiency. Then parameters alpha and beta are determined by nonlinear regression of impactor mass concentration data on ATOFMS single particle data, using equation E. It is important to reiterate that this is a more sophisticated and accurate regression model that does not rely on averaging of the ATOFMS data into narrow size intervals. Rather, it scales the single particle data directly based on their measured aerodynamic diameters.

7.3 Results and Discussion

7.3.1 Aerosol Mass Concentration

During 1996 and 1997, four field experiments were conducted in which an ATOFMS instrument and a micro orifice impactor (MOI) simultaneously sampled the ambient aerosol at Riverside, California. Because of instrument modifications between these field experiments, the transmission efficiency of the laboratory-based ATOFMS instrument varied slightly from one experiment to the next. The regression model described above was used to calculate most likely parameter values that describe the ATOFMS particle detection efficiency during each experiment. These parameter values for the lab-based ATOFMS in Riverside are listed in Table 7.1. By looking at these values for the different studies, one can see the values for the parameters change from one study to another. These changes can be explained by a discovery that was made after this study was completed. We determined that the nozzle we had been using

for the experiment was being etched away by the cleaning process thus changing the expansion conditions and associated transmission for the nozzle.

Table 7.1. Parameter Values Fit to the Scaling Function $F = aD_a^b$

Experiment	α^a	β^a	applicable range of D_a (μm)
V1	1452 \pm 435	-3.90 \pm 0.519	0.32 – 1.8
V2	1080 \pm 633	-4.48 \pm 0.463	0.32 – 1.8
N3	5201 \pm 2155	-4.68 \pm 1.028	0.32 – 1.8

^a Most likely parameter values and 95% confidence intervals

(Note: values for T96 using the modified regression model described above are $\alpha=5036 \pm 1192$ and $\beta=-3.1285 \pm 0.6393$ and are not identical to those published in Allen et al.)

Allen et al. demonstrated that ATOFMS particle detection efficiencies during the 1996 sampling at Riverside did not depend on aerosol chemical composition. Following the same procedure, the regression model residuals for each of the 1997 experiments are analyzed to determine whether or not the ATOFMS particle detection efficiencies were significantly affected by aerosol chemical composition, when averaged over the size-segregated ambient aerosol. Extensive aerosol composition data are available from chemical analyses of the impactor samples collected during each experiment. The correlations of regression model residuals and aerosol chemical composition are listed in Table 7.2.

Table 7.2. Correlation Coefficients Squared (R^2) for Residual Aerosol Mass Concentrations and Aerosol Concentrations of Individual Analytes.

	V1		V2		N3	
	R^2	$R^2_{crit}{}^a$ (n^b)	R^2	$R^2_{crit}{}^a$ (n^b)	R^2	$R^2_{crit}{}^a$ (n^b)
Mass	0.007	0.66 (6)	0.22	0.50 (8)	0.004	0.66 (6)
OC	0.26	0.99 (3)	0.51	0.66 (6)	0.28	0.90 (4)
NH4	0.11	0.77 (5)	0.02	0.57 (7)	0.001	0.66 (6)
NO3	0.67	0.99 (3)	0.37	0.44 (9)	0.001	0.66 (6)
SO4	0.008	0.77 (5)	0.002	0.57 (7)	0.26	0.99 (3)
Na	0.17	0.90 (4)	0.001	0.57 (7)	0.13	0.77 (5)
As	0.11	0.99 (3)	^c		^c	
K	^c		^c		0.80	0.99 (3)
La	0.05	0.77 (5)	^c		^c	

^a Threshold R^2 value significantly different from zero with 95% confidence

^b Number of impactor measurements with analyte concentrations =2 SD above zero

^c Fewer than 3 impactor measurements for given analyte significantly different from zero

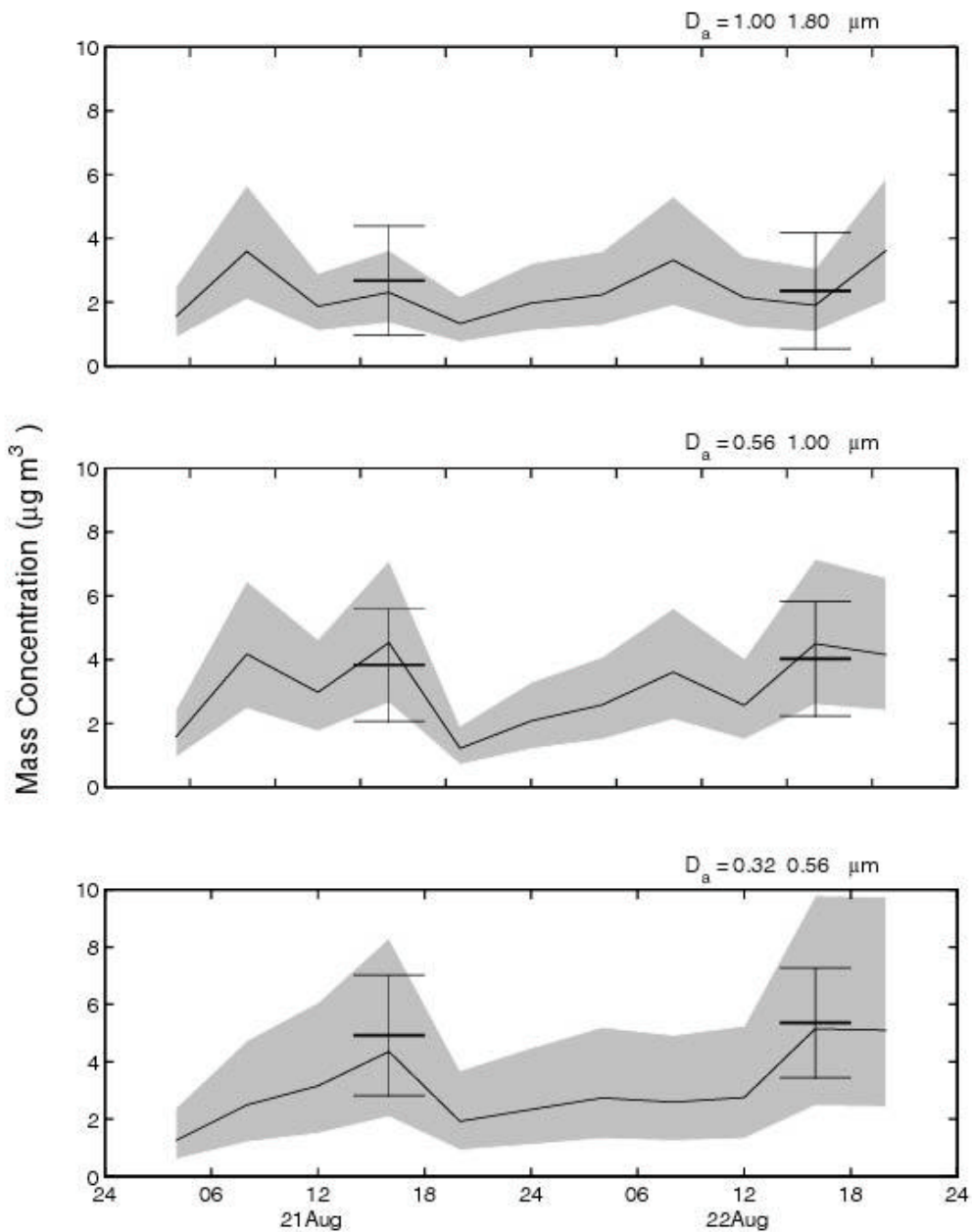


Figure 7.1: Continuous fine aerosol mass concentration as determined from the scaled ATOFMS data at Riverside during V1. Scaled ATOFMS data are shown as a solid line with shading indicating the 95% confidence intervals; impactor data are shown as heavy horizontal bars of 4-hour duration with error bars indicating 2 standard deviations.

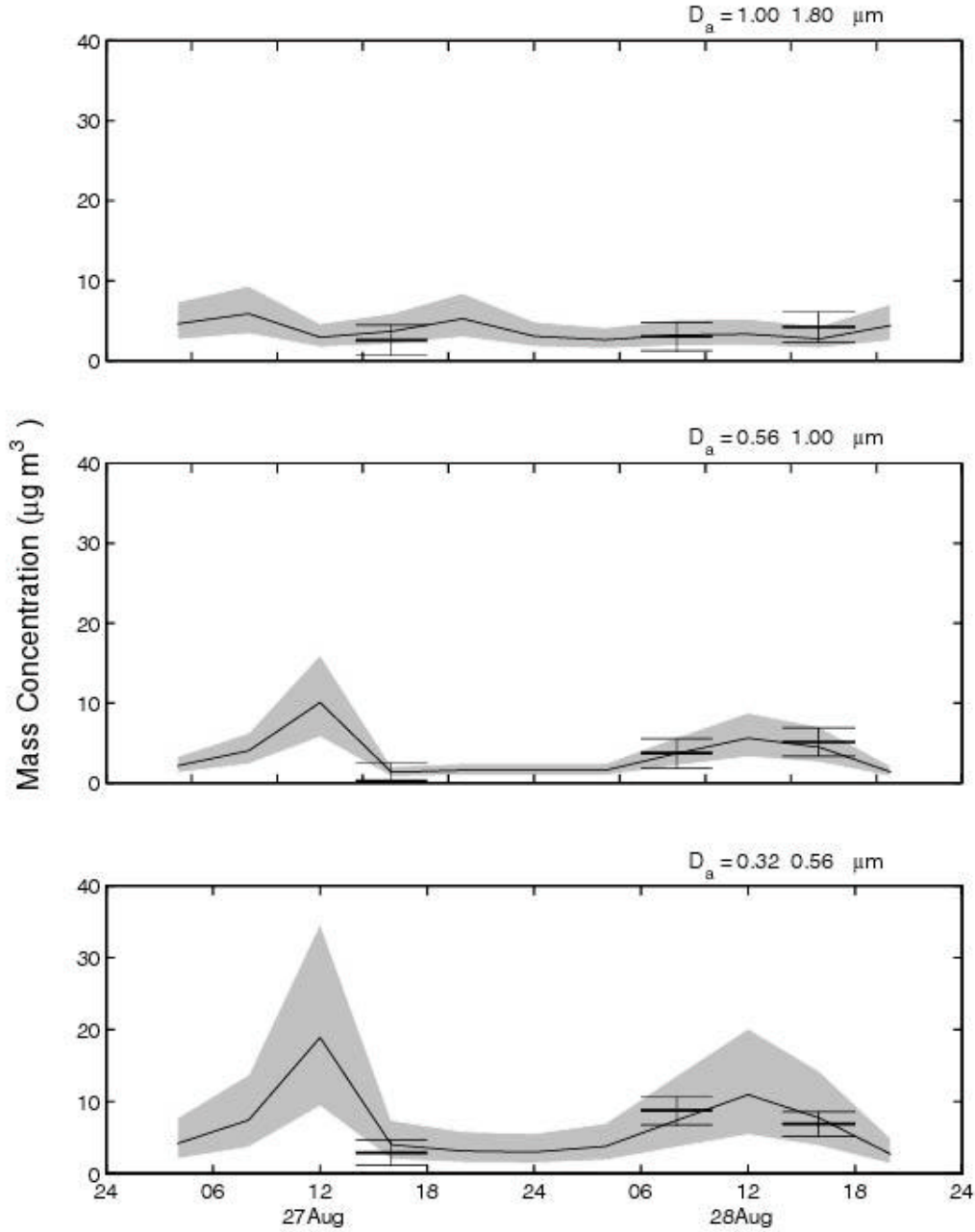


Figure 7.2: Continuous fine aerosol mass concentration as determined from the scaled ATOFMS data at Riverside during V2. Scaled ATOFMS data are shown as a solid line with shading indicating the 95% confidence intervals; impactor data are shown as heavy horizontal bars of 4-hour duration with error bars indicating 2 standard deviations.

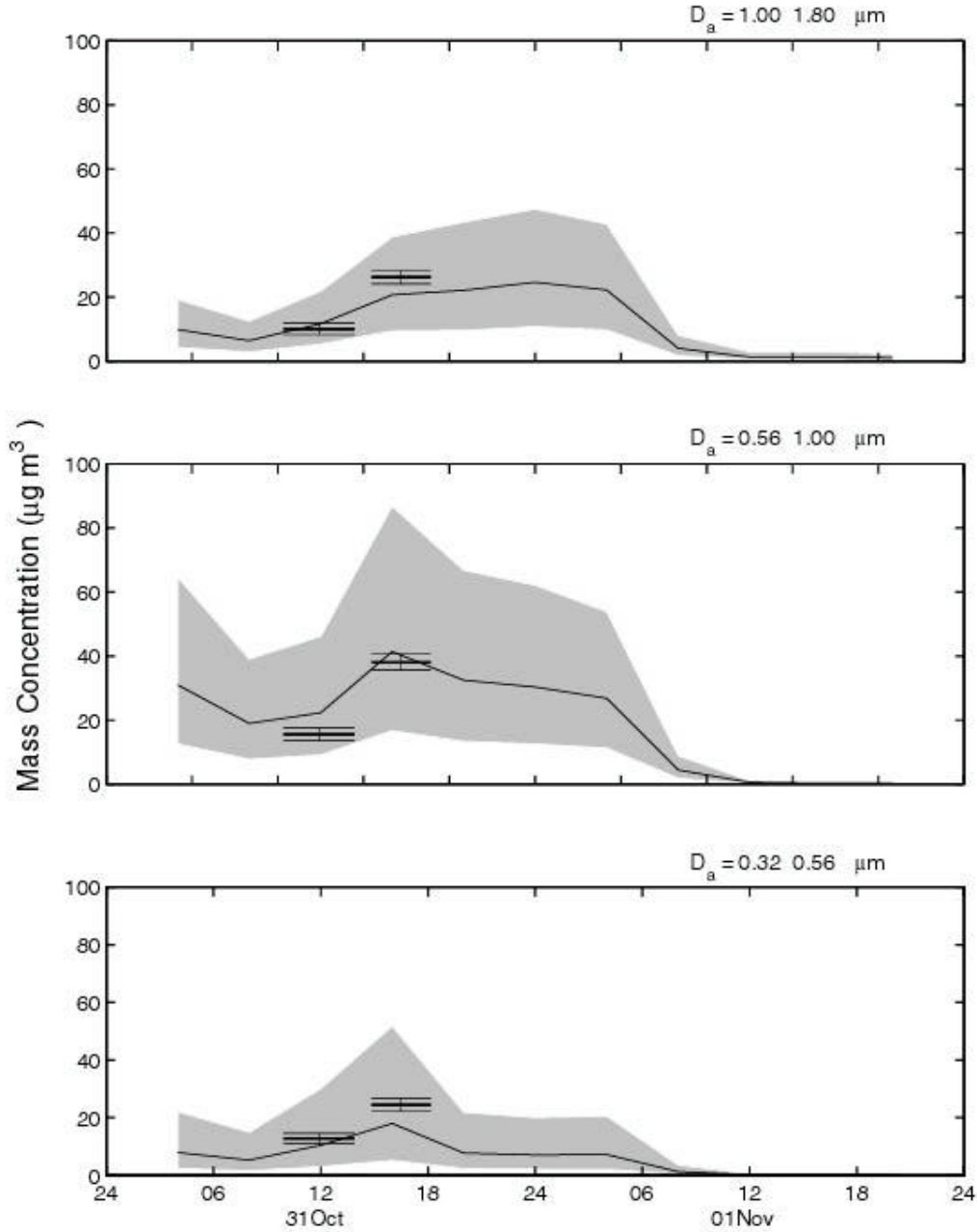


Figure 7.3: Continuous fine aerosol mass concentration as determined from the scaled ATOFMS data at Riverside during N3. Scaled ATOFMS data are shown as a solid line with shading indicating the 95% confidence intervals; impactor data are shown as heavy horizontal bars of 4-hour duration with error bars indicating 2 standard deviations.

None of the correlation coefficients are found to be significantly different from zero, with 95% confidence. These results indicate that particle detection efficiencies averaged over the size-segregated ambient aerosol were not significantly affected by aerosol chemical composition during the 1997 field experiments at Riverside. One application of the regression model described above is to recreate the time series of aerosol concentrations from ATOFMS data over an extended period. This has been demonstrated using the 1996 dataset by Allen et al. In an analogous fashion, Figures 7.1-7.3 illustrate continuous aerosol mass concentration data obtained from ATOFMS measurements during each of the 1997 periods with impactors and ATOFMS sampling side-by-side in Riverside. The y-axis scales of Figures 7.1–7.3 are 10, 40, and 100, respectively. Since this represented the first long term field study for the transportable version of the instruments, there was significant variability in the comparisons between the MOUDI impactor and the ATOFMS data that could be attributed to major instrument modifications in the field due to equipment not being robust enough (i.e. replacement of scattering lasers, LDI lasers, ion detectors, etc.). Since this study was conducted, we have acquired products that are much more robust under field conditions and thus the scaling factors are more stable and consistent over long sampling periods, similar to the lab-based data shown in this section.

7.3.2 Ammonium and Nitrate Concentrations

In the present study, we hypothesize that the chemical sensitivity of ATOFMS instruments to ammonium (NH_4^+) and nitrate (NO_3^-) is unaffected by minor variations in the instrument transmission efficiencies. Following this hypothesis, the ATOFMS estimates of size-segregated mass concentrations during each experiment are pooled together to maximize the number of data points available for evaluating the ATOFMS instrument sensitivities to NH_4^+ and NO_3^- . Comparisons of the pooled ATOFMS mass concentrations to corresponding impactor measurements are shown in Figure 7.4. In this figure, dotted lines represent the 2:1, 1:1, and 1:2 lines of correspondence. The vast majority of data points fall between the 2:1 and 1:2 lines, demonstrating that the particle detection efficiency scaling procedures are accurate within a factor of two.

The most striking feature in Figures 7.5 and 7.6 is the clustering of data points according to particle size, as represented by different shading patterns. For both NH_4 and NO_3 , the ratio of summed ion signal to mass concentration is largest for particles in the 0.32 - 0.56 μm size range, and smallest for particles in the 1.0 - 1.8 μm size range. A qualitatively similar trend has also been reported in laboratory experiments (Reents et al, 1994, Carson et al, 1997). Further investigation is needed to explain this apparent size dependence, as well as the variations observed among particles in the same size range. In the future, it may be possible to parameterize the dependence of ion signal per unit mass on particle size, under ambient sampling conditions. Such a parameterization may permit the quantification of NH_4 and NO_3 ions in size-segregated ambient aerosols.

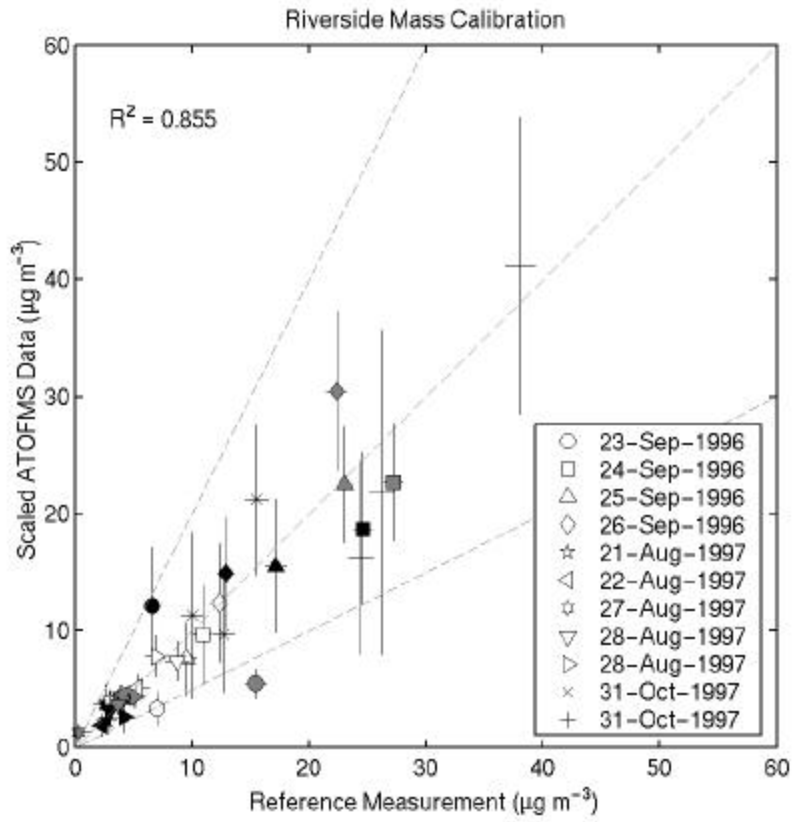


Figure 7.4: Pooled aerosol mass concentration data, scaled ATOFMS data versus impactor.

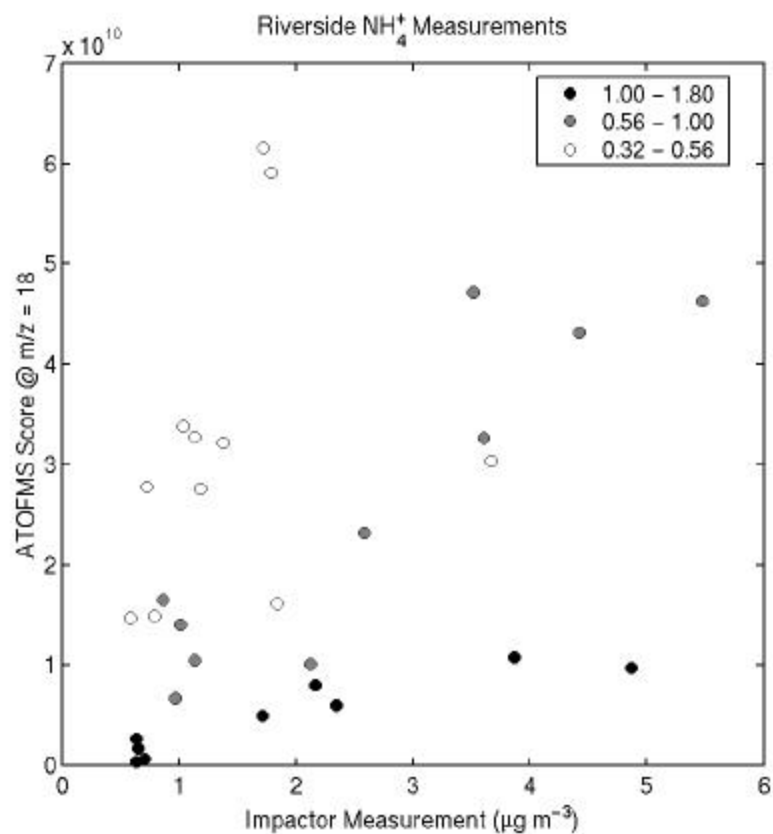


Figure 7.5: Comparison of the ATOFMS ammonium “score” (quantity of ions that would have been detected by the ATOFMS instrument if it had sized and hit all particles drawn from the atmosphere) and corresponding impactor measurements for the same time and size interval.

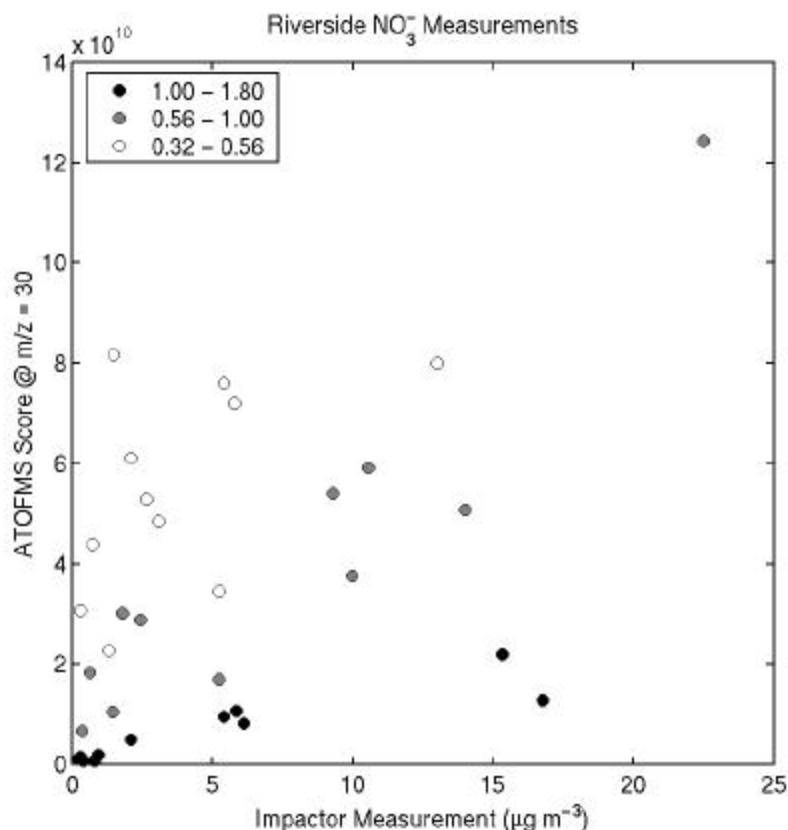


Figure 7.6: Comparison of the ATOFMS nitrate “score” (quantity of ions that would have been detected by the ATOFMS instrument if it had sized and hit all particles drawn from the atmosphere) and corresponding impactor measurements for the same time and size interval.

7.4 Conclusions

This chapter demonstrates the potential for calibrating the ATOFMS instruments using off-line mass concentration data simultaneously obtained with a MOUDI impactor. The comparison is demonstrated for the lab-based system because it was the most stable instrument over the course of this study. As mentioned, the field transportable instruments, being much newer instruments, had some difficulties over the course of the experiment with certain electronic components that were not as robust in the field as the instrument specifications of the manufacturers claimed. As a result, from one IOP side-by-side calibration to another, there were significant changes to the instruments, resulting in too few data points for precise calibration of the instruments. However, since this study was complete, these components have been changed and the systems are now as stable as the lab-based instrument. They have proven this in a number of recent field campaigns in Japan, Hawaii, Atlanta, Texas and New York. The instruments will be calibrated for various species in these studies using the analysis and calibration techniques developed as part of SCOS97. In addition, the procedures will be tested on sulfate, organic carbon, elemental carbon, and various metals detected by ATOFMS.

Summary and Conclusions

This report summarizes key findings from a major field campaign conducted using ATOFMS instruments during SCOS97. This project was the first long term study conducted with multiple ATOFMS instruments. The project has resulted in the evolution of ATOFMS instruments from relatively unstable field instrument to rugged systems. In addition, the single particle data have been shown to be reproducible from study to study. Analysis and calibration procedures have been developed and the first attempts have been made at using single particle data for source apportionment.

The study allowed for initial testing of the transportable ATOFMS instrumental stability over time. Some instability was encountered due to certain key electrical components of the transportable instruments not operating at the specifications reported by the manufacturers. However in spite of these fluctuations, unique insights were obtained on the temporal and spatial variability of aerosol size and composition at several locations in southern California. The evolution of the complexity of particles was monitored as they moved inland through areas of high pollution. For the first time, source signatures obtained in vehicular characterization experiments were used to identify individual particles in ambient air in real time, monitoring how the emitted particle evolved over time and distance. Major advancements were made in developing analysis methods and calibration procedures that will allow for rapid processing of future ATOFMS datasets. These procedures were developed using the data from the more stable lab-based ATOFMS instruments. The transportable ATOFMS instruments have been improved based on findings during SCOS97 to be able to detect higher fractions of the ambient aerosol (improved by 5 orders of magnitude at 200 nm). Also, the stability of the instruments has been improved so they are as stable as the lab-based ATOFMS instrument.

Recommendations

Oposing theories exist as to whether coarse ($>2.5 \mu\text{m}$) or fine ($<2.5 \mu\text{m}$) particles produce health effects (Brunekreef 2002). This can be attributed to the fact that during certain times, one size range of particles has been shown to produce a certain effect, while at other times this same size range of particles has shown no effect. These conflicting results are most likely due to the fact that at different times and locations, the size cut at $\text{PM}_{2.5}$ does not separate compositions from different sources (i.e. coarse particles (i.e. dust, sea salt) from accumulation mode particles (i.e. combustion (organic)), and therefore cannot separate the effects due to compositional differences in fine and coarse particulate matter. Particles from such different sources have been shown to have quite different health effects (Laden 2000; Morawska 2002). This study confirms $\text{PM}_{1.0}$ would be more effective at separating particles from these sources which produce drastically different compositions. This same size-composition trend has been shown previously in other ATOFMS studies conducted in other regions of the United States and world including the Indian Ocean (Guazzotti 2001), Atlanta (Liu 2003; Wenzel 2003), Texas, as well as bulk source combustion studies and ambient size distribution measurements (Kleeman 1999; Morawska 2002; Salma 2002). Based on these findings, in future health effects studies, using a cut-point at $1 \mu\text{m}$ (as opposed to $2.5 \mu\text{m}$) would most likely provide results which are less ambiguous and easier to interpret from day to day and location to location.

Further calibration studies of the ATOFMS instruments will be conducted to test the stability and versatility of the calibration procedures over time as well as at different locations. The ATOFMS data will be scaled using data from instruments with higher temporal response than filter-based methods such as the Hering continuous nitrate monitor and the PILS system developed by Prof. Rodney Weber of Georgia Tech. In addition the calibration procedures will be applied to other particle phase species including sulfates, organic carbon, elemental carbon, and various metal species. Unique mass spectral types derived from source characterization studies will be used for source apportionment of ambient particles at the single particle level. Additional studies will be conducted with the more robust transportable instruments, using a newly implemented (highly efficient) focusing inlet which allows detection of particles down to 50 nm. Longer term instrument stability of the transportable instruments will allow correlations to be made on short timescales between particle size and composition and deleterious health effects, reduced visibility, and climate change. Establishment of the correlations with specific components in the aerosol will allow for better control strategies to be developed specifically aimed at the sources of particles of concern.

Glossary of Terms

AMS	aerosol mass spectrometer
APCI-MS	atmospheric pressure chemical ionization mass spectrometry
APS	aerodynamic particle sizer
ATOFMS	aerosol time-of-flight mass spectrometry
CCN	cloud condensation nuclei
CI	chemical ionization
DOAS	differential optical absorption spectroscopy
DMA	differential mobility analyzer
EC	elemental carbon
EI	electron impact
EPA	Environmental Protection Agency
FTIR	Fourier transform infrared spectroscopy
GC	gas chromatography
GC/MS	gas chromatography mass spectrometry
He-Ne	helium-neon
HPLC	high performance liquid chromatography
IC	ion chromatography
IOP	intensive operating period
INDOEX	Indian Ocean Experiment
IR	infrared spectroscopy
ITMS	ion trap mass spectrometry
LC	liquid chromatography
LDI	laser desorption ionization
LIDAR	light detection and ranging
MCP	microchannel plate detector
MOUDI	microorifice uniform deposit impactor
m/z	mass-to-charge
Nd:YAG	neodymium-yttrium aluminum garnet laser
NMR	nuclear magnetic resonance
OC	organic carbon
PM _{2.5}	particulate matter with aerodynamic diameter = 2.5 µm
PM ₁₀	particulate matter with aerodynamic diameter = 10 µm
PMT	photomultiplier tube detector
PSL	polystyrene latex spheres
SCOS97-NARSTO	1997 Southern California Ozone Study – North American Research Strategy for Tropospheric Ozone (SCOS97-NARSTO)
SMPS	scanning mobility particle sizing system
SPMS	single particle mass spectrometry
TEOM	tapered element oscillating microbalance
TOF	time-of-flight
UF	ultrafine (<100 nm)
VF	vigilance factor (used in ART-2a analysis)
VOC	volatile organic carbon
VUV	vacuum ultraviolet

List of Appendices

Appendix A: Possible positive ion m/z assignments for mass spectra.

Appendix B: Possible negative ion m/z assignments for mass spectra.

Appendix C: ART-2a positive-ion weight vectors for Riverside ambient August 21-23, 1997: m/z ratio and normalized intensity (vigilance factor = 0.5; top 20 of 57 clusters)

Appendix D: Matching results for particles in Los Angeles, Azusa, and Mira Loma matched to top 20 Riverside clusters (shown in Appendix C). Note matching procedure only uses positive ion spectra since lab-based instrument could only run with one ion polarity. Matching is for total particles sampled.

Appendix E: Matching results for particles in Los Angeles and Azusa matched to top 20 Riverside clusters (shown in Appendix C). Note matching procedure only uses positive ion spectra since lab-based instrument could only run with one ion polarity. Matching is sub-divided into sub- and super- μm particles.

Appendix F: ART-2a dual-ion weight vectors for Los Angeles ambient August 21, 1997 12:40-15:40: m/z ratio and normalized intensity (vigilance factor = 0.7; 20 clusters)

Appendix G: ART-2a dual-ion weight vectors for Azusa ambient August 21, 1997 17:30-22:30: m/z ratio and normalized intensity (vigilance factor = 0.7; 8 clusters). New clusters for particles that did not match the Los Angeles dataset.

Appendix H: ART-2a positive-ion weight vectors for diesel vehicle dynamometer: mass-to-charge ratio and normalized intensity (vigilance factor = 0.5; 6 clusters)

Appendix I: ART-2a dual-ion weight vectors for diesel vehicle dynamometer: mass-to-charge ratio and normalized intensity (vigilance factor = 0.5; 12 clusters)

Appendix J: ART-2a positive-ion weight vectors for car vehicle dynamometer: mass-to-charge ratio and normalized intensity (vigilance factor = 0.5; 14 clusters).

Appendix K: ART-2a dual-ion weight vectors for car vehicle dynamometer: mass-to-charge ratio and normalized intensity (vigilance factor = 0.5; 22 clusters)

Appendix L: ART-2a dual-ion weight vectors for diesel vehicle dynamometer: mass-to-charge ratio and normalized intensity (vigilance factor = 0.7; 11 clusters)

Appendix M: ART-2a dual-ion weight vectors for car vehicle dynamometer: mass-to-charge ratio and normalized intensity (vigilance factor = 0.7; 27 clusters)

Appendix N: Table showing matching of Azusa to ART-2a dual-ion weight vectors for car vehicle dynamometer: m/z ratio and normalized intensity (vigilance factor = 0.7; 27 clusters)

Appendix O: ART-2a positive-ion weight vectors for Diamond Bar, Mira Loma, and Riverside ambient during trajectory-matched times September 27-29, 1997: m/z ratio and normalized intensity (vigilance factor = 0.7; 57 clusters)

Appendix P: Color versions of similarity plots presented in the body of the report in grayscale. A red to blue color-coding replaces the white to black grayscale coding. See the body of the report for captions and additional information.

Appendix Q: Temporal plots of clusters #1-20 in Riverside over 40 consecutive days between August 19, 1997 and September 27, 1997 during SCOS97-NARSTO.

Appendix R: List of product references directly supported by this contract.

References

- Allen, J. O., D. P. Fergenson, E. E. Gard, L. S. Hughes, B. D. Morrical, M. J. Kleeman, D. S. Gross, M. E. Gaelli, K. A. Prather and G. R. Cass (2000). "Particle detection efficiencies of aerosol time of flight mass spectrometers under ambient sampling conditions." *Environmental Science and Technology* **34**(1): 211-217.
- Angelino, S., D. T. Suess and K. A. Prather (2001). "Formation of aerosol particles from reactions of secondary and tertiary alkylamines: Characterization by aerosol time-of-flight mass spectrometry." *Environmental Science and Technology* **35**(15): 3130-3138.
- Bhave, P. V., J. O. Allen, B. D. Morrical, D. P. Fergenson, G. R. Cass and K. A. Prather (2002). "A field-based approach for determining ATOFMS instrument sensitivities to ammonium and nitrate." *Environmental Science & Technology* **36**(22): 4868-4879.
- Bhave, P. V., D. P. Fergenson, K. A. Prather and G. R. Cass (2001). "Source apportionment of fine particulate matter by clustering single-particle data: Tests of receptor model accuracy." *Environmental Science and Technology* **35**(10): 2060-2072.
- Bhave, P. V., M. J. Kleeman, J. O. Allen and L. S. Hughes (2002). "Evaluation of an air quality model for the size and composition of source-oriented particle classes." *Environmental Science and Technology* **36**(10): 2154-2163.
- Brunekreef, B. and S. T. Holgate (2002). "Air pollution and health." *Lancet* **360**(9341): 1233-1242.
- Cahill, T. A., R. Morales and J. Miranda (1996). "Comparative aerosol studies of Pacific Rim cities - Santiago, Chile (1987); Mexico city, Mexico (1987-1990); and Los Angeles, U.S.A. (1973 and 1987)." *Atmospheric Environment* **30**(5): 747-9.
- Carpenter, G. A., S. Grossberg and D. B. Rosen (1991). "Art 2a - An adaptive resonance algorithm for rapid category learning and recognition." *Neural Networks* **4**(4): 493-504.
- Charlson, R. J., J. E. Lovelock, M. O. Andreae and S. G. Warren (1987). "Oceanic phytoplankton, atmospheric sulfur, cloud albedo and climate." *Nature (London, United Kingdom)* **326**: 655-661.
- Chow, J. C., C. S. Liu, J. Cassmassi, J. G. Watson, Z. Lu and L. C. Pritchett (1992). "A neighborhood-scale study of PM10 source contributions in Rubidoux, California." *Atmospheric Environment, Part A: General Topics* **26A**(4): 693-706.
- Chow, J. C., J. G. Watson, E. M. Fujita, Z. Lu, D. R. Lawson and L. L. Ashbaugh (1994). "Temporal and spatial variations of PM2.5 and PM10 aerosol in the Southern California Air Quality Study." *Atmospheric Environment* **28**(12): 2061-80.
- Collins, D. R., H. H. Jonsson, H. Liao, R. C. Flagan, J. H. Seinfeld, K. J. Noone and S. V. Hering (2000). "Airborne analysis of the Los Angeles aerosol." *Atmospheric Environment* **34**(24): 4155-4173.
- Dockery, D. W. (2001). "Epidemiologic evidence of cardiovascular effects of particulate air pollution." *Environmental Health Perspectives* **109**: 483-486.
- Dockery, D. W., C. A. Pope III, X. Xu, J. D. Spengler, J. H. Ware, M. E. Fay, B. G. Ferris and F. E. Speizer (1993). "An association between air pollution and mortality in six US cities." *New England Journal of Medicine* **329**(24): 1753-1759.
- Dolislager, L. J. and N. Motellebi (1999). "Characterization of particulate matter in California." *Journal of the Air and Waste Management Association* **49**: PM-45-PM-56.
- Eldering, A. and G. R. Cass (1996). "Source-oriented model for pollutant effects on visibility." *Journal of Geophysical Research* **101**(D14): 19343-19369.

- Fergenson, D. P., X.-H. Song, Z. Ramadan, J. O. Allen, L. S. Hughes, G. R. Cass, P. K. Hopke and K. A. Prather (2001). "Quantification of ATOFMS data by multivariate methods." *Analytical Chemistry* **73**(15): 3535-3541.
- Gao, N., M.-D. Cheng and P. K. Hopke (1994). "Receptor modeling of airborne ionic species collected in SCAQS." *Atmospheric Environment* **18**(8): 1447-1470.
- Gard, E., J. E. Mayer, B. D. Morrical, T. Dienes, D. P. Fergenson and K. A. Prather (1997). "Real-time analysis of individual atmospheric aerosol particles: Design and performance of a portable ATOFMS." *Analytical Chemistry* **69**(20): 4083-4091.
- Gard, E. E., M. J. Kleeman, D. S. Gross, L. S. Hughes, J. O. Allen, B. D. Morrical, D. P. Fergenson, T. Dienes, M. E. Galli, R. J. Johnson, G. R. Cass and K. A. Prather (1998). "Direct observation of heterogeneous chemistry in the atmosphere." *Science (Washington, D. C.)* **279**(5354): 1184-1187.
- Goodin, W. R., G. J. McRae and J. H. Seinfeld (1979). "A comparison of interpolated methods for sparse data: Application to wind and concentration fields." *Journal of Applied Meteorology* **18**: 761-771.
- Guazzotti, S. A., K. R. Coffee and K. A. Prather (2001). "Continuous measurements of size-resolved particle chemistry during INDOEX-IFP 99." *Journal of Geophysical Research, [Atmospheres]* **106**(D22): 28607-28627.
- Guazzotti, S. A., J. R. Whiteaker, D. Suess, K. R. Coffee and K. A. Prather (2001). "Real-time measurements of the chemical composition of size-resolved particles during a Santa Ana wind episode, California USA." *Atmospheric Environment* **35**(19): 3229-3240.
- Held, A., K. P. Hinz, A. Trimborn, B. Spengler and O. Klemm (2002). "Chemical classes of atmospheric aerosol particles at a rural site in central Europe during winter." *Journal of Aerosol Science* **33**(4): 581-594.
- Hinz, K. P., M. Greweling, F. Drews and B. Spengler (1999). "Data processing in on-line laser mass spectrometry of inorganic, organic, or biological airborne particles." *Journal of the American Society for Mass Spectrometry* **10**(7): 648-660.
- Hopke, P. K. and X. H. Song (1997). "Classification of single particles by neural networks based on the computer-controlled scanning electron microscopy data." *Analytica Chimica Acta* **348**(1-3): 375-388.
- Hughes, L. S., J. O. Allen, P. Bhave, M. J. Kleeman, G. R. Cass, D. Y. Liu, D. P. Fergenson, B. D. Morrical and K. A. Prather (2000). "Evolution of atmospheric particles along trajectories crossing the Los Angeles basin." *Environmental Science and Technology* **34**(15): 3058-3068.
- Hughes, L. S., J. O. Allen, M. J. Kleeman, R. J. Johnson, G. R. Cass, D. S. Gross, E. E. Gard, M. E. Gaelli, B. D. Morrical, D. P. Fergenson, T. Dienes, C. A. Noble, D.-Y. Liu, P. J. Silva and K. A. Prather (1999). "Size and composition distribution of atmospheric particles in southern California." *Environmental Science and Technology* **33**(20): 3506-3515.
- Hughes, L. S., J. O. Allen, L. G. Salmon, P. R. Mayo, R. J. Johnson and G. R. Cass (2002). "Evolution of nitrogen species air pollutants along trajectories crossing the Los Angeles area." *Environmental Science & Technology* **36**(18): 3928-3935.
- Jacobson, M. Z. (1999). "Studying the effects of calcium and magnesium on size-distributed nitrate and ammonium with EQUISOLV ii." *Atmospheric Environment* **33**(22): 3635-3649.
- John, W., S. M. Wall, J. L. Ondo and W. Winklmayr (1990). "Modes in the size distributions of atmospheric inorganic aerosol." *Atmospheric Environment* **24A**(9): 2349-2359.

- Johnston, M. V. (2000). "Sampling and analysis of individual particles by aerosol mass spectrometry." *Journal of Mass Spectrometry* **35**(5): 585-505.
- Kane, D. B. and M. V. Johnston (2001). "Enhancing the detection of sulfate particles for laser ablation aerosol mass spectrometry." *Analytical Chemistry* **73**(22): 5365-5369.
- Kane, D. B., J. J. Wang, K. Frost and M. V. Johnston (2002). "Detection of negative ions from individual ultrafine particles." *Analytical Chemistry* **74**(9): 2092-2096.
- Kegler, S. R., W. E. Wilson and A. H. Marcus (2001). "PM1, intermodal (PM2.5-1) mass, and the soil component of PM2.5 in Phoenix, AZ, 1995-1996." *Aerosol Science and Technology* **35**(5): 914-920.
- Kim, B. M., S. Teffera and M. D. Zeldin (2000). "Characterization of PM2.5 and PM10 in the South Coast Air Basin of southern California: Part 1 - spatial variations." *Journal of the Air & Waste Management Association* **50**(12): 2034-2044.
- Kim, B. M., S. Teffera and M. D. Zeldin (2000). "Characterization of PM2.5 and PM10 in the South Coast Air Basin of southern California: Part 2 - temporal variations." *Journal of the Air & Waste Management Association* **50**(12): 2045-2059.
- Kleeman, M. J. and G. R. Cass (2001). "A 3d Eulerian source-oriented model for an externally mixed aerosol." *Environmental Science and Technology* **35**(24): 4834-4848.
- Kleeman, M. J., G. R. Cass and A. Eldering (1997). "Modeling the airborne particle complex as a source-oriented external mixture." *Journal of Geophysical Research-Atmospheres* **102**(D17): 21355-21372.
- Kleeman, M. J., J. J. Schauer and G. R. Cass (1999). "Size and composition distribution of fine particulate matter emitted from wood burning, meat charbroiling, and cigarettes." *Environmental Science and Technology* **33**: 3516-3523.
- Klouda, G. A., C. W. Lewis, D. C. Stiles, J. L. Marolf, W. D. Ellenson and W. A. Lonneman (2002). "Biogenic contributions to atmospheric volatile organic compounds in Azusa, California." *Journal of Geophysical Research, [Atmospheres]* **107**(D7 & D8): ACH 7/1-ACH 7/14.
- Laden, F., L. M. Neas, D. W. Dockery and J. Schwartz (2000). "Associations of fine particulate matter from different sources with daily mortality in six U.S. Cities." *Environmental Health Perspectives* **108**(10): 941-955.
- Lawson, D. R. (1990). "The Southern California Air Quality Study." *J. Air Waste Man. Ass.* **40**: 156-165.
- Lee, S.-H., D. M. Murphy, D. S. Thomson and A. M. Middlebrook (2002). "Chemical components of single particles measured with particle analysis by laser mass spectrometry (PALMS) during the Atlanta Supersite project: Focus on organic/sulfate, lead, soot, and mineral particles." *Journal of Geophysical Research-Atmospheres* **107**(D1): AAC 1-13.
- Liu, D.-Y., K. A. Prather and S. V. Hering (2000). "Variations in the size and chemical composition of nitrate-containing particles in Riverside, CA." *Aerosol Science and Technology* **33**(1-2): 71-86.
- Liu, D.-Y., R. J. Wenzel and K. A. Prather (2003). "Aerosol time-of-flight mass spectrometry during the Atlanta Supersite experiment: Part 1 measurements." *Journal of Geophysical Research-Atmospheres* **108**: 14-1: 14-16.
- Lurmann, F. W., A. S. Wexler, S. N. Pandis, S. Musarra, N. Kumar and J. H. Seinfeld (1997). "Modelling urban and regional aerosols .II. Application to California's South Coast Air Basin." *Atmospheric Environment* **31**(17): 2695-2715.

- Mallina, R. V., A. S. Wexler, K. P. Rhoads and M. V. Johnston (2000). "High speed particle beam generation: A dynamic focusing mechanism for selecting ultrafine particles." *Aerosol Science and Technology* **33**(1-2): 87-104.
- McMurry, P. H. (2000). "A review of atmospheric aerosol measurements." *Atmospheric Environment* **34**: 1959-1999.
- Middlebrook, A. M., D. M. Murphy, S. H. Lee, D. S. Thomson, K. A. Prather, R. J. Wenzel, D. Y. Liu, D. J. Phares, K. P. Rhoads, A. S. Wexler, M. V. Johnston, J. L. Jimenez, J. T. Jayne, D. R. Worsnop, I. Yourshaw, J. H. Seinfeld and R. C. Flagan (2003). "A comparison of particle mass spectrometers during the 1999 Atlanta Supersite project." *Journal of Geophysical Research-Atmospheres* **108**(D7).
- Morawska, L. and J. F. Zhang (2002). "Combustion sources of particles. 1. Health relevance and source signatures." *Chemosphere* **49**(9): 1045-1058.
- Motallebi, N., J. Pederson, B. E. Croes, T. VanCuren, S. V. Hering, K. A. Prather and M. A. Allan (1998). "The 1997 Southern California Ozone Study-NARSTO: Aerosol program and radiation study." *Proceedings, Annual Meeting - Air & Waste Management Association* **91st**: WP7506/1-WP7506/20.
- Murphy, D. M. and D. S. Thomson (2000). "Halogen ions and NO⁺ in the mass spectra of aerosols in the upper troposphere and lower stratosphere." *Geophysical Research Letters* **27**(19): 3217-3220.
- Murphy, D. M., D. S. Thomson and T. M. J. Mahoney (1998). "In situ measurements of organics, meteoritic material, mercury, and other elements in aerosols at 5 to 19 kilometers." *Science* **282**(5394): 1664-1669.
- Neubauer, K. R., M. V. Johnston and A. S. Wexler (1998). "Humidity effects on the mass spectra of single aerosol particles." *Atmospheric Environment* **32**(14-15): 2521-2529.
- Noble, C. A. and K. A. Prather (1996). "Real-time measurement of correlated size and composition profiles of individual atmospheric aerosol particles." *Environmental Science & Technology* **30**(9): 2667-2680.
- Pandis, S. N., R. A. Harley, G. R. Cass and J. H. Seinfeld (1992). "Secondary organic aerosol formation and transport." *Atmospheric Environment, Part A: General Topics* **26A**(13): 2269-82.
- Pastor, S. H., J. O. Allen, L. S. Hughes, P. Bhawe, G. R. Cass and K. A. Prather (2003). "Ambient single particle analysis in Riverside, CA by aerosol time-of-flight mass spectrometry during SCOS97-NARSTO." *Atmospheric Environment* **in press**.
- Pastor, S. H. and K. A. Prather (2000). "The evolution of single particle size and composition in the South Coast Air Basin during SCOS97." *Proceedings of the Air & Waste Management Association's Annual Conference & Exhibition, 93rd, Salt Lake City, UT, United States, June 18-22, 2000*: 137-144.
- Penner, J. E., C. C. Chuang and K. Grant (1998). "Climate forcing by carbonaceous and sulfate aerosols." *Climate Dynamics* **14**(12): 839-851.
- Penner, J. E., D. Hegg, R. Leitch and . (2001). "Unraveling the role of aerosols in climate change." *Environmental Science & Technology* **35**(15): 332A-340A.
- Phares, D. J., K. P. Rhoads, A. S. Wexler, D. B. Kane and M. V. Johnston (2001). "Application of the ART-2a algorithm to laser ablation aerosol mass spectrometry of particle standards." *Analytical Chemistry* **73**(10): 2338-2344.
- Pope, C. A. (2000). "Review: Epidemiological basis for particulate air pollution health standards." *Aerosol Science and Technology* **32**(1): 4-14.

- Pope III, C. A., M. J. Thun, M. M. Namboodiri, D. W. Dockery, J. S. Evans, F. E. Speizer and C. W. Heath (1995). "Particulate air pollution as a predictor of mortality in a prospective study of U.S. Adults." *American Journal of Respiratory and Critical Care Medicine* **151**: 669-674.
- Prather, K. A., T. Nordmeyer and K. Salt (1994). "Real-time characterization of individual aerosol particles using time-of-flight mass spectrometry." *Anal. Chem.* **66**(9): 1403-7.
- Russell, A. G., K. F. McCue and G. R. Cass (1988). "Mathematical modeling of the formation of nitrogen-containing air pollutants. 1. Evaluation of an Eulerian photochemical model." *Environmental Science and Technology* **22**(3): 263-71.
- Salma, I., M. D. Maso, M. Kulmala and G. Zaray (2002). "Modal characteristics of particulate matter in urban atmospheric aerosols." *Microchemical Journal* **73**: 19-26.
- Silva, P. J., R. A. Carlin and K. A. Prather (2000). "Single particle analysis of suspended soil dust from southern California." *Atmospheric Environment* **34**(11): 1811-1820.
- Singh, M., P. A. Jaques and C. Sioutas (2002). "Size distributions and diurnal characteristics of particle-bound metals in source and receptor sites of the Los Angeles basin." *Atmos. Environ.* **36**: 1675-1689.
- Solomon, P. A., S. M. Larson, T. Fall and G. R. Cass (1988). "Basinwide nitric acid and related species concentrations observed during the claremont nitrogen species comparison study." *Atmospheric Environment (1967-1989)* **22**(8): 1587-94.
- Song, X.-H., N. M. Faber, P. K. Hopke, D. T. Suess, K. A. Prather, J. J. Schauer and G. R. Cass (2001). "Source apportionment of gasoline and diesel by multivariate calibration based on single particle mass spectral data." *Analytica Chimica Acta* **446**(1-2): 329-343.
- Song, X.-H., P. K. Hopke, D. P. Fergenson and K. A. Prather (1999). "Classification of single particles analyzed by ATOFMS using an artificial neural network, art-2a." *Analytical Chemistry* **71**(4): 860-865.
- Suess, D. T. and K. A. Prather (1999). "Mass spectrometry of aerosols." *Chemical Reviews (Washington, D. C.)* **99**(10): 3007-3035.
- Tan, P. V., O. Malpica, G. J. Evans, S. Owega and M. S. Fila (2002). "Chemically-assigned classification of aerosol mass spectra." *Journal of the American Society for Mass Spectrometry* **13**(7): 826-838.
- Thomas, S. and L. Morawska (2002). "Size-selected particles in an urban atmosphere of Brisbane, Australia." *Atmospheric Environment* **36**(26): 4277-4288.
- Turpin, B. A. and J. J. Huntzicker (1995). "Identification of secondary organic aerosol episodes and quantitation of primary and secondary organic aerosol concentrations during SCAQS." *Atmos. Environ.* **29**(23): 3527-3544.
- Vedal, S. (1997). "Ambient particles and health: Lines that divide." *Journal of the Air and Waste Management Association* **47**: 551-581.
- Vuilleumier, L., R. A. Harley, N. J. Brown, J. R. Slusser, D. Kolinski and D. S. Bigelow (2001). "Variability in ultraviolet total optical depth during the Southern California Ozone Study (SCOS97)." *Atmospheric Environment* **35**(6): 1111-1122.
- Watson, J. G. (2002). "Visibility: Science and regulation." *Journal of the Air & Waste Management Association* **52**(6): 628-713.
- Wenzel, R. J., D. Y. Liu, E. Edgerton and K. A. Prather (2003). "Aerosol time-of-flight mass spectrometry during the Atlanta Supersite experiment: Part 2 scaling procedures." *Journal Of Geophysical Research-Atmospheres* **108**: 15-1:15-8.

- Wexler, A. S. and J. H. Seinfeld (1992). "Analysis of aerosol ammonium nitrate: Departures from equilibrium during SCAQS." *Atmospheric Environment* **26A**(4): 579-591.
- Wilson, W. E., J. C. Chow, C. Claiborn, F. S. Wei, J. Engelbrecht and J. G. Watson (2002). "Monitoring of particulate matter outdoors." *Chemosphere* **49**(9): 1009-1043.
- Wood, S. H. and K. A. Prather (1998). "Real-time analysis of individual aerosol particles during SCOS97." *Book of Abstracts, 215th ACS National Meeting, Dallas, March 29-April 2*: ANYL-071.
- Woods, E., G. D. Smith, R. E. Miller and T. Baer (2002). "Depth profiling of heterogeneously mixed aerosol particles using single-particle mass spectrometry." *Analytical Chemistry* **74**(7): 1642-1649.